Feary, D.A., Hine, A.C., Malone, M.J., et al., 2000
Proceedings of the Ocean Drilling Program, Initial Reports Volume 182

8. Site 1130[1]

Shipboard Scientific Party[2]

BACKGROUND AND OBJECTIVES

Site 1130 is located on the Great Australian Bight upper slope in 488.0 m of water (Fig. F1). The primary objective at Site 1130 was to intersect and characterize Neogene shelf edge and slope sequences and, particularly, to sample the distal (to contrast with the proximal section at Site 1132) portion of an inferred Paleocene–middle Eocene progradational siliciclastic wedge identified and mapped as seismic Sequence 7 (Feary and James, 1998, reprinted as Chap. 2). This sequence forms an east-west-oriented, elongate sediment body that extends at least 300 km along the Eucla Basin, seaward of a prominent basement high (Fig. F2; see "Seismic Stratigraphy," p. 30).

Sequence 7 appears to represent the first depositional episode overlying the top Mesozoic erosional event. The uppermost portion of this sequence is probably the seaward equivalent of the middle Eocene Hampton Sandstone found in the subsurface of the onshore Eucla Basin. The youngest parts of Sequence 7 were inferred to be thin, uppermost lower or lowermost middle Eocene mudstones intersected at the base of the Tertiary succession in the Jerboa-1 well (Bein and Taylor, 1981; Stagg et al., 1990), and interpreted by Feary and James (1998, reprinted as Chap. 2) as a thin foredelta apron. This top part of the sequence is an aggradational component reflecting increased accommodation space, probably resulting from sediment compaction and sag within the Mesozoic rift basin (Eyre Sub-basin) underlying the Eyre Terrace.

Site 1130 was located to intersect thin portions of Paleogene Sequence 6A and Neogene Sequence 4, overlain by a thick interval of Pleistocene Sequence 2. Regional seismic stratigraphy shows that Sequences 6A and 4 are deep-water carbonate accumulations with lobate and aggradational geometries, respectively (see "Seismic Stratigraphy," p. 30). Sequence 2 at Site 1130 offered the opportunity to describe

F1. Map showing Site 1130 in relation to other Leg 182 sites and the AGSO160 seismic lines, p. 35.

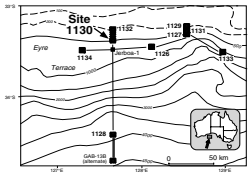

F2. Portion of seismic line AGSO169/13a showing seismic stratigraphic sequences at Site 1130, p. 36.

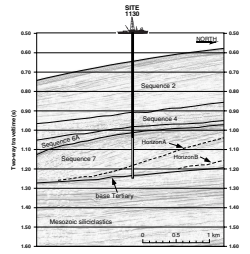

[1]Examples of how to reference the whole or part of this volume.
[2]Shipboard Scientific Party addresses.

Ms 182IR-108

along-slope variations in sedimentation rates and facies, in comparison with the much thicker interval of Sequence 2 intersected at Sites 1127, 1129, and 1131.

The scientific objectives for Site 1130 were to

1. Recover a detailed record of shelf edge siliciclastic deposition at a distal site to evaluate the sedimentary response to Paleogene sea-level fluctuations and to evaluate the complex interaction between sea-level variation, accommodation space, and subsidence;
2. Determine the characteristics of cool-water carbonate facies within the Neogene/Quaternary succession;
3. Determine paleoceanographic parameters within a shelf edge to slope setting from Sequences 2 to 6A to complement other components of the shelf-to-basin transect;
4. Evaluate sea-level control on Neogene/Quaternary facies within an upper slope/shelf edge setting; and
5. Evaluate the diagenetic history and processes within Neogene/Quaternary facies in an upper slope/shelf edge setting.

OPERATIONS

Transit to Site 1130

The 45-nmi transit to Site 1130 required 4.5 hr at an average speed of 10.0 kt (Table T1). A beacon was launched at 2207 hr on 11 November, followed by a second beacon, initiating Site 1130.

T1. Site 1130 coring summary, p. 71.

Hole 1130A

The ship was stabilized on position and an advanced hydraulic piston corer (APC) bottom-hole assembly (BHA) was run to 476 meters below rig floor (mbrf), based on the readings from the precision depth recorder (PDR). The first two attempts to spud the hole resulted in no recovery, indicating that the PDR depth was inaccurate. The PDR computer was reinitialized and the bit was positioned at 497 mbrf, closer to the estimated water depth in the leg prospectus. Hole 1130A was spudded at 0200 hr on 11 November, and Core 1H recovered 8.48 m, indicating a water depth of 486.7 meters below sea level (mbsl). Advanced hydraulic piston coring advanced to 170.0 meters below seafloor (mbsf), ceasing when 90 kilopounds (kips) could not dislodge Core 18H, which required drilling over the core barrel to release it. The nonmagnetic shoe, flapper, and liner seal sub were deployed on Cores 3H, 5H, 7H, and 9H. The bottom portion of Core 3H was lost when the single nonmagnetic flapper core catcher failed. Cores 3H–18H were oriented and Adara tool heat-flow measurements were taken on Cores 4H and 8H. The Davis-Villinger temperature probe (DVTP) was deployed after Core 12H at 113.0 mbsf.

Coring resumed with the extended core barrel (XCB) from 170.0 to 380.5 mbsf. The last six cores (Cores 182-1130A-36X through 41X) had 3.4% recovery in interbedded cherts and chalks. Two soft-formation XCB shoes were destroyed when chert beveled out the throat of each shoe. As a safety precaution before penetrating Sequence 7 sandstones, operations were slowed (after Core 33X) to allow hydrocarbon gas monitoring to be completed before proceeding with each succeeding core.

Only background levels of gas were detected. The pipe became stuck at 378 mbsf after Core 41X; however, it was pulled free with 70 kips overpull. Hole 1130A was terminated because of poor recovery in the sandstones with the XCB system. The hole was filled with mud and the drill string was recovered, clearing the seafloor at 1815 hr on 13 November.

Hole 1130B

The ship was moved 20 m west and Hole 1130B was spudded at 1915 hr on 13 November. The bit was positioned at 494 mbrf, and Core 1H recovered 3.93 m, indicating a water depth of 488.1 mbsl. Advanced hydraulic piston coring advanced to 156.0 mbsf. Cores 3H–17H were oriented and an Adara heat-flow measurement was taken on Core 6H. The nonmagnetic core barrel assembly was deployed on Cores 3H, 5H, 7H, 9H, 11H, and 13H. Core 3H was lost when it slipped past the single nonmagnetic flapper catcher; thus, a steel 10-finger core catcher was added to the nonmagnetic core barrel assembly thereafter. XCB coring was advanced to the depth objective of 310.4 mbsf with 101.2% recovery in chalk. After plugging the hole with mud, the drill string was recovered, clearing the rig floor at 1530 hr on 14 November.

Hole 1130C

The ship was moved 20 m north and Hole 1130C was spudded with the rotary core barrel (RCB) at 1830 hr on 14 November. The interval from 0 to 299.2 mbsf was drilled, followed by a one-stand wiper trip to 331 mbsf to condition the hole. Coring resumed with the RCB from 299.2 to 395.2 mbsf. The rotary stalled while cutting Core 9R; however, the pipe was worked free in 15 min with 50 kips overpull. Rotation and circulation were regained and a mud sweep was circulated. Core 10R was cut from 385.6 to 395.2 mbsf, after which the pipe became stuck again in presumably friable and variably indurated sandstones. The pipe could not be freed, so the bit was released with the mechanical bit release. The pipe was worked free after 2.5 hr, and circulation and rotation were reestablished. However, coring operations were terminated because hole conditions were too unstable to continue under shallow-water operational guidelines. The end of pipe was pulled to 106 mbsf in preparation for logging. Logging tools were run in the following order: (1) triple combination logging tool (triple combo) (368.5 mbsf, 26.7 m off bottom, to the mudline) in two runs because of failure of the wireline heave compensator (WHC) on the first run; (2) Formation MicroScanner (FMS)/sonic (368.9–90.5 mbsf) in two runs; and (3) well seismic tool (WST) (363.5 mbsf to the end of the pipe) with eight stations ~30 m apart. After conclusion of logging operations, the hole was plugged with mud, the rig was secured for transit, and the vessel departed for Site 1131 at 0845 hr on November 16.

LITHOSTRATIGRAPHY

Introduction

Site 1130 is located at a water depth of 488.0 m on the upper slope of the eastern Eyre Terrace. The objective at this site was to intersect the thick Pleistocene carbonate succession and the distal parts of the Paleocene–Eocene? progradational siliciclastic wedge in an upper slope depo-

sitional setting. Four major sedimentary units were recognized and subdivided (Fig. F3) on the basis of major sediment type, texture, composition, color change, presence of firmgrounds, and soft sediment deformation. The lowest package consists of calcareous sandstone of presumed Eocene age that was probably deposited in a marginal marine setting. The overlying, poorly recovered interval consists of chert (silicified nannofossil planktonic foraminiferal ooze) intervals. The third sedimentary unit is dominated by pelagic calcareous ooze and chalk. The shallowest and thickest unit is characterized by a repetitive succession of bioclastic packstones, punctuated by bioclastic wackestone layers and occasional calcareous ooze to chalk intervals.

Recovery was more than 95% within the upper 329 mbsf of the cored interval but then dropped abruptly because of the presence of soft calcareous chalks and interbedded hard chert layers. Unit boundaries in these low recovery intervals are defined by first and last occurrence (FO and LO, respectively) of particular lithologies (e.g., silicified planktonic foraminiferal ooze or calcareous sandstone)

F3. Site 1130 sediment lithostratigraphy, p. 37.

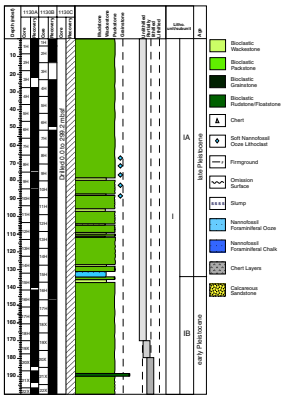

Lithostratigraphic Units

Unit I

Intervals: Core 182-1130A-1H through Section 28X-2, 143 cm; Core 182-1130B-1H through Section 28X-6, 123 cm
Depth: 0–257.23 mbsf (Hole 1130A); 0–261.43 mbsf (Hole 1130B)
Age: Pleistocene–late Pliocene

Unit I consists of light gray to pale olive, strongly bioturbated, unlithified bioclastic packstone punctuated by intervals of unlithified bioclastic wackestone and nannofossil ooze. Unit I is divided into three subunits on the basis of different sedimentation patterns, textural changes, and the presence of hardgrounds and nannofossil ooze intervals (Fig. F3). Subunits IA and IB are characterized by a repetitive succession of uniform bioclastic packstones in the upper part punctuated by bioclastic wackestone layers in the lower part. The two subunits are separated by a distinct calcareous ooze interval. Subunit IC is dominated by bioclastic packstones, with a slump at its base.

Subunit IA

Intervals: Core 182-1130A-1H through Section 15H-2, 10 cm; Core 182-1130B-1H through Section 15H-2
Depth: 0–133.60 mbsf (Hole 1130A); 0–130.50 mbsf (Hole 1130B)
Age: late Pleistocene

Subunit IA consists of a succession of massive, uniform bioclastic packstone in the upper part and alternating layers of wackestone to packstone in the lower part. The lowermost bed in Subunit IA is a nannofossil ooze.

The matrix of the unlithified packstones is dominated by calcareous nannofossils, abundant bioclasts, benthic and planktonic foraminifers, sponge spicules, and tunicate spines. The sand-sized fraction (>63 µm) contains varying amounts of bioclasts and planktonic foraminifers and common to abundant benthic foraminifers and sponge spicules. Echinoid and tunicate spines are present. The silt- to sand-sized unlithified bioclastic packstones have subtle but distinct color alternations ranging from light olive gray to light gray. Generally, the lighter layers are finer

grained and planktonic foraminifer rich, whereas the darker layers are coarser grained and contain more bioclasts. The sediments are moderately to strongly bioturbated.

Deposits between 67.7 and 99.73 mbsf are characterized by the presence of scattered soft lumps of nannofossil ooze. These white unlithified clasts "float" in the wackestone or packstone matrix, and they appear out of context with respect to the major lithology.

Below 78 mbsf, the sediment pattern changes to alternating layers of unlithified wackestone and packstone. The generally light gray, very fine grained wackestones are compositionally and texturally similar to nannofossil ooze. The wackestone matrix is mostly calcareous nannofossils, common benthic foraminifers, sponge spicules, bioclasts, and tunicate spines. Echinoid spines and planktonic foraminifers are present. The wackestone coarse fraction (>63 µm) is dominated by bioclasts, common planktonic and benthic foraminifers, and sponge spicules. There are rare bryozoans and traces of dark brown grains, quartz, tunicate spines, bivalves, and ostracodes. The wackestones contain a greater proportion of nannofossils, sponge spicules, and tunicate spines than the packstones. The deposits are moderately bioturbated, as shown by color mottling. Interval 182-1130B-11H-5, 0–113 cm, in particular, contains a large *Thalassinoides* network.

The lower boundary of Subunit IA is at the base of a white nannofossil ooze with bioclasts. The ooze contains well-defined burrows that are usually stiffer and better lithified than the surrounding sediment, with deep *Thalassinoides* burrowing present in interval 182-1130B-15H-1, 127–150 cm.

Subunit IB

Intervals: Sections 182-1130A-15H-2, 10 cm, through 26X-3, 80 cm; Sections 182-1130B-15H-3 through 26X-3, 120 cm
Depth: 133.60–238.80 mbsf (Hole 1130A); 130.50–237.70 mbsf (Hole 1130B)
Age: late Pliocene–early Pleistocene

The boundary between Subunits IA and IB is a sharp contact between the upper thin but distinct layer of white to light gray nannofossil ooze and the lower light olive-gray, very fine grained bioclastic packstone.

The sedimentary pattern in Subunit IB is similar in style to the succession in Subunit IA, with the main difference being the lack of firmgrounds. The uppermost part of the subunit is composed of uniform unlithified packstone with a few wackestone interbeds in the lower part.

The unlithified bioclastic packstones of Subunit IB are characterized by alternating light olive-gray and pale olive color changes. Grain size ranges from silt to fine sand, but the unlithified packstones in the lower part of the subunit are generally finer grained and contain more mud. Components of the >63-µm fraction are planktonic foraminifers, benthic foraminifers, sponge spicules, blackened grains, and glauconite grains. The matrix is dominantly calcareous nannofossils, abundant bioclasts, common planktonic foraminifers, and sponge spicules.

The sediments are moderately to strongly bioturbated and change from unlithified to partially lithified in a transition zone between 170 and 180 mbsf. The gray, fine-grained, unlithified rudstone bed that grades upward into a light gray bioclastic floatstone and then into a bioclastic packstone at ~187–188 mbsf is interpreted as a turbidite. It contains pebble-sized bryozoan fragments (vagrant and delicate

branching growth forms), granule-sized shell fragments, an azooxanthellate coral, and benthic foraminifers. The deposit has a sharp erosional base, whereas the contact with the overlying bioclastic packstone lithology is transitional due to bioturbation.

In the lower part of Subunit IB, below 200 mbsf, the deposits are alternating layers of bioclastic wackestone and packstone, with a thin bed of nannofossil ooze overlying a firmground at the base. The matrix in grain-supported intervals is dominantly calcareous nannoplankton, abundant to common bioclasts, with minor planktonic and benthic foraminifers and sponge spicules (see **"Site 1130 Smear Slides,"** p. 83). The coarse fraction is mostly bioclasts. Lighter layers contain abundant planktonic foraminifers, whereas darker layers are rich in blackened grains and glauconite. Benthic foraminifers, sponge spicules, and echinoid spines are also present.

The fine-grained wackestones in the lower part of the subunit are light gray to light olive gray in color, with gradational changes between colors. The wackestone matrix is dominated by calcareous nannofossils, abundant bioclasts, varying amounts of benthic and planktonic foraminifers, common tunicate spines, and sponge spicules. There are traces of quartz and pyrite grains. The coarse fraction has the same composition as the packstones, but with large numbers of planktonic and benthic foraminifers.

Both packstones and wackestones are strongly bioturbated throughout, which is shown as color mottling. *Thalassinoides* and *Chondrites* burrows of the uppermost parts of burrows are best shown in transition zones from darker grain-supported to lighter mud-supported intervals. Shell fragments, bivalve fragments, gastropods, and benthic foraminifers are scattered throughout.

A turbidite with pebble-sized gray bryozoan debris, blackened grains, and echinoid spines is present at 229.37–229.80 mbsf. It is characterized by inverse to normal grading and is poorly sorted (Fig. **F4**). The boundary between Subunits IB and IC is defined by a hardground and facies change.

F4. Turbidite from the lower part of Subunit IB, **p. 39.**

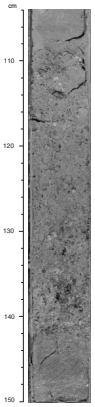

Subunit IC

Intervals: Sections 182-1130A-26X-3, 80 cm, through 28X-2, 143 cm; Sections 182-1130B-26X-3, 120 cm, through 28X-6, 123 cm
Depth: 238.80–257.23 mbsf (Hole 1130A); 237.70–261.43 mbsf (Hole 1130B)
Age: late Pliocene

The upper boundary of Subunit IC is marked by the presence of a firmground and a change in lithology; the lower boundary is placed at the base of a bed characterized by synsedimentary deformation and interpreted as a slump.

The bioclastic packstone is characterized by color alternation ranging from olive to light gray. The matrix of the packstones is dominated by calcareous nannofossils, with varying amounts of bioclasts and benthic and planktonic foraminifers. The sediment also contains sponge spicules, tunicate spines, diatoms, ostracodes, and dolomite (see **"Site 1130 Smear Slides,"** p. 83).

The components of the >63-µm fraction are fine-grained abundant to dominant bioclasts, abundant to common benthic and planktonic foraminifers, and minor amounts of blackened grains, glauconite, echinoid spines, sponge spicules, tunicates, and ostracodes. Lighter layers contain more planktonic foraminifers, whereas darker layers are richer

in blackened grains. The deposits are moderately to strongly bioturbated and partially lithified. The slump at the base of the Subunit IC (Fig. F5) consists of alternating layers of glauconitic bioclastic packstone and white nannofossil bioclastic packstone, suggesting entrainment of the underlying lithology.

F5. Slump marking the boundary between lithostratigraphic Units I and II, p. 40.

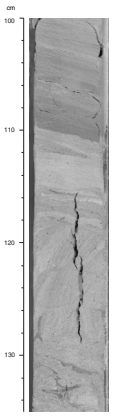

Unit II

Intervals: Sections 182-1130A-28X-2, 143 cm, through 35X-CC, 24 cm; Sections 182-1130B-28X-6, 123 cm, through 33X; 182-1130C-1R through 3R
Depth: 257.23–328.86 mbsf (Hole 1130A); 261.43–310.56 mbsf (Hole 1130B); 299.20–328.10 mbsf (Hole 1130C)
Age: late Miocene–early Pliocene

Lithologies in Unit II are calcareous nannofossil foraminiferal chalk and ooze, punctuated by two grainstone to floatstone intervals in the lower part. Texturally, these sediments range from mudstone to packstone, and lithification varies from unlithified to partially lithified (Fig. F3), resulting in alternating layers of soft oozes and harder chalks. The matrix is dominated by calcareous nannofossils, common planktonic foraminifers, and some bioclasts. Components of the >63-µm fraction are abundant planktonic foraminifers, some benthic foraminifers, and few bioclasts. Glauconite and blackened grains are scattered throughout the unit and are common in the lower part. The sediments are moderately to strongly bioturbated, which is manifested by color mottling.

The deposits in the lower 30 m of Unit II are characterized by firmgrounds, two grainstone beds, and thin, alternating wackestone-packstone layers punctuated by omission surfaces. The upper grainstone bed (intervals 182-1130A-34X-1, 46–51 cm, and 182-1130C-2R-4, 123–126 cm) is a light olive-gray, partially lithified, fine sand-sized planktonic foraminiferal grainstone that texturally grades upward to a grainstone to packstone with a sharp base and gradational bioturbated top. In addition to the planktonic foraminifers, some of which are filled with glauconite, it also contains benthic foraminifers, well-cemented packstone to grainstone clasts, bivalve fragments, sponge spicules, ovoid fine- to medium-sized brown bioclasts (limonite?), and minor amounts of pyrite. The grain size is fine sand. In Hole 1130C, the underlying nannofossil foraminiferal chalk underwent some minor synsedimentary deformation (slump).

The lower grainstone bed (intervals 182-1130A-34X-4, 59–76 cm, and 182-1130C-3R, 56–59 cm) is a fine to medium sand-sized bioclastic grainstone (Hole 1130A) containing skeletal fragments, glauconite, planktonic foraminifers, benthic foraminifers, bryozoans, and bivalve fragments. Both upper and lower contacts are sharp. The equivalent layer in Hole 1130B is a partially lithified floatstone with bioclasts and planktonic foraminifers. The upper contact is sharp, whereas the lower one was not recovered. Both intervals are interpreted as turbidites. Omission surfaces and firmgrounds were recognized in Hole 1130C only. This is probably the result of different drilling techniques (XCB vs. RCB), with frequent biscuiting observed in XCB cores.

Unit III

Intervals: Sections 182-1130A-35X-CC, 24 cm, through Core 39X; Cores 182-1130C-4R through 7R

Depth: 328.86–369.50 mbsf (Hole 1130A); 328.10–366.40 mbsf (Hole 1130C)
Age: late Oligocene

This unit was poorly recovered. The only sediments recovered were fragments of silicified nannofossil foraminiferal chalk, some of which are draped with a thin layer of unlithified nannofossil ooze to partially lithified chalk. A reasonable inference is that the entire unit consists of ooze and that beds or lenses of preferentially silicified nannofossil foraminiferal ooze were the only materials recovered. Unit boundaries were defined by the FO and LO of silicified nannofossil foraminiferal chalk. The lithified white to very dark gray, silicified nannofossil planktonic foraminiferal ooze (chert/porcellanite) has a wackestone to packstone texture and a grain size ranging from very fine sand to silt. Major components are large to small benthic foraminifers, very small planktonic foraminifers, and blackened grains. The matrix is dominated by calcareous nannofossils, but it also contains planktonic and benthic foraminifers, bioclasts, and sponge spicules. Most fragments have burrows filled with white, fine to very fine grained nannofossil foraminiferal chalk, ranging from packstone to grainstone in texture. No macrofossils were recorded in Unit III.

Unit IV

Intervals: Core 182-1130A-40X; Cores 182-1130C-8R through 10R
Depth: 369.50–369.87 mbsf (Hole 1130A); 366.40–386.51 mbsf (bottom of the hole; Hole 1130C)
Age: late Eocene

The upper boundary of the unit was defined by the first occurrence (FO) of calcareous sandstone in Core 182-1130C-8R. Overall recovery was poor, and sediments were biscuited or fragmented during drilling.

Four lithologies were recovered in this interval: (1) calcareous sandstone, (2) bioclastic glauconitic wackestone, (3) bryozoan grainstone, and (4) bivalve grainstone (see **"Site 1130 Thin Sections,"** p. 84).

The red calcareous sandstone is poorly sorted. The grain distribution is bimodal with fine sand- to granule-sized grains within a carbonate bioclastic wackestone to packstone matrix. Terrigenous components consist of sand-sized, subrounded iron-coated grains, quartz, feldspar, opaque minerals, and glauconite. Carbonate components are bryozoans, benthic foraminifers, minor bioclasts, and a piece of azooxanthellate coral, all of which are filled with light brown carbonate mud.

Thin-section analysis (Sample 182-1130B-40X-1, 5–6 cm) shows that the red to orange sediment varies from a calcareous sandstone to a sandy limestone and is distinguished by very coarse to sand-sized grains and pink to orange carbonate. Texturally, the sediment is a packstone to wackestone. The composition of the terrigenous clastic components is bimodal, comprising very coarse subrounded quartz and feldspar particles and fine, more subrounded to angular quartz grains. The feldspar is altered to clay along cleavage planes. Both polycrystalline and single-crystal quartz grains are present. Most of the grains are iron coated, and some are cemented together by limonite?. Small fractures within the grains are also zones of Fe oxide precipitation. Fine sand-sized glauconite is present, and the periphery of many glauconite particles are altered to limonite. Fine sand-sized ovoid limonite/goethite grains

typically have an oolitic texture; in some instances, small angular quartz grains are also coated with layers of limonite.

Carbonate components are dominated by bryozoan and echinoid grains with lesser benthic foraminifers. Echinoid remains consist of spines and plates, whereas the bryozoans are fragmented and composed of delicate, articulated, and flat robust branching forms. Benthic foraminifers are miliolids, amphisteginids?, textularids, and some encrusting growth forms. Other grains include brachiopod and ostracode fragments. Many particles are also sites of Fe oxide precipitation, especially in microborings and echinoderm stoma. The fine-grained, mud-sized matrix is entirely microbioclastic carbonate, containing some planktonic foraminifers. Fe oxides are also present throughout the matrix.

Diagenesis is visible in a few minor spar-filled molds, but positive identification of origin is difficult. Overall, there is little obvious neomorphism, but fuzzy grain boundaries suggest minor crystal enlargement.

The red bioclastic glauconitic wackestone (or bioclastic wackestone with glauconite) contains varying amounts of fine to very fine sand-sized glauconite, coarse- to fine-grained bioclasts, echinoid spines, bryozoans, and other unidentifiable particles. Some fragments show grading from glauconite-poor to glauconite-rich intervals, and some possible cross lamination. One fragment at interval 182-1130C-8R-1, 82–85 cm, contains a fine gray carbonate mudstone to very fine grained carbonate siltstone layer.

The medium to very coarse grained bryozoan grainstone is white to light red. Its diverse bryozoan assemblage ranges from mainly articulate to fenestrate and flat robust branching bryozoans. It also contains abundant angular to rounded and moderately sorted quartz grains and common bioclasts. Serpulid worm tubes, gastropods, bivalves, echinoid spines, and opaque grains are present.

The bivalve grainstone is very coarse grained and pink in color. It contains abundant bivalve fragments and quartz. Articulate and delicate branching bryozoans and serpulid worm tubes are common. The components are subangular to rounded and well sorted.

Discussion

The basal calcareous sandstones at Site 1130 (Unit IV) were poorly recovered and thus provide little information about the development of the succession (Fig. **F3**). However, both the bryozoan assemblage and benthic foraminifer assemblage (see **"Biostratigraphy,"** p. 10) suggest a shelf environment. Further marine indicators are benthic foraminifers in the matrix, carbonate mud indicating a quiet-water depositional environment, and bioturbation. The calcareous sandstones are barren of datable microfauna (see **"Biostratigraphy,"** p. 10), but tentative correlation with a succession drilled in Jerboa 1 (Bein and Taylor, 1981) suggests an Eocene age. Unit IV is equivalent to the top part of the seismic Sequence 7 (Feary and James, 1998, reprinted as **Chap. 2;** see **"Seismic Stratigraphy,"** p. 30).

A dramatic change of sedimentation style from shelf-dominated Eocene calcareous sandstones to pelagic Oligocene–lower Pliocene sediments (Units III and II) occurs at 366.40 mbsf. The boundary was not recovered; very poor recovery in the silicified nannofossil planktonic foraminiferal ooze (chert) beds of Unit III prevents further interpretation of the development of the depositional realm. The abrupt change

from silicified nannofossil planktonic foraminiferal ooze to partially lithified nannofossil ooze coincides with a hiatus of 15 m.y. (see "Biostratigraphy," p. 10) and with the top of seismic Sequence 6A (see "Seismic Stratigraphy," p. 30). The well-recovered Unit II is a succession of chalk and ooze in which the lower part is characterized by discontinuous sedimentation, represented by firmgrounds or omission surfaces and by redeposition of sediment shed from the shelf in the form of turbidites. The upper part of Unit II is uniform upper Miocene–lower Pliocene nannofossil chalk and ooze and is represented by seismic Sequence 3.

The boundary to Unit I is an abrupt change in depositional style at the base of a slump (Fig. F5), from pelagic deposition to shelf-dominated deposition of bioclastic packstones. This coincides with a 2-m.y. hiatus recognized in the microfauna (see "Biostratigraphy," p. 10), an abrupt decrease in natural gamma radiation (NGR) (see "Physical Properties," p. 25), and the disappearance of aragonite (see "Inorganic Geochemistry," p. 23).

The upper Pliocene bioclastic packstones of Subunit IC record variations in input of shelf-derived material, with intervals containing blackened and glauconitic grains alternating with mud-supported intervals rich in planktonic foraminifers. The boundary between Subunits IC and IB coincides with the Pliocene/Pleistocene boundary and coincides with the base of Sequence 2, a regional unconformity (see "Seismic Stratigraphy," p. 30).

Subunits IA and IB span the lower–upper Pleistocene and were deposited as sigmoidal clinoforms (see "Seismic Stratigraphy," p. 30). The sedimentary record indicates that these clinoforms can be divided into two depositional packages separated by a flooding interval consisting of nannofossil ooze. This interval corresponds to a prominent reflector within seismic Sequence 2 in the seismic line, separating lower from upper Pleistocene sediments. The lower parts of Subunits IA and IB consist of alternating wackestone and packstone layers, with occasional turbidites (Fig. F4) representing the bottomset style of clinoform sedimentation, whereas uniform bioclastic packstone represents the topset style.

BIOSTRATIGRAPHY

Introduction

Calcareous nannofossils and planktonic foraminifers indicate that sediments recovered at Site 1130 are mainly of Pleistocene–middle Oligocene age. Part of the Pliocene is either missing or highly condensed into the Pleistocene–upper Miocene succession. Pleistocene–upper Pliocene calcareous packstones extend down to ~260 mbsf, overlying lowermost Pliocene and upper Miocene (260–328 mbsf) foraminifer nannofossil oozes. Middle–upper Oligocene wackestones and cherts occur between 328 and 367 mbsf, overlying a calcareous sandstone of middle–late Eocene age at the base of Holes 1130A and 1130C. Calcareous nannofossils and planktonic foraminifers indicate that the disconformity between the Neogene and Oligocene sections represents a hiatus of at least 14 m.y. The contact between Oligocene sediments and the sandstone is also probably disconformable, although its nature cannot be determined because of the absence of nannofossils and age-diagnostic planktonic foraminifers.

The three benthic foraminifer assemblages occurring within the Site 1130 succession correspond respectively to the Oligocene, Miocene–Pliocene, and upper Pliocene–Pleistocene, and indicate a shallowing-upward trend through these time periods. The Oligocene and Neogene assemblages are typically cosmopolitan, middle bathyal assemblages. The upper Pliocene–Pleistocene assemblage is a mixed assemblage of upper bathyal paleodepths, containing many well-sorted specimens redeposited from shelf environments.

The combined results from nannofossils, planktonic foraminifers, and paleomagnetism indicate that the sedimentation rate was as high as 240–260 m/m.y. during most of the Pleistocene. During the Pliocene–Miocene, the sedimentation rate fluctuated between 12 and 32 m/m.y. A similar rate of 10–30 m/m.y. was estimated for middle–upper Oligocene deposition, although datum constraint in this part of the section is limited by poor core recovery.

Calcareous Nannofossils

A Pleistocene–middle Oligocene succession of calcareous nannofossil assemblages is recorded from Site 1130. Common chert layers in the Oligocene section hampered both core recovery and biostratigraphic refinement (see **"Operations,"** p. 2), and a calcareous sandstone below the Oligocene is barren of calcareous nannofossils. Two disconformities are indicated in the Pleistocene–middle Oligocene section, separating three discrete biostratigraphic packages: Pleistocene–upper Pliocene, lower Pliocene–upper Miocene, and upper–middle Oligocene. These disconformities coincide with significant lithologic changes and seismic stratigraphic boundaries (see **"Lithostratigraphy,"** p. 3, and **"Seismic Stratigraphy,"** p. 30). The Pleistocene–upper Pliocene package of calcareous packstones is relatively thick (~255 m), in contrast to both the lower Pliocene–Miocene oozes (~175 m) and the Oligocene calcareous grainstones (~30 m).

The hiatus at the Paleogene/Neogene boundary has a longer duration than the younger hiatus recorded in the Pliocene. It is >14 m.y., with the lower and middle Miocene nannofossil Zones NN1–NN9 missing (Fig. **F6**).

Pleistocene

The three Quaternary calcareous nannofossil zones, NN21–NN19, are recorded. Preservation is good to moderate, and is poor only in the lower part of the section. Reworking is very minor and detected only in two samples at 150.88 and 170.38 mbsf from the uppermost part of Zone NN19. The assemblages from the lowermost part of the combined Zones NN21–NN20 show some evidence of sorting in favor of small species, such as *Reticulofenestra minuta*. Assemblages from the Pleistocene section at Site 1127 showed similar evidence of sorting (see **"Biostratigraphy,"** p. 9, in the "Site 1127" chapter).

The key species for Zone NN21, *Emiliania huxleyi,* is identified down section to Sample 182-1130B-1H-CC (21.95 mbsf), in association with *Braarudosphaera bigelowii, Coccolithus pelagicus, Gephyrocapsa caribbeanica, Gephyrocapsa oceanica, Helicosphaera carteri, Helicosphaera hyalina, Helicosphaera wallichi,* and *Umbilicosphaera sibogae*. Assemblages indicative of the combined Zones NN21–NN20 are recorded down to Sample 182-1130A-14H-CC (131.91 mbsf). Species present throughout this interval include *B. bigelowii, Calcidiscus leptoporus, G. caribbeanica,* small

F6. Calcareous nannofossil and planktonic foraminifer zones and benthic foraminifer assemblages, **p. 41.**

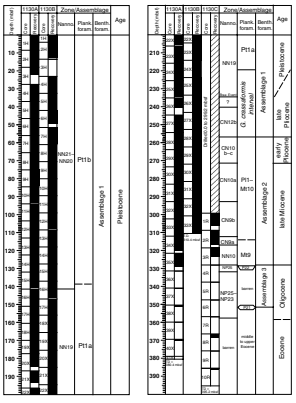

Gephyrocapsa spp. (including *Gephyrocapsa aperta*), *Helicosphaera carteri,* and *Syracosphaera pulchra*. The warm-water *Gephyrocapsa omega* occurs in the upper part of the interval, indicating the influence of the Leeuwin Current.

The LO of *Pseudoemiliania lacunosa,* which indicates Zone NN19, occurs in Sample 182-1130A-15H-CC (140.32 mbsf), in which small *Gephyrocapsa* spp. have their greatest abundance. Similar Zone NN19 assemblages are recorded down to Sample 182-1130A-25X-CC (234.34 mbsf). In addition to those listed above, the assemblage in Samples 182-1130A-16H-CC (150.88 mbsf) and 17H-CC (170.38 mbsf) from the uppermost part of Zone NN19 also contains *Calcidiscus macintyrei, Coccolithus miopelagicus, Cyclicargolithus floridanus, Dictyococcites productus, Helicosphaera carteri, Helicosphaera sellii, Pontosphaera japonica, P. lacunosa, Syracosphaera globulosa,* and *Rhabdosphaera clavigera*. Reworking in these samples is indicated by the presence of *Cyclicargolithus floridanus* and *C. miopelagicus* from older sediments, probably of Miocene age. *Helicosphaera sellii* and *Calcidiscus macintyrei* are represented by a few poorly preserved specimens and appear to be also reworked. The highest occurrences of these two species could not be confidently located during our shipboard study.

An abundance peak of *B. bigelowii* is recorded at the base of Zone NN19 in Sample 182-1130A-25X-CC (234.34 mbsf). This species also shows an abundance peak within a narrow interval in the lower part of the expanded Pleistocene section at Site 1127 (see **"Biostratigraphy,"** p. 9, in the "Site 1127" chapter).

Pliocene

Subzone CN12b (Zone NN16 in part) of late Pliocene age is indicated by the presence of rare *Discoaster surculus* in association with *Calcidiscus macintyrei, Calcidiscus leptoporus, C. pelagicus, Discoaster brouweri, Helicosphaera carteri, Pontosphaera japonica,* and *P. lacunosa* in Sample 182-1130A-26X-CC (240.59 mbsf). Whether the two short Subzones CN12c–d (Zones NN17 and NN18) of the upper Pliocene are represented between this sample and Zone NN19 in Sample 182-1130A-25X-CC (234.34 mbsf) was not determined in our shipboard study.

A disconformity at the sharp lithologic contact between lithostratigraphic Units I and II, at ~259 mbsf (see **"Lithostratigraphy,"** p. 3), separates assemblages of the upper Pliocene Subzone CN12b from that of the lower Pliocene Subzones CN10b–c. The missing Subzone CN12a and Zone CN11 suggest a hiatus of ~1.7 m.y. duration.

Both *Amaurolithus ninae* and *Amaurolithus tricorniculatus* are recorded in association with *Discoaster asymmetricus, Discoaster brouweri, Discoaster pentaradiatus, D. surculus, Discoaster variabilis, Reticulofenestra pseudoumbilicus, Reticulofenestra minutula, Sphenolithus abies,* and *Sphenolithus neoabies* in Sample 182-1130A-28X-3, 124–128 cm (258.54 mbsf), below the lithostratigraphic Unit I/Unit II boundary. In the absence of *Triquetrorhabdulus rugosus,* this association suggests the combined Subzones CN10b–c. Species of *Ceratolithus* (*Ceratolithus acutus, Ceratolithus armatus,* or *Ceratolithus rugosus*) are very scarce or completely absent. The assemblage in Sample 182-1130A-28X-2, 58–62 cm (256.38 mbsf), from above the lithostratigraphic Unit I/Unit II boundary, lacks species of *Amaurolithus* and *Sphenolithus,* as well as the key taxa *R. pseudoumbilicus* and *Discoaster tamalis,* but contains *Ceratolithus rugosus, P. lacunosa,* and *D. surculus,* indicating Subzone CN12b.

Miocene

Assemblages assignable to Subzone CN10a of latest Miocene age are recorded in Samples 182-1130B-29X-CC (272.71 mbsf) through 31X-CC (291.46 mbsf). These are characterized by the presence of *T. rugosus* and species of the genus *Amaurolithus*. Also occurring in this subzone are *Reticulofenestra gelida, Scyphosphaera* spp., and *Triquetrorhabdulus farnsworthii*. Evidence of some reworking from Paleogene sediments into the upper part of Subzone CN10a is recorded by the presence of *Coccolithus formosus, Coccolithus eopelagicus,* and *Discoaster trinidadensis*.

Assemblages assignable to Subzone CN9b occur in Samples 182-1130B-32X-CC (301.05 mbsf) through 182-1130A-33X-CC (312.07 mbsf). These include the association *Amaurolithus amplificus, A. ninae, A. tricorniculatus,* and *Discoaster quinqueramus*. Sample 182-1130C-2R-CC (316.42 mbsf) contains rare *Discoaster berggrenii* and *Minylitha convallis,* and lacks the species of *Amaurolithus,* indicating Subzone CN9a.

Assemblages from Samples 182-1130A-34X-CC (320.12 mbsf), 3R-CC (323.34 mbsf), and 35X-5, 87–92 cm (328.57 mbsf), lack *D. berggrenii,* but contain rare *Discoaster bellus, Discoaster calcaris, Discoaster neohamatus,* and *D. pentaradiatus,* as well as few *Helicosphaera rhomba, M. convallis,* and *T. rugosus,* indicating Zone NN10 (or Zone CN8).

The Zone NN10 assemblage (upper Miocene) in Sample 182-1130A-35X-5, 87–92 cm (328.57 mbsf), is immediately underlain by a Zone NP25 assemblage (upper Oligocene) in Sample 182-1130A-35X-CC (328.89 mbsf). This indicates a major disconformity with the lower, middle, and the basal upper Miocene missing.

Oligocene

Assemblages of Zone NP25 of late Oligocene age are recorded from Samples 182-1130C-4R-CC (328.18 mbsf), 182-1130A-35X-CC (328.89 mbsf), and 182-1130A-36X-CC (331.30 mbsf). *Sphenolithus distentus* is absent from these assemblages, and *Sphenolithus ciperoensis* occurs only in the lower sample at 331.30 mbsf. The association *B. bigelowii, Chiasmolithus altus, Cyclicargolithus abisectus, C. floridanus, Dictyococcites bisectus, Discoaster deflandrei, Helicosphaera recta, Reticulofenestra lockeri,* and *Zygrhablithus bijugatus,* present in the other two samples, supports a Zone NP25 assignment.

Sample 182-1130C-6R-CC (357.06 mbsf) contains an impoverished assemblage, although the assemblages in Samples 182-1130A-38X-CC (351.37 mbsf) and 182-1130C-7R-CC (357.06 mbsf) are rich. The latter samples contain the association *B. bigelowii, C. altus, Coronocyclus nitescens, Cyclicargolithus abisectus, C. floridanus, D. bisectus, Discoaster deflandrei* "group," *Helicosphaera euphratis, Helicosphaera intermedia, Helicosphaera obliqua, Helicosphaera recta, Sphenolithus predistentus, Sphenolithus* sp. aff. *Sphenolithus distentus,* and *Z. bijugatus,* which suggests the zonal interval NN25–23.

Chiasmolithus altus is abundant throughout the Oligocene section at Site 1130, indicating a cool-water regime, although the presence of *S. ciperoensis* in Zone NP25 suggests warm-water influence. This supports the conclusion (Shafik, 1990) that a cool-water regime prevailed in the Great Australian Bight during the middle and late Oligocene, although with an intermittent warm-water influence inferred to result from a surface current intermittently bringing warm water from the Indian Ocean. Core-catcher samples examined from the calcareous sandstone

at the bottom of both Holes 1130A and 1130C are barren of calcareous nannofossils.

Planktonic Foraminifers

Sediments recovered at Site 1130 contain planktonic foraminifer assemblages of the Pleistocene, Pliocene, upper Miocene, and Oligocene. Few planktonic foraminifers were detected in the calcareous sandstone from the lower part of Hole 1130B, between 365 and 390 mbsf. On the basis of the standard zonal scheme of Berggren et al. (1995a; 1995b), the Neogene and Oligocene successions are divided into relevant zones or zonal equivalents that can be correlated between sites and to regional biostratigraphy. The Pleistocene–upper Miocene succession appears to be truncated by a disconformity at the lower/upper Pliocene boundary. The disconformity between the upper Miocene and Oligocene represents a break in sedimentation of at least 14 m.y. (Fig. F6).

Pleistocene to Upper Pliocene

Planktonic foraminifers are relatively rare from Cores 182-1130A-1H through 5H and 182-1130B-1H through 5H in sediments dominated by shell debris consisting mainly of bivalves and gastropods. Their abundance increases downhole, comprising 10%–20% of the >63-µm residue, although preservation deteriorates. The faunal succession consists of two main assemblages characterized respectively by *Globorotalia truncatulinoides* and *Globorotalia crassaformis*. The *G. truncatulinoides* assemblage occurs down to ~225 mbsf (Cores 182-1130A-1H to 24X and 182-1130B-1H to 24X), whereas the *G. crassaformis* assemblage extends from this level down to a lithostratigraphic boundary at ~257 mbsf within Cores 182-1130A-28X and 182-1130B-29X (see "Lithostratigraphy," p. 3).

The *G. truncatulinoides* assemblage typifies the Pleistocene zone Pt1 of Berggren et al. (1995a; 1995b) and SN14 of Jenkins (1993) (Fig. F6). It is a cool temperate assemblage that mainly comprises *Globorotalia inflata, G. truncatulinoides, Globigerina bulloides,* and *Globigerinoides ruber.* In the 63- to 150-µm fraction, however, *Globigerina falconensis, Globigerina quinqueloba,* and *Neogloboquadrina pachyderma* are dominant. Minor constituents include *Globigerinoides rubescens, Globigerinoides tenellus, Orbulina universa,* and *Neogloboquadrina dutertrei*. *Globorotalia hirsuta* is recorded downhole to Sample 182-1130A-5H-CC, 9–11 cm (55.95 mbsf). The co-occurrence of typical *Globorotalia tosaensis* and *G. truncatulinoides* from Sample 182-1130A-15H-CC, 22–25 cm (140.32 mbsf), downhole can be used to define Subzone Pt1a.

As observed earlier at Site 1127 (see "Biostratigraphy," p. 9, in the "Site 1127" chapter), the Pleistocene (Pt1) planktonic foraminifer assemblage as a whole is of the southern temperate type (Li et al., in press), and in only a few levels did we observe rare specimens of (sub)tropical species. They include *Globigerinoides sacculifer* s.l. in Samples 182-1130A-3H-CC, 10–12 cm, 5H-CC, 9–11 cm, and 7H-CC, 18–21 cm; *Globorotalia tumida* in Samples 182-1130A-10H-CC, 19–22 cm, and 14H-CC, 17–20 cm; and *Sphaeroidinella dehiscens* in Sample 182-1130A-22X-CC, 35–38 cm. These typical low-latitude species reflect warmer climatic conditions and/or stronger flows of the Leeuwin Current (McGowran et al., 1997a), probably in response to global climatic cycles.

The Pleistocene/Pliocene boundary cannot be positively identified, partly because temperate planktonic foraminifers contain few species suitable for age dating. The boundary in the region has been placed at the FO of *G. truncatulinoides* (Jenkins, 1993; McGowran et al., 1997b). If this traditional measure is applied, the Pleistocene/Pliocene contact lies within Core 182-1130A-24X, where the species first appears. However, this datum level seems to be diachronous: in the uppermost Pliocene (2.0 Ma; Berggren et al., 1995a), or even in the lower part of the upper Pliocene (Hornibrook et al., 1989). At Site 1130, the FO of *G. truncatulinoides* was found at two levels: 224.7 mbsf in Hole 1130A (Sample 182-1130A-24X-CC, 17–20 cm) and 214.03 mbsf in Hole 1130B (Sample 182-1130B-23X-CC, 28–31 cm). The interval encompassing this datum level between the holes is within a paleomagnetic normal zone, probably the Olduvai or older (see **"Paleomagnetism,"** p. 19), and at the base of seismic Sequence 2 (see **"Seismic Stratigraphy,"** p. 30).

Cores 182-1130A-25X through 28X and 182-1130B-25X through 27X contain abundant, poorly preserved globorotaliid planktonic foraminifers, characterizing the tentatively termed "*G. crassaformis* interval" (Fig. **F6**). Together with some species that are common also in the cores above (such as *Globorotalia inflata, Globigerina bulloides,* and *Globigerinoides ruber*), the assemblage is mainly composed of *Globorotalia puncticulata, G. crassaformis,* and *Globorotalia crassula*. It has been also observed from Cores 182-1127A-45X through 50X at Site 1127. The assemblage is similar in composition to the upper Pliocene fauna of New Zealand (Hornibrook et al., 1989). Calcareous nannofossils indicate that this interval is either fully equivalent to the lowermost part of the Pleistocene Zone NN19 (see **"Biostratigraphy,"** p. 9, in the "Site 1127" chapter), or covers parts of Zone NN19 through the upper Pliocene Subzone CN12b (see **"Calcareous Nannofossils,"** p. 11). Further study of the stratigraphy and related foraminifer datum levels is necessary to clarify the age of this interval.

Lower Pliocene and Upper Miocene

Moderately preserved planktonic foraminifers occur in Samples 182-1130A-28X-3, 124–128 cm, through 35X-5, 87–92 cm (258.54–328.57 mbsf). This faunal change coincides with a lithologic change from grayish, glauconite-rich packstones above to light-colored foraminifer nannofossil oozes (see **"Lithostratigraphy,"** p. 3). The assemblage is characterized by *Globorotalia margaritae, Zeaglobogerina nepenthes,* and, in the lower part, by *Globorotalia* cf. *cibaoensis,* indicating early Pliocene to late Miocene age (Berggren et al., 1995a). In Cores 182-1130A-29X to 30X and 182-1130B-29X to 30X, the FO of *G. crassaformis* and *G. puncticulata* was also recorded, although they become more frequent in the *G. crassaformis* interval in cores above. In contrast to those from above, however, *G. crassaformis* is represented mainly by sinistral specimens, similar to the lower Pliocene record from New Zealand (Hornibrook et al., 1989). Their association with upper Miocene taxa, such as *Globorotalia sphericonomiozea,* indicates that the uppermost part of the lower Pliocene is probably either condensed or missing. Therefore, if it is a disconformity, the lower/upper Pliocene contact represents a hiatus of ~1.7 m.y. duration.

Cores 182-1130A-31X through 33X and 182-1130B-31X through 33X contain assemblages more typical of Zones Pl1 and Mt10, as indicated by the coexistence of *Z. nepenthes, G. margaritae, G.* cf. *cibaoensis, Globorotalia conomiozea, Globorotalia plesiotumida,* and *Globorotalia*

conoidea (including *Globorotalia miotumida*), as well as other upper Miocene to Pliocene taxa. The zones are combined at this site because the marker species *G. sphericonomiozea* was recorded, although discontinuously, throughout this interval (~260–310 mbsf). Some specimens resembling this species are also present in Sample 182-1130C-3R-CC, 16–19 cm (323.34 mbsf).

Planktonic foraminifers indicating the upper Miocene Zone Mt9 (upper part) occur in the interval of ~315–328.57 mbsf in Samples 182-1130A-34X-CC, 51–52 cm, 35X-5, 87–92 cm, 182-1130C-2R-CC, 8–11 cm, and 3R-CC, 16–19 cm. Common species include *G. conoidea, G.* cf. *cibaoensis, G. plesiotumida, Z. nepenthes, Z. woodi, Globigerinoides extremus,* and *O. universa* s.l.

According to Berggren et al. (1995a; 1995b), the Pliocene/Miocene boundary lies within Subzone Pl1a. Hornibrook et al. (1989), however, placed it at the FO of *G. crassaformis* in New Zealand, which occurs at 273.71 mbsf in Hole 1130A and at 281.79 mbsf in Hole 1130B. With an estimated age of 4.5 Ma (see **"Planktonic Foraminifers,"** p. 10, in the "Explanatory Notes" chapter), the datum level is 0.75 m.y. younger than the Pliocene/Miocene boundary defined in Berggren et al. (1995a). Pending further studies, we tentatively placed the boundary at ~273 mbsf (Fig. **F6**).

Oligocene

A sharp contact between the upper Miocene sediments in Core 182-1130A-35X and the core-catcher sample represents a hiatus of at least 14 m.y., as indicated by planktonic foraminifers of late Oligocene age found in Sample 182-1130A-35X-CC, 27–30 cm (328.89 mbsf). The assemblage is poorly preserved and contains numerous small *Globigerina praebulloides, Globigerina officinalis, Globorotaloides suteri, Globorotaloides testarugosa,* and tenuitellids, as well as some specimens of *Globigerina euapertura, Globoquadrina venezuelana, Paragloborotalia nana,* and *Globigerina* cf. *ciperoensis*. Further downhole in Samples 182-1130A-38X-CC, 17–20 cm (351.37 mbsf), and 182-1130C-7R-CC, 6–8 cm (356.96 mbsf), these species were found together with *Catapsydrax dissimilis, Zeaglobigerina labiacrassata,* and *Paragloborotalia* cf. *opima,* indicating Zone P21 of the middle Oligocene. The assemblage contains few specimens of *Chiloguembelina cubensis,* a species most common in the lower Oligocene and Eocene of middle to high latitudes (Berggren, 1992; Li et al., 1992).

The Oligocene succession at Site 1130 (328–365 mbsf) contains many chert intervals. The poor core recovery from these intervals yielded no suitable material for planktonic foraminifer study. Calcareous nannofossils, however, indicate that several chert samples are also of Oligocene age (see **"Calcareous Nannofossils,"** p. 11).

Eocene

An orange-brown, porous calcareous sandstone was recovered underlying the Oligocene cherts and wackestones. No planktonic foraminifers were detected at 369.85 mbsf in the single washed core-catcher sample (Sample 182-1130A-40X-CC, 35–37 cm). A thin section (Sample 182-1130A-40X-CC, 5–6 cm) prepared for lithologic analysis contains a few planktonic foraminifer tests resembling *Subbotina linaperta-Subbotina angiporoides* from the middle to upper Eocene. Therefore, the sandstone probably accumulated during the upper Eocene, although post-

cruise studies are needed to clarify this age (see "Lithostratigraphy," p. 3, and "Seismic Stratigraphy," p. 30).

Benthic Foraminifers

Benthic foraminifers were studied from every fourth core-catcher samples in Cores 182-1130A-1H through 21X and from every core-catcher sample below Core 21X. Benthic foraminifers are generally abundant and well preserved at Hole 1130A, except between Cores 23X and 27X, where abundance fluctuates markedly and significant numbers of abraded and corroded tests with glauconite infilling are found in some of the samples examined. No benthic foraminifers were found in the disaggregated core-catcher sample (Sample 182-1130A-40X-CC) from the brown-orange calcareous sandstone recovered at the base of Hole 1130A. However, examination of a thin section (interval 182-1130A-40X-CC, 5–6 cm) revealed that the calcareous matrix contained miliolids and bolivinids, as well as the planktonic foraminifer tests of middle–late Eocene age noted above.

Between 100 and 300 benthic foraminifers were picked from the >63-µm fraction, except in Samples 182-1130A-23X-CC, 25X-CC, and 27X-CC, where abundance was low. The benthic foraminifer assemblages studied include mainly calcareous taxa and only a few species and specimens of agglutinated taxa. They show some similarity to shelf assemblages documented by Li and McGowran (in press) from Lakes Entrance in southeastern Australia. Although many of the species have a cosmopolitan distribution, some of the shelf species within the assemblages probably represent endemic taxa with a more restricted distribution. Further taxonomic studies are needed to clarify the distribution of benthic foraminifers in the Great Australian Bight during the Paleogene and Neogene. Three benthic foraminifer assemblages are recognized in the Cenozoic succession of Hole 1130A, which indicate a shallowing-upward trend from middle bathyal paleodepths in the upper Oligocene to upper bathyal paleodepths in the Pleistocene.

Assemblage 1 (Pleistocene)

Cores 182-1130A-1H through 27X

This Pleistocene assemblage is characterized by fluctuating abundances of Triloculina spp., *Spiroloculin*a spp., *Quinqueloculina* spp., *Elphidium* spp., *Bolivina* spp., *Loxostomum* spp., *Loxostomoides* spp., and *Uvigerina hispidicostata*. Also present as rare to few constituents of the assemblage are *Patellina corrugata, Spirillina* spp., *Sigmoilopsis schlumbergeri, Neolenticulina peregrina, Hoeglundina elegans, Heterolepa dutemplei, Uvigerina hispida, Planulina wuellerstorfi, Sphaeroidina bulloides, Cancris auriculus, Bulimina marginata, Siphonina australis, Anomalinoides* spp., *Textularia* spp., *Trifarina* spp., *Nodogenerina* spp., *Fissurina* spp., *Cibicidoides* spp., *Palliolatella* spp., *Pyrgo* spp., *Sigmoilina* spp., *Rosalina* spp., *Glandulina* spp., *Ehrenbergina* sp., and various nodosariids. In some samples, the assemblage is dominated by small specimens (63–150 µm) of taxa typical of inner to middle neritic environments (*Triloculina* spp., *Spiroloculina* spp., *Elphidium* spp., *Quinqueloculina* spp., and *Patellina* spp.). This suggests that a large proportion of the tests within these samples originated from the adjacent shelf, before being sorted and redeposited further offshore. Upper bathyal paleodepths are otherwise indicated by the presence of the depth-sensitive species *Sigmoilopsis schlumbergeri, Hoeglundina elegans, H. dutemplei, Uvigerina proboscidea,*

and *S. bulloides*. Fluctuations in the relative proportions of redeposited neritic taxa within the samples may relate to changes in climate, sea level, and oceanic circulation during the Pleistocene (McGowran et al., 1997a). However, high-resolution studies are needed to resolve the changes in benthic foraminifer distribution patterns and to integrate them within a sequence stratigraphic framework.

Site 1130 is situated ~50 km west of Site 1127, at comparable water depths. Expanded Pleistocene sedimentary successions were recovered at these two sites, although sedimentation rates were significantly lower at Site 1130 than at Site 1127 (see Fig. **F7,** p. 37, and Fig. **F6,** p. 36, in the "Site 1127" chapter). Although the Pleistocene benthic foraminifer assemblages at these two sites show close similarity in composition, the assemblage at Site 1127 contains a greater proportion of small, reworked tests than the coeval assemblage at Site 1130 and does not exhibit such marked fluctuations in composition. Variations in assemblage composition and in sediment accumulation rates at the two sites probably reflect different hydrographic regimes at these two upper slope settings during the Pleistocene.

Assemblage 2 (Early Pliocene–Late Miocene)

Cores 182-1130A-28H through 34X

The FO of Assemblage 2 coincides with the marked lithologic change from glauconite-rich, bioclastic packstones to nannofossil foraminifer oozes in Core 182-1130A-28X (see **"Lithostratigraphy,"** p. 3). Assemblage 2 is characterized by the few to common occurrence of *H. dutemplei, Stilostomella* spp., and *Loxostomum* spp. Also present are *U. hispidicostata, U. proboscidea, Bulimina marginata, Globocassidulina subglobosa, P. wuellerstorfi, Oridorsalis umbonatus, Laticarinina pauperata, Eggerella bradyi, Martinottiella communis, S. bulloides, Anomalinoides globulosus, Vulvulina spinosa, Osangularia* spp., *Pyrgo* spp., *Siphonina* spp., *Cibicidoides* spp., *Trifarina* spp., *Bolivina* spp., and various nodosariids. Abundance is generally low and there is no strong evidence of preferential test size sorting within the assemblage. Middle bathyal paleodepths are suggested by the presence of the depth-indicative species *L. pauperata, Globocassidulina subglobosa,* and *Eggerella bradyi*. Assemblage 2 differs markedly in composition from the Miocene benthic foraminifer assemblage identified at Site 1127, which was indicative of upper bathyal paleodepths, but also contained a significant proportion of reworked neritic taxa.

Assemblage 3 (Late Oligocene)

Cores 182-1130A-35X through 38X

A major lithologic change from nannofossil foraminiferal ooze to chert occurs at ~328 mbsf. This change coincides with a major unconformity, spanning ~14 m.y. between the upper Miocene and upper Oligocene (see **"Calcareous Nannofossils,"** p. 11, and **"Planktonic Foraminifers,"** p. 14). The benthic foraminifer assemblage within this interval of poor core recovery is characterized by numerous, relatively well-preserved, small tests of *Bolivina* spp., *Trifarina* spp., and *Stilostomella* spp. Also present as rare to few constituents of the assemblage are *Globocassidulina subglobosa, Cibicidoides laurisae, V. spinosa, Siphonina tenuicarinata,* and *Cibicidoides* spp. Middle bathyal paleodepths are suggested for this assemblage by the presence of *Cibicidoides laurisae,* a

predominantly middle bathyal to abyssal species (van Morkhoven et al., 1986), and by the absence of deeper bathymetric indicators. *Cibicidoides laurisae* is also a stratigraphically significant species within this interval, with a stratigraphic range extending from the middle Eocene (P10) to the upper Oligocene (P22), according to van Morkhoven et al. (1986).

Sedimentation Rates

Sediment accumulation rates shown in Figure F7 were calculated from preliminary biostratigraphic and paleomagnetic results (see "Paleomagnetism," p. 19). The onset of the Brunhes Chron was identified with confidence, but the onsets and terminations of the Jaramillo and Olduvai Subchrons are less certain (see "Paleomagnetism," p. 19). The paleomagnetic datum levels are generally consistent with the biostratigraphic datum levels. The biostratigraphic datum levels and relevant paleomagnetic data used to calculate sedimentation rates are listed in Table T2.

A very high sedimentation rate, between 240 and 260 m/m.y., is calculated for the greater part of the Pleistocene section. In contrast, the rates recorded below the Brunhes/Matuyama boundary are significantly lower, between 15 and 20 m/m.y. The Pliocene record is punctuated at ~258 mbsf by a hiatus of ~1 m.y. duration. This is clearly delineated by the simultaneous LOs of the nannofossil species *Amaurolithus* and *Sphenolithus,* as well as *R. pseudoumbilicus*. However, the most spectacular hiatus recorded at Site 1130 is at the Neogene/Paleogene boundary, from which the entire lower Miocene–lower upper Miocene succession is missing. The duration of this hiatus is ~14 m.y.

The middle–upper Oligocene section registered relatively low sedimentation rate of 10–30 m/m.y. At Site 1128, by comparison, sedimentation rates of 50–60 m/m.y. were recorded for the lower–middle Oligocene section (see "Sedimentation Rates," p. 22, in the "Site 1128" chapter).

F7. Sedimentation rate curve from datum levels for Site 1130, p. 42.

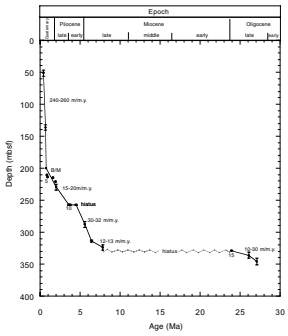

T2. Datum levels used in the graph of sedimentation rate, p. 74.

PALEOMAGNETISM

All cores from Holes 1130A and 1130B with sufficient recovery to make long-core measurements feasible were measured as half cores using the 2-G 760-R magnetometer. Measurements were made of natural remanent magnetization (NRM) and after 20-mT demagnetization. The experimental nonmagnetic shoe was used for odd-numbered cores in Hole 1130A from Core 182-1130A-3H to 7H, and the experimental nonmagnetic APC core barrel assembly, which was also used at Site 1128, was again used for the odd-numbered cores from Core 182-1130B-3H to 7H. The nonmagnetic shoe and the core barrel assembly both made reductions in the "radial" component contamination, although the effects were not as dramatic as at Site 1128 (see "Appendix: Magnetics Experiment"). Discrete samples were taken from both soft sediments cored by the APC and from biscuits in the XCB and RCB cores for NRM and rock magnetic analysis. The analyses were performed using the methods described in "Paleomagnetism," p. 19, in the "Explanatory Notes" chapter.

Long-Core Measurements

The long-core measurements revealed an extensive record of normal magnetization and a sharp switch to reverse polarity at 200 mbsf in both Holes 1130A and 1130B. Below this was ~10 m of reversed polarity, and then mixed polarities were found. Intensities of magnetization varied from 0.01 to 1 mA/m with an overall decreasing trend throughout the core. Superposed on this decreasing trend are higher frequency fluctuations with dominant wavelengths of a few tens of meters (Fig. F8). The overall decreasing trend is consistent with dissolution of the fine-grained magnetite that carries the bulk of the paleomagnetic record. Toward 350 mbsf, the intensity approaches the noise level of the 2-G 760-R. Fluctuations in intensity are similar to those seen at Site 1127, although they do not show the same correlation with field intensity fluctuations. They are, however, accompanied by inclination features with comparable wavelength.

F8. Paleomagnetic intensity of magnetization and magnetic susceptibility downhole, Hole 1130A, p. 43.

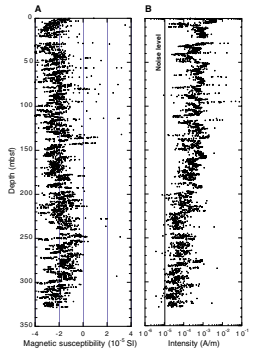

Discrete Samples

Discrete samples were taken for demagnetization analysis of the NRM and for rock magnetic investigations. Zijderveld plots from APC and XCB cores yielded high-quality plots with good convergence to the origin over the major part of the demagnetization and well-determined characteristic directions of magnetization (Fig. F9). However, other samples from deeper in the hole were noisy, and the magnetization directions were less well determined.

Rock magnetic analysis revealed interesting downhole trends in the magnetic material. As noted above, the intensity of magnetization decreases with depth downhole. The ratio of anhysteretic remanent magnetization (ARM) to isothermal remanent magnetization (IRM), which is a measure of the relative importance of single-domain to multidomain behavior, decreases downcore (Fig. F10). This indicates that the role of biogenic magnetite is reduced downhole and, because this corresponds to a decrease in magnetization, it strongly suggests that the fine magnetite of biogenic origin is undergoing preferential dissolution.

F9. Demagnetization analysis for Sample 1130A-9H-5, 51–53 cm, p. 44.

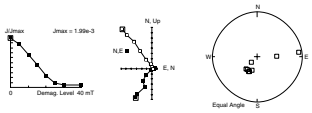

F10. Plots of demagnetization of NRM, ARM, and IRMs and of the acquisition of IRM for samples from Hole 1130A, p. 45.

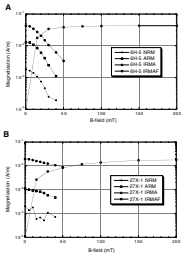

Susceptibility

Magnetic susceptibility from multisensor track (MST) measurements is shown in Figure F8. These data do not display any downhole trend comparable to the magnetization intensity trend. However, a decrease in the negative, diamagnetic-dominated susceptibility values between 200 and 320 mbsf is consistent with increased multidomain magnetite at this depth.

Magnetostratigraphy

The Brunhes/Matuyama boundary is very clearly seen in both Hole 1130A and Hole 1130B at 200 mbsf (Fig. F11). It occurs at Section 1130A-22X-3, 30 cm, and at Section 1130B-22X-4, 70 cm. These depths then yield sedimentation rates of 255 m/m.y. The depth of reversed magnetization below is only between 10 and 15 m before dominantly normal magnetizations occur again. This is too short a length of core to represent the ~200,000 yr between the Brunhes/Matuyama reversal and the termination of the Jaramillo; thus, there must either be a major change in sedimentation rate or missing sediment. Tentative depth as-

F11. Magnetostratigraphy of Holes 1130A and 1130B, p. 46.

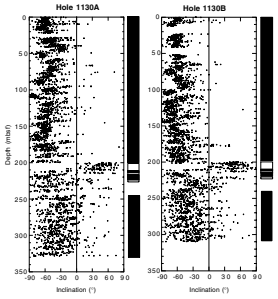

signments have been made for the Jaramillo and Olduvai but require testing with onshore analysis. Below this, no useful magnetostratigraphy could be established.

COMPOSITE DEPTHS

Introduction

Construction of the composite and spliced section from Holes 1130A and 1130B followed the methods outlined in **"Composite Depths,"** p. 14, in the "Explanatory Notes" chapter. Table **T3** (also in **ASCII format**) relates mbsf to meters composite depth (mcd) for each core and section at Holes 1130A and 1130B and provides offset values for the conversion of mbsf to mcd. The composite section indicates that a nearly complete record of the Pleistocene–upper Miocene sedimentary section was recovered at Site 1130.

T3. Site 1130 core and section depths in mcd and mbsf, **p. 75.**

Data Input

The primary lithologic parameters used to create the composite section were NGR emissions data collected by the MST on whole-round cores and a ratio of the 700- to 400-nm color reflectance data measured on split cores (Fig. **F12**). The 700- and 400-nm color reflectance data were also used individually but proved not to be as effective as the 700:400 ratio. Gamma-ray attenuation (GRA) bulk density and *P*-wave velocity data collected by the MST were disturbed by voids within the cores and were, therefore, not used for correlation purposes. Magnetic susceptibility was also not used for correlation because of a low signal-to-noise ratio. For specifics regarding data collection procedures and parameters, see **"Physical Properties,"** p. 25.

Biostratigraphic data aided in correlation by providing additional datums that were compared between holes (Table **T4;** see **"Biostratigraphy,"** p. 10). Planktonic foraminifers were particularly useful in constraining correlative intervals of the recovered section. Because most biostratigraphic samples were taken from core catchers, the stratigraphic error associated with a particular datum is generally on the order of 10 m (the distance between core catchers in consecutive cores). The position of the last appearance datum (LAD) of *G. tosaensis* ties the base of Core 182-1130A-15H to the top of Core 182-1130B-16H and implies an age of ~0.65 Ma (or older) for this interval. Overlap of the *G. truncatulinoides* first appearance datum ties the top of Core 182-1130A-25X and the bottom of Core 182-1130B-24X and constrains the age of this interval to ~2 Ma (or younger). The LAD of *Z. nepenthes* overlaps and ties the base of Core 182-1130A-29X to the top of Core 182-1130B-30X and implies an age of ~4.2 Ma for this stratigraphic interval (Table **T4**).

F12. Composite depth section produced using Splicer software, **p. 47.**

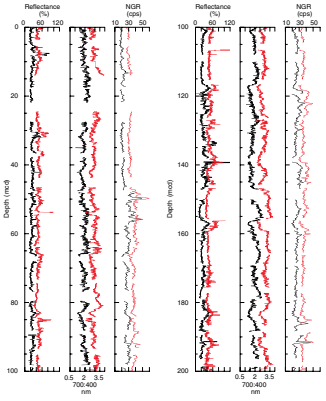

T4. Site 1130 biostratigraphic data used for correlations, **p. 82.**

Composite Section Construction

The primary difficulties encountered in the correlation of Holes 1130A and 1130B were dissimilarities in the data records between the holes, which resulted partly from core distortion and partly from actual, though minor, lithologic variations between holes. Color reflectance data correlate poorly using small-scale (<1 m) features, most likely because of the relative homogeneity of the sediments on these scales (uniform packstones over much of the section; see **"Lithostratigra-**

phy," p. 3). Larger scale (>1 m) distinctive events are infrequent in the single-band color reflectance data. At several places, the data are interrupted by an erroneous shift to much higher values that do not correspond to any lithologic variation but, rather, are a result of an error in the output of the color reflectance scanner. To circumvent these problems, a ratio of the 700:400 nm color reflectance data was used with great success. The ratio data exhibit less noise and reveal more distinctive events that were more easily correlated between holes than simply using a single color reflectance band. Core overlap between holes averaged ~2–3 m where recovery was high and allowed for a statistical evaluation of ties used to create the composite section.

The upper 139 mcd (132 mbsf) are late Pleistocene in age, based upon biostratigraphic data (Fig. F13). The data record in this stratigraphic range is divided into one lithostratigraphic unit and two physical properties units. Physical properties Unit (PP Unit) 1 (above 47 mcd) was difficult to correlate, as data exhibit low-amplitude oscillations over long wavelengths with few clearly distinctive events. Below PP Unit 1, data (color reflectance ratio) exhibit higher amplitude oscillations with more distinctive characteristics that are more easily recognized between holes. At ~180 mcd, the data clearly change to higher frequency but lower amplitude oscillations that correlate well between holes. This characteristic signal is maintained to 252 mcd, the Pleistocene/Pliocene boundary. The upper Pliocene section is characterized by a 20-m-thick, uniform packstone in 1130B, which is interrupted by a nannofossil ooze in Hole 1130A. This packstone exhibits very low reflectance values (30%–40%) in the 700- and 400-nm ranges, but a high 700:400 nm ratio (1.75–2.5). The characteristics of this lower Pliocene bed are correlative between holes and easily distinguished from the overlying Pleistocene strata and underlying lower Pliocene strata. Below this unique bed, beginning at ~275 mcd, the data change character again to low-amplitude oscillations with very few easily correlated distinctive events (lithostratigraphic Unit II; upper Miocene–lower Pliocene). These relatively uniform data are maintained to the base of Core 182-1130B-35X (327.70 mbsf; 342.29 mcd), the last core analyzed by the MST.

The composite section indicates the existence of several unrecovered intervals in the record (Fig. F12). Low recovery in Core 182-1130A-3H and no recovery in Core 182-1130B-3H produced a gap in the record at 22–24 mbsf. The record below this is apparently continuous to ~188 mcd (Table T5, also in ASCII format). Below 188 mcd there are a number of gaps in the record resulting from the loss of overlap between cores in adjacent holes and requiring cores to be appended to the splice rather than tied. The mcd scale expansion relative to the mbsf scale is ~6%.

An initial age model was produced using the biostratigraphic datums (Table T4). The 700:400 nm reflectance data were tuned to a composite seawater $\delta^{18}O$ curve (Raymo et al., 1989; Shackleton et al., 1990; Shackleton et al., 1995) using the initial age model as a constraint. Results of the tuning were positive, with good agreement with paleomagnetic and biostratigraphic data to ~0.7 Ma, and indicate that the variability apparent in color reflectance data are probably of Milankovitch-scale cyclicity in the Pleistocene section (Fig. F14).

F13. Spliced section of smoothed color reflectance data produced using Splicer software, p. 49.

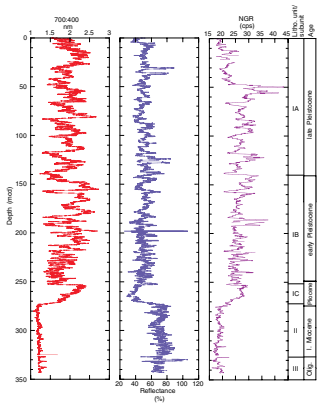

T5. Site 1130 splice tie points, p. 83.

F14. Spliced and tuned color reflectance record compared to the Site 656 composite seawater $\delta^{18}O$ curve, p. 50.

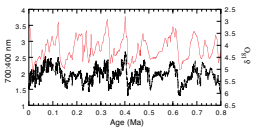

ORGANIC GEOCHEMISTRY

At Site 1130, in addition to routine monitoring of hydrocarbon gases for safety, inorganic carbon (IC) analyses were made. The analytical procedures are described in "Organic Geochemistry," p. 16, in the "Explanatory Notes" chapter.

Volatile Hydrocarbons and Hydrogen Sulfide

Concentrations of volatile hydrocarbons were routinely determined in every core from Holes 1130A and 1130C using standard ODP headspace sampling procedures. Only low concentrations of methane were detected; the maximum concentration was 11.3 ppm and most samples have <7 ppm (Table T6). No heavier hydrocarbon gases (C_{2+}) were detected.

Hydrogen sulfide (H_2S) was detected in headspace samples from 13 to 126.7 mbsf and was much lower in concentration than at Sites 1127, 1129, and 1131. The maximum concentration (3800 ppmv) was observed at 41.50 mbsf.

Inorganic and Organic Carbon, Sulfur, and Nitrogen

Inorganic carbon concentrations were converted to calcium carbonate percentages (see "Organic Geochemistry," p. 16, in the "Explanatory Notes" chapter). Calcium carbonate content in Hole 1130A ranges from 80.9 to 93.2 wt%, with most samples having 85 to 90 wt% (Table T7; Fig. F15).

Concentrations of methane in the headspace samples at Site 1130 were only slightly above background level.

INORGANIC GEOCHEMISTRY

Interstitial Waters

Interstitial water samples from Hole 1130A were taken at a rate of one per core for the first 15 cores and one every other core thereafter, recovery permitting. No samples were taken from Hole 1130B, and only one sample was taken from Hole 1130C. Samples were analyzed according to the procedures outlined in "Inorganic Geochemistry," p. 18, in the "Explanatory Notes" chapter. The data are presented in Table T8 and Figures F16, F17, F18, and F19.

Salinity and Chlorinity

Salinity values increase rapidly below the third core, reaching 82 in Core 182-1130A-5H (41.4 mbsf), and remain stable to the base of the cored interval (Fig. F16). Chlorinity shows the same rapid increase from values close to those of normal seawater to 1323 mM at 41.4 mbsf. Below this depth, values remain relatively constant (Fig. F16). We interpret the increase in salinity and chlorinity as a result of the presence of a saline brine within and below the cored interval (see "Discussion," p. 25).

T6. Headspace gases, p. 84.

T7. Calcium carbonate content, p. 85.

F15. Calcium carbonate content in samples from Site 1130, p. 51.

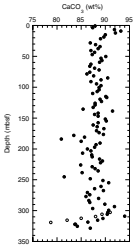

T8. Interstitial water geochemistry, p. 86.

F16. Concentration depth profiles of salinity, Cl^-, K^+, Ca^{2+}, Mg^{2+}, and Sr^{2+}, p. 52.

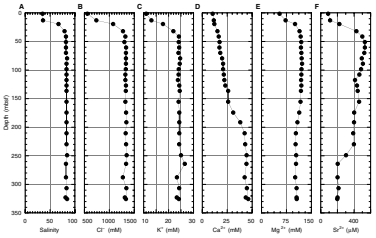

F17. Concentration depth profiles of Li^+, SO_4^{2-}, H_4SiO_4, NH_4^+, Fe^{2+}, and pH, p. 53.

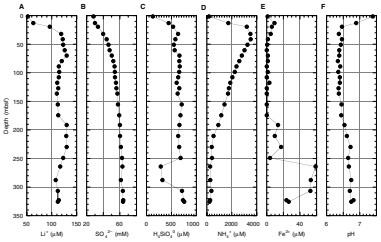

Calcium, Magnesium, Potassium, Lithium, Silica, Strontium, and Iron

The concentration of Ca^{2+} increases from 10.5 to 26.0 mM within the upper 136.4 mbsf (Fig. F16). Between 174.4 and 210.6 mbsf, the rate of Ca^{2+} change increases, reaching a relatively stable concentration between 210.6 and 321.4 mbsf. The increase is a result of the increasing influence of the brine noted previously. The concentration of Ca^{2+} relative to Cl^- is lower than that of seawater to a depth of 155.4 mbsf (Fig. F18). This depletion is caused by the precipitation of carbonate, triggered by increased alkalinity. Below a depth of 155.4 mbsf, excess Ca^{2+} indicates net dissolution of carbonate. As is the case with Ca^{2+}, the Mg^{2+} concentration increases from 54.1 to 119.0 mM as a result of the increasing influence of the underlying brine. However, Mg^{2+} concentration decreases slightly to 105.0 mM at 321.4 mbsf (Fig. F16). This is even more apparent for the excess Mg^{2+} concentration shown in Figure F18 and is probably caused by the precipitation of dolomite. Note, however, that even a complete Mg^{2+} depletion of the interstitial water would only result in the precipitation of minor amounts of dolomite (Swart and Guzikowski, 1988). The concentration of K^+ increases from 11.1 to 23.3 mM at 321.4 mbsf (Fig. F16). The increase is caused entirely by the increase in salinity, and the K^+/Cl^- ratio remains close to that of seawater throughout. The Sr^{2+} concentration reaches a maximum of 530 µM at 50.9 mbsf, gradually decreasing to 198 µM at 326.1 mbsf (Fig. F16; see "Discussion," p. 25). The Li^+/Cl^- ratio shows a highly variable signal, roughly coincident with changes in lithology (see "Lithostratigraphy," p. 3). Silica shows an almost fourfold increase (128 to 633 µM) within the upper 27 mbsf, maintaining values between 580 and 758 µM, until a marked decrease to values as low as 284 µM between 249 and 287.5 mbsf (Fig. F17). The observed variations are probably caused by variations in the silica content of the sediment. This is particularly evident for the interval between 263.6 and 302.1 mbsf where the silica values decrease by ~50%, and the sediment type changes from a bioclastic packstone to a nannofossil ooze (lithostratigraphic Unit II; see "Lithostratigraphy," p. 3). The concentration of Fe^{2+} increases from values below the detection limit to 7.8 µM at 13.0 mbsf. As a result of the presence of H_2S, which causes Fe^{2+} to precipitate as iron sulfides, Fe^{2+} concentration decreases with depth and is lower than the detection limit below 60.4 mbsf. With the exception of some scatter in the data, possibly related to contamination, Fe^{2+} concentrations remain low until 174.4 mbsf. With decreasing H_2S content in pore water, Fe^{2+} concentration increases below 174.4 mbsf and reaches a maximum of 58.81 µM at 268.3 mbsf (Fig. F17).

Sulfate, Alkalinity, Ammonium, and pH

As a result of the influence of the underlying brine, the concentration of SO_4^{2-} increases steadily with depth and reaches a maximum of 64 mM at 321.4 mbsf (Fig. F17). This increase is slower than the increase in salinity, which indicates sulfate reduction is occurring. As a by-product of organic matter decomposition within the sulfate reduction zone, the concentration of NH_4^+ increases from 171 µM to 3508 µM at 41.4 mbsf. Below this depth, the concentration of NH_4^+ steadily decreases to 257 µM at 321.4 mbsf (Fig. F17). The pH declines from 7.4

F18. Concentration depth profiles of alkalinity, Ca^{2+}, Mg^{2+}, silica, lithium, p. 54.

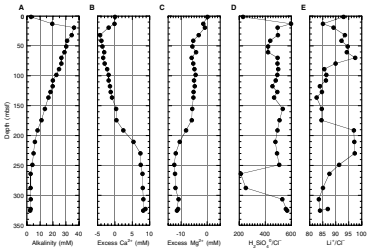

at 4.5 mbsf to 6.4 at 27.5 mbsf, remains almost constant until 132 mbsf, and increases slightly thereafter (Fig. F17).

Discussion

Sulfate reduction at Site 1130 is approximately one-third that of Site 1127 (see "Inorganic Geochemistry," p. 19, in the "Site 1127" chapter). Because both sites have an abundant supply of SO_4^{2-} from the underlying brine, the difference is probably a result of variations in the initial organic carbon content of the sediment (see "Organic Geochemistry," p. 23). As a consequence of the lower sulfate reduction activity, alkalinity values are also lower (Fig. F17; see "Inorganic Geochemistry," p. 19, in the "Site 1127" chapter) and less carbonate precipitation occurs (4.2 mM Ca^{2+} depletion, compared to 8.8 mM at Site 1127). Furthermore, the SO_4^{2-} concentration is never lower than that of seawater, and interstitial waters are saturated with respect to $SrSO_4$, thus limiting Sr^{2+} pore-water concentrations (Fig. F18).

The most striking feature of the pore-water chemistry at Site 1130 is the steep salinity gradient of 5.7/m, which compresses the interface between pore waters with normal seawater salinity and the brine into a zone between 13.0 and 31.9 mbsf. By comparison, Site 1126, which yielded the highest salinity values of Leg 182 (106 at 153.8 mbsf; see "Inorganic Geochemistry," p. 30, in the "Site 1126" chapter), had a salinity/depth gradient of 1.7/m. Despite the steep gradient, salinity reaches only a maximum value of 82. Furthermore, salinity values remain constant, within the error limits, below 41.4 mbsf. The steep gradient, as well as the constant salinity concentrations below 41.4 mbsf (Fig. F16), suggests nonsteady-state conditions.

X-Ray Mineralogy

The mineralogy of the Pleistocene section at Site 1130 is characterized by variations between low-Mg calcite (LMC) and high-Mg calcite (HMC), whereas dolomite, aragonite, and quartz show only minor variations (Table T9, also in ASCII Format; Fig. F19). Although the upper part of the section is dominated by HMC, LMC becomes increasingly dominant with depth, and almost no HMC is observed below the Pliocene/Pleistocene boundary at 230 mbsf (see "Biostratigraphy," p. 10). Below the Pliocene/Pleistocene boundary, aragonite shows its first marked decrease. Variations in the abundance of dolomite may relate to dolomite formation during periods of nondeposition and/or periods of high sea level, such as at the present time, when Mg^{2+} is supplied through diffusion.

PHYSICAL PROPERTIES

Introduction

Measurements of physical properties at Site 1130 followed the procedures outlined in "Physical Properties," p. 19, in the "Explanatory Notes" chapter. These included nondestructive measurements of *P*-wave velocity (PWL) (every 4 cm; Table T10, also in ASCII format), GRA bulk density (every 4 cm; Table T11, also in ASCII format), magnetic susceptibility (MS) (every 8 cm; Table T12, also in ASCII format), and NGR (every 16 cm; Table T13, also in ASCII format) using the MST. The PWL

T9. XRD data, p. 87.

F19. Variations in mineral concentrations, p. 55.

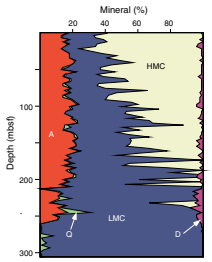

T10. *P*-wave velocity measurements, p. 89.

T11. GRA densiometry measurements, p. 90.

T12. Magnetic susceptibility measurements, p. 91.

T13. Natural gamma-ray measurements, p. 92.

was activated only on APC cores. Thermal conductivity was measured in unconsolidated sediment at a frequency of one per core (Table T14, also in ASCII format), increasing to three samples per core after deployment of the Adara and DVTP tools. A minimum of two discrete *P*-wave velocity measurements (PWS) per section were made on the working half of the split cores (Table T15, also in ASCII format). Measurement frequency was increased to five per section after the PWL was turned off. Standard index properties (Table T16, also in ASCII format) and undrained shear strength were measured at a frequency of one per section in unconsolidated sediments (Table T17, also in ASCII format). Difficulties occurred with the pycnometer used for determination of dry volume. For index properties measurements, see "Index Properties," p. 21, in the "Explanatory Notes" chapter.

The following sections describe the downhole variations in sediment physical properties and their relationships to lithology and downhole logging measurements. Variations in MS are described within "Paleomagnetism," p. 19.

T14. Thermal conductivity measurements, p. 93.

T15. Discrete *P*-wave velocity measurements, p. 94.

T16. Index properties measurements, p. 95.

T17. Undrained shear strength measurements, p. 96.

Index Properties, *P*-wave Velocity, Natural Gamma Radiation, and GRA Densiometry

Sediment physical properties data at Site 1130 reflect the homogeneous nature of the recovered sediments. In contrast to Sites 1129 and 1131, Site 1130 has relatively low concentrations of methane and H_2S, and PWL velocities were the only data set that showed interference caused by sediment degassing. The small voids and airspaces resulting from degassing caused interference in transmission of the sonic signal and unacceptable variability in the data set.

Physical properties data can be divided into three units on the basis of trends in the measured parameters. Physical properties Unit 1 (0–43 mbsf) is characterized by increasing NGR values with a sharp increase at the lower boundary of Unit 1. Porosity decreases sharply throughout the unit (55% to 30%; Fig. F20). Physical properties Unit 1 correlates well with increasing pore-water salinity, potassium, and strontium concentrations, indicating active sediment diagenesis (see "Inorganic Geochemistry," p. 23). *P*-wave velocity increases within PP Unit 1 from 1.5 to 1.7 km/s. An offset to higher values is seen between the PWS3 data because of compression-induced increases in *P*-wave velocity during analysis with the PWS3 probe (see "Sonic Velocity," p. 23, in the "Explanatory Notes" chapter). Bulk density shows a steady increase within PP Unit 1 from 1.5 to 1.6 g/cm³ (Fig. F20).

Velocities of *P*-wave within PP Unit 2 (43–254 mbsf) remain constant near 1.75 km/s (Fig. F20). Bulk density increases slightly throughout the unit from 1.7 to 2 g/cm³, whereas porosity remains relatively constant (32%–37%) (Fig. F20). The increases in *P*-wave velocity and bulk density are likely to be a response to lithostatic compaction. The most intriguing result from PP Unit 2 is the cyclic variability in NGR data (Fig. F20). These variations are well correlated to changes in color reflectance and are likely to be driven by changes in the carbonate/terrigenous sediment ratio. The lower boundary of PP Unit 2 (254 mbsf; Fig. F20) is characterized by a marked drop in NGR (20–<10 cps). This boundary correlates with the lower boundary of lithostratigraphic Unit I, corresponding to a sediment change from packstone to nannofossil ooze (see "Lithostratigraphy," p. 3).

F20. Discrete *P*-wave velocities, bulk densities, porosity, magnetic susceptibility, and NGR measurements, p. 56.

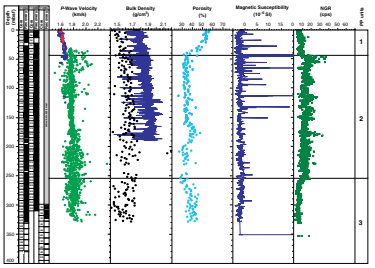

Physical properties Unit 3 (254–330 mbsf) is characterized by low NGR (<10 cps), an increase in porosity (~30%–40%), and bulk density values between 1.4 and 1.75 km/s (Fig. F20). *P*-wave velocity data show no change from PP Unit 2 to PP Unit 3. Poor recovery precludes recognition of further PP units below 330 mbsf.

Correlation of Physical Properties and Downhole Logging Data

The trends in NGR values from both whole-core and downhole logging measurements are well correlated, although downhole values are greater (Fig. F21). This supports the integrity of both data sets. Moisture and density and GRA data are consistently lower than downhole logging density data (Fig. F21). This difference results from the fact that in situ density includes the influence of sediment overburden and hydrostatic pressure, whereas the laboratory measurements do not. A similar effect is seen in the *P*-wave velocities, particularly deeper than 140 mbsf, where in situ velocities are higher than those measured on discrete samples. Log data confirm the location of the boundary at 254 mbsf, as similar shifts are seen in both data sets (Fig. F21).

Shear Strength

Undrained peak and residual shear strength were measured on unconsolidated sediments from 0 to 180 mbsf (Fig. F22; Table T17). Shear strength at Site 1130 increases linearly with depth (0–40 kPa), with peaks in the data corresponding to more indurated portions of the sedimentary section. Shear-strength variability increases downhole. In part, this is a result of differences in lithification, but it may also result from drilling disturbance or cracking of the sediment before failure.

Thermal Conductivity

Thermal conductivity values from Site 1130 range from 0.8 to 1.38 W/(m·K) (Fig. F23; Table T14). In general, thermal conductivity data increase with depth (0–254 mbsf) and correlate best with bulk density and discrete *P*-wave velocity (Fig. F23). The increase in thermal conductivity is primarily caused by lithostatic compaction and the resulting increase in bulk density. Thermal conductivity decreases below 270 mbsf (1.4–1.0 W/[m·K]) because of a lithologic change below the PP Unit 2/Unit 3 boundary.

In Situ Temperature Measurements

Four in situ temperature measurements were made at Site 1130: three using the Adara tool and one using the DVTP (Fig. F24). A good linear fit can be obtained ($r^2 = 0.95$, $N = 10$) if the lower estimates of mudline temperature are used. The geothermal gradient derived from this regression is 35° ± 3°C/km. As a result of the increase in thermal conductivity with depth, the geometric mean of the interval 0–150 mbsf was used for the determination of heat flow (0.968 ± 0.069 W/[m·K]). Using this value and the geothermal gradient determined above, heat flow is estimated at 33.9 mW/m².

F21. Downhole logging data and physical properties measurements, p. 57.

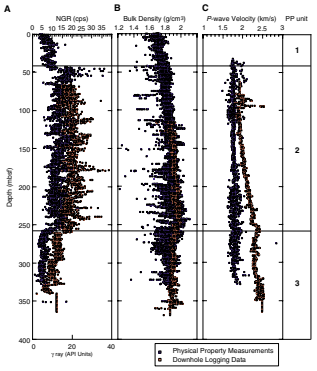

F22. Shear strength measurements, p. 58.

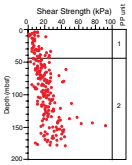

F23. Thermal conductivity measurements, p. 59.

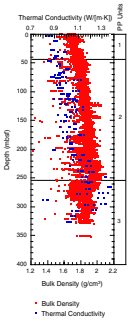

F24. Variation of in situ formation temperature with depth, p. 60.

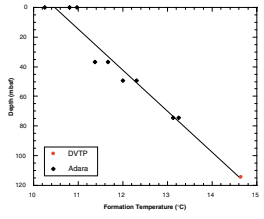

DOWNHOLE MEASUREMENTS

Logging Operations

To free the pipe at the conclusion of drilling at Hole 1130C, the bit was released and, accordingly, no wiper trip was possible before logging. Hole preparation was limited to circulating with seawater. The lower limit of the BHA was placed at 108 mbsf. The WHC was used throughout logging and generally coped well with the moderate heave conditions.

Three different logging strings were deployed in the following order: (1) triple combo, (2) FMS/sonic, and (3) WST (Table T18; see "Downhole Measurements," p. 25, in the "Explanatory Notes" chapter). To increase the maximum depth of logging with the triple combo, and thereby increase the chances of logging across the carbonate/siliciclastic boundary at the base of the hole, the Lamont-Doherty Earth Observatory high-resolution temperature/acceleration/pressure tool was not deployed. Three passes with the triple combo were made. The first was a short quality-control run from 239.5 to 179.5 mbsf, with the accelerator porosity sonde (APS) switched off. A main pass was initiated at the base of the hole (371.5 mbsf); however, the WHC failed because of overheating caused by a water-pump failure when the triple combo was ~20 m off bottom. As a result, the WHC had to be closed down. The logging speed was then doubled to 550 m/hr to protect the tools, and the hole was logged to mudline without the WHC. A second full run of the triple combo with the WHC working was made from 322.5 mbsf to the mudline. Two passes of the FMS/sonic were made at Site 1130. The first pass was from 368.5 to 152.5 mbsf. For the second FMS run, the BHA was raised by 10 m, and the hole was logged from 367.5 to 132.5 mbsf. Eight check-shot stations (stacks of seven shots), spaced ~30 m apart, were recorded with the WST between 358 and 140 mbsf, adjacent to significant boundaries indicated by acquired logs and potential seismic sequence boundaries. As a result of the shallow water depth, the generator-injector (GI) gun pressure was lowered to the minimum level of 600 psi to avoid saturating the WST geophone.

T18. Tool strings, intervals logged, and logging speeds for Hole 1130C, p. 97.

Data Quality

Conditions in Hole 1130C were good, despite the minimal hole preparation. The borehole diameter indicated by the caliper log identified only slight rugosity, with a maximum diameter of ~38 cm in the interval from 300 to 335 mbsf (Figs. F25, F26). Data from the first pass of the triple combo was of poor quality above 342.5 mbsf as a result of the high logging speed and significant tool heave after the WHC failed. The second pass with the operational WHC and normal logging speed produced good quality data in the open-hole interval between 322.5 mbsf and 107 mbsf. Neutron loading of the formation by the APS from the first triple combo significantly degraded gamma-ray measurements through pipe during the second pass, but not in the open-hole interval. The uniform hole diameter produced good quality FMS logs on both passes, with heave effects largely removed by shipboard processing. The sonic log was of high quality, even for the analog channels. Check-shot data were generally of good quality, although the last four stations clipped slightly on the first arrival, despite the GI being run at minimum pressure. The low gun pressure reduced the bubble-suppression benefits of the GI gun, causing multiples to appear in the signal.

F25. Spectral gamma-ray logs from HNGS vs. depth, p. 61.

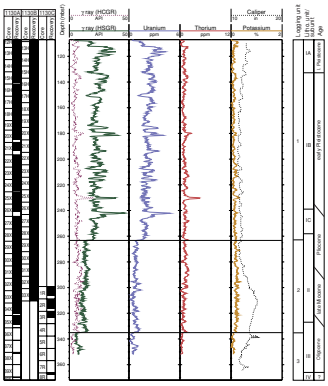

F26. Comparison between geophysical logs and physical properties measured on the recovered cores, p. 62.

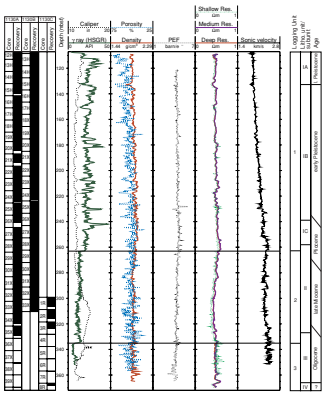

Comparison of logging data to physical properties measurements (see "Physical Properties," p. 25) shows good agreement between the gamma-ray log (standard [total] gamma ray [HSGR] from the hostile environment natural gamma-ray sonde [HNGS]) and NGR from core, although there seem to be small depth discrepancies possibly caused by heave, poor core recovery, and/or core expansion (Fig. F27). Downhole sediment density and GRA bulk density measured from core also correlate well (Fig. F27). Downhole sonic velocity shows a greater increase with depth when compared to discreet *P*-wave velocity measurements from cores. This difference occurs because discrete *P*-wave velocities are not measured under in situ pressure. In addition, discrete velocity measurements from cores show higher amplitude excursions than measurements seen in the sonic log (Fig. F27), probably as a result of the limited vertical resolution of the sonic digital tool.

F27. Spectral gamma-ray logs from the HNGS vs. depth, p. 63.

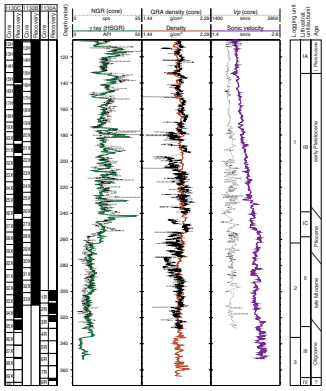

F28. Geophysical logs vs. depth from triple combo and FMS/sonic string, p. 64.

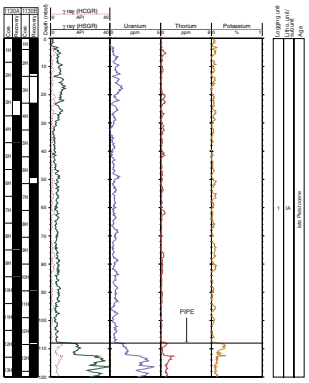

Preliminary Interpretations

Three logging units were defined at Site 1130, primarily from variations in NGR (Figs. F25, F26, F28). Boundaries between the defined logging units are characterized by abrupt shifts in gamma-ray, suggesting sharp boundaries between distinct lithostratigraphic units as observed in the recovered core (see "Lithostratigraphy," p. 3).

Logging Unit 1: 0–263 mbsf

The upper portion of Unit 1 that was logged through pipe (0–108 mbsf) is characterized by very low gamma-ray levels (Fig. F28), whereas the open-hole logged interval has distinct cyclic variations in gamma radiation, with excursions of as much as 45 American Petroleum Institute (API) units (Fig. F25). The frequency of this cyclicity increases near 173 mbsf. Uranium is the dominant source of gamma radiation throughout Unit 1 (Figs. F25, F28). Sonic velocity (1.9–2.3 km/s) and sediment density (1.8–2.0 g/cm^3) increase linearly with depth in Unit 1, consistent with a normal compaction profile. Photoelectric effect (PEF) increases slightly downhole from 4.4 barn/e$^-$ at the top to 4.7 barn/e$^-$ at the base of the unit. These values are characteristic of calcium carbonate-rich sediments. The slight positive separation of the porosity and density curves may result from the increased magnesium carbonates in this part of the section, as confirmed by XRD analyses (see "Inorganic Geochemistry," p. 23). The base of Unit 1 is defined at an abrupt drop in uranium gamma radiation and a decrease in the slope of the sonic velocity profile (Fig. F26). This boundary roughly correlates to lithostratigraphic Unit I.

Logging Unit 2: 263–329 mbsf

Unit 2 is characterized by nearly constant values of all parameters measured (Fig. F26). The lower gamma-ray values in this unit relative to Unit 1 reflect a decrease in uranium content (Fig. F25). The separation between the porosity and density logs is less than in Unit 1 and is characteristic of a clean calcium carbonate (see "Lithostratigraphy," p. 3). Several low-porosity peaks, crossing over the density curve, may indicate the occurrence of partially silicified beds within this unit. The reduced gradient in sonic velocity within logging Unit 2 (Fig. F26) may indicate slight fluid overpressure of this unit. Some degree of overpressure is also indicated by the large difference between in situ velocities

and velocities measured on the recovered core (Fig. F27). The base of Unit 2 is defined by an abrupt decrease in NGR (Fig. F25). This boundary is clearly identified on FMS images (Fig. F29) and correlates to the base of lithostratigraphic Unit II.

Logging Unit 3: 329–359 mbsf

Unit 3 is characterized by low gamma-ray values compared with overlying units (Fig. F25), and the PEF log displays increased variability. The jagged appearance of both shallow-resistivity and sonic logs indicates a thinly bedded (1–2 m) succession of varying lithification (Fig. F26). This is confirmed by limited core recovery (see "Lithostratigraphy," p. 3) and FMS images that indicate a sequence of highly resistive thin chert beds (~20 cm) alternating with 1- to 3-m intervals of more conductive chalk or ooze (Fig. F29).

SEISMIC STRATIGRAPHY

Introduction

Site 1130 (Fig. F30) intersects Cenozoic seismic Sequences 2, 3, 6A, and 7 (sequences defined in Feary and James, 1998, reprinted as Chap. 2), although hole instability restricted penetration of Sequence 7 sandstones to only the top 27 m. The high-resolution site-survey seismic data (Fig. F31), together with the regional seismic database, indicate that significant hiatuses should occur at sequence boundaries corresponding to the base of Sequence 2, the base of Sequence 3 (missing the basal part of Sequence 3 and all of Sequence 4), and the top of Sequence 7 (missing all but the youngest part of Sequence 6A).

Time–Depth Conversion

A check-shot survey using the single-channel WST was undertaken at this site to establish the time–depth relationship within the Cenozoic succession and to correct the integrated sonic curve for drift and for the pipe interval. The parameters and procedures undertaken during the check-shot survey at Site 1130 are described in "Downhole Measurements," p. 28. The eight time–depth tie points derived from the check-shot survey are presented in Figure F32. These points were plotted on a depth to two-way–traveltime graph (Fig. F33A) to (1) determine the relationship between depths encountered at Site 1130 and sequence boundaries and horizons located on seismic data and (2) compare the check-shot-corrected time–depth relationship with predictions based on stacking velocities. This plot shows that the actual time–depth relationship defined by the check-shot survey falls slightly below the envelope defined by the six stacking velocity curves for the immediate vicinity of Site 1130 (resulting from stacking velocities providing an underestimate of true traveltimes). These velocity underestimates correspond to depth errors of as great as 17 m between predicted and corrected depths to boundaries (Table T19).

Seismic Sequence Characteristics

The data collected at Site 1130, particularly lithostratigraphic and biostratigraphic information, provide an opportunity to interpret the

F29. FMS image of boundary between logging Units 2 and 3, and boundary between lithostratigraphic Units II and III, p. 65.

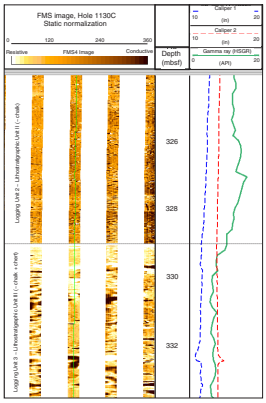

F30. Seismic site-survey tracks for Site 1130 in relation to other Leg 182 sites and the AGSO169 site-survey seismic lines, p. 66.

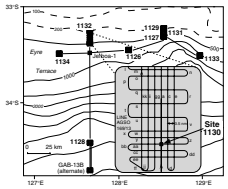

F31. Portion of seismic Line AGSO169/13a, p. 67.

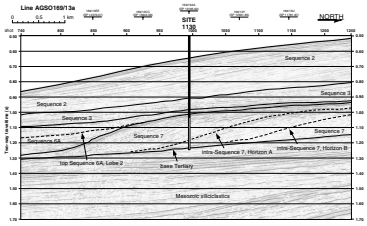

F32. Check-shot stations and acquisition geometry for the WST survey, p. 68.

Depth (mbrf)	Depth (mbsl)	Transit time (ms)	True path length (m)	Corrected TWT (ms)	Interval velocity (m/s)
640.0	628.5	401.92	628.7	805.36	1780.00
670.2	658.7	418.82	658.9	839.29	2041.31
699.9	688.4	433.31	688.6	868.39	2303.19
730.1	718.6	448.36	718.8	894.61	2102.69
760.0	748.5	460.53	748.7	923.05	2348.99
799.8	788.3	477.40	788.5	956.94	2505.43
830.1	818.6	489.45	818.8	981.13	2234.48
858.0	846.5	501.90	846.7	1006.10	

Corrected TWT is TWT from sea level to WST tool along a vertical path

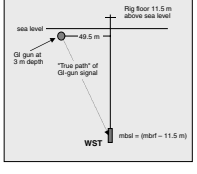

site data within a more regional context and also allow a description of the characteristics of seismic sequences intersected at this site (see "Lithostratigraphy," p. 3, and "Biostratigraphy," p. 10). The correlation of lithostratigraphic and biostratigraphic data with seismic stratigraphy (Fig. F34) was based on the regional moderate-resolution multichannel seismic data collected by the Japan National Oil Corporation (JNOC) in 1990 (Feary and James, 1998, reprinted as Chap. 2) and the high-resolution site-survey seismic data collected by the Australian Geological Survey Organisation (AGSO) in 1996 (Feary, 1997).

Sequence 2

Comparison of the high-resolution site-survey seismic data at Site 1130 to regional seismic data indicates that the Sequence 2 interval intersected at Site 1130 should represent a relatively complete succession; however, the 259-m thickness represents a lower sedimentation rate and decreased resolution compared with the ~550-m thickness of Sequence 2, which forms the spectacular clinoforms at Sites 1127, 1129, and 1131. Seismic data show that the component of Sequence 2 intersected at Site 1130 should represent an expanded upper part and a relatively condensed middle part of this sequence, with the oldest parts either highly condensed or absent. The high-resolution site-survey seismic data indicate that there should be significant facies differences between the succession intersected at this site compared with Site 1132, with reflectors at Site 1130 being more evenly stratified and continuous compared with the mounded reflection geometry at Site 1132. Lithostratigraphic analysis shows that these evenly stratified and continuous reflections correspond to strongly bioturbated bioclastic packstones interbedded with bioclastic wackestone and nannofossil ooze. The basal sequence boundary correlates to the transition from lithostratigraphic Unit I to Unit II, corresponding to a transition from slumped glauconitic bioclastic packstone and nannofossil bioclastic packstone of Subunit IC to the undeformed nannofossil foraminiferal chalk and ooze of Unit II. Biostratigraphic data show that the hiatus associated with this boundary represents ~1.7 m.y. missing, corresponding to the lower/upper Pliocene boundary. The prominent reflector intersected at ~0.8 s two-way traveltime (Fig. F31) correlates with a marked finer wackestone unit at 132 mbsf, which is interpreted as a flooding surface (see "Lithostratigraphy," p. 3).

Sequence 3

From a regional perspective, Sequence 3 is thickest (~240 m) beneath the modern shelf and thins downslope to a feather edge beneath the modern middle shelf (Feary and James, 1998, reprinted as Chap. 2). Site 1130 intersects Sequence 3 beneath the uppermost slope, where it is only 69 m thick. Sequence 3 correlates with lithostratigraphic Unit II, of late Miocene to early Pliocene age, which is dominated by calcareous nannofossil foraminiferal chalk and ooze. The lower one-third of this unit contains many omission surfaces and firmgrounds, as well as two prominent turbidite horizons. The sequence boundary at the base of Sequence 3 represents a very substantial hiatus, with the older (middle Miocene) parts of Sequence 3 and all of Sequence 4 (lower Miocene) completely missing. This hiatus corresponds to an interval of 14–15 m.y. (see "Biostratigraphy," p. 10).

F33. Predicted and corrected depths and interval velocities, p. 69.

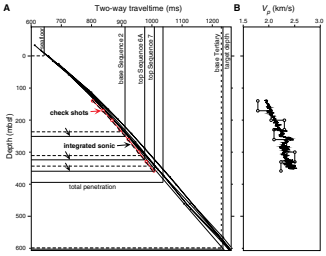

T19. Differences between depths to key horizons and corrected depths, p. 98.

F34. Lithostratigraphic units, seismic sequences, biostratigraphic hiatuses, and ages, p. 70.

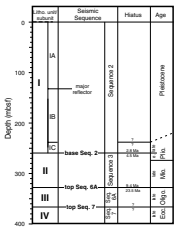

Sequence 6A

Sequence 6A is represented at Site 1130 by a 40-m-thick, poorly recovered upper Oligocene interval corresponding to lithostratigraphic Unit III. Because of limited recovery, it was only possible to conclude that Sequence 6A at this site consists of a nannofossil foraminiferal chalk/ooze interval containing preferentially silicified thin beds and lenses.

Sequence 7

The basal interval intersected at Site 1130 consists of 27 m of poorly recovered and diverse lithologies corresponding to lithostratigraphic Unit IV. The calcareous sandstone, bioclastic glauconitic wackestone, bryozoan grainstone, and bivalve grainstone are assigned to seismic Sequence 7. The absence of either calcareous nannofossils or planktonic foraminifers within core catcher samples means that the only direct indications of age are based on a few foraminifer tests observed in thin sections in the calcareous sandstone. These indicate a middle–late Eocene age (see **"Biostratigraphy,"** p. 10), although it is likely that postcruise studies will enable this age to be further refined. Hole instability, presumably caused by poorly cemented sandstone portions of this sequence, prevented penetration to the base of Sequence 7 and attainment of one of the major objectives at this site.

REFERENCES

Bein, J., and Taylor, M.L., 1981. The Eyre Sub-basin: recent exploration results. *APEA J.,* 21:91–98.

Berggren, W.A., 1992. Paleogene planktonic foraminifer magnetobiostratigraphy of the Southern Kerguelen Plateau (Sites 747–749). *In* Wise, S.W., Jr., Schlich, R., et al., *Proc. ODP, Sci. Results,* 120 (Pt. 2): College Station, TX (Ocean Drilling Program), 551–568.

Berggren, W.A., Hilgen, F.J., Langereis, C.G., Kent, D.V., Obradovich, J.D., Raffi, I., Raymo, M.E., and Shackleton, N.J., 1995a. Late Neogene chronology: new perspectives in high-resolution stratigraphy. *Geol. Soc. Am. Bull.,* 107:1272–1287.

Berggren, W.A., Kent, D.V., Swisher, C.C., III, and Aubry, M.-P., 1995b. A revised Cenozoic geochronology and chronostratigraphy. *In* Berggren, W.A., Kent, D.V., Aubry, M.-P., and Hardenbol, J. (Eds.), *Geochronology, Time Scales and Global Stratigraphic Correlation*. Spec. Publ.—Soc. Econ. Paleontol. Mineral. (Soc. Sediment. Geol.), 54:129–212.

Feary, D.A., 1997. ODP pollution prevention and safety panel: Leg 182 safety package—Cenozoic cool-water carbonates of the Great Australian Bight. *Aust. Geol. Surv. Org.,* 28.

Feary, D.A., and James, N.P., 1998. Seismic stratigraphy and geological evolution of the Cenozoic, cool-water, Eucla Platform, Great Australian Bight. *AAPG Bull.,* 82:792–816.

Hornibrook, N. de B., Brazier, R.C., and Strong, C.P., 1989. Manual of New Zealand Permian to Pleistocene foraminiferal biostratigraphy. *Paleontol. Bull. N.Z. Geol. Surv.,* 56:1–175.

Jenkins, D.G., 1993. Cenozoic Southern mid- and high-latitude biostratigraphy and chronostratigraphy based on planktonic foraminifera. *In* Kennett, J.P., and Warnke, D.A. (Eds.), *The Antarctic Paleoenvironment: A Perspective on Global Change*. Antarct. Res. Ser., 60:125–144.

Li, Q., James, N.P., Bone, Y., and McGowran, B., 1999. Palaeoceanographic significance of Recent foraminiferal biofacies on the southern shelf of Western Australia: a preliminary study. *Palaeogeogr., Palaeoclimatol., Palaeoecol.,* 147:101–120.

Li, Q., and McGowran, B., in press. Miocene foraminifera from Lakes Entrance oil shaft, southeastern Australia. *Assoc. Australas. Paleontol. Mem. Ser.*

Li, Q., Radford, S.S., and Banner, F.T., 1992. Distribution of microperforate tenuitellid planktonic foraminifers in Holes 747A and 749B, Kerguelen Plateau. *In* Wise, S.W., Jr., Schlich, R., et al., *Proc. ODP, Sci. Results,* 120: College Station, TX (Ocean Drilling Program), 569–594.

McGowran, B., Li, Q., Cann, J., Padley, D., McKirdy, D.M., and Shafik, S., 1997a. Biogeographic impact of the Leeuwin Current in southern Australia since the late middle Eocene. *Palaeogeogr., Palaeoclimatol., Palaeoecol.,* 136:19–40.

McGowran, B., Li, Q., and Moss, G., 1997b. The Cenozoic neritic record in southern Australia: the biogeohistorical framework. *In* James, N.P., and Clarke, J., *Cool-Water Carbonates*. Spec. Publ.— Soc. Econ. Petrol. Mineral., 56:185–203.

Raymo, M.E., Ruddiman, W.F., Backman, J., Clement, B.M., and Martinson, D.G., 1989. Late Pliocene variation in Northern Hemisphere ice sheets and North Atlantic deep water circulation. *Paleoceanography,* 4:413–446.

Shackleton, N.J., Berger, A., and Peltier, W.A., 1990. An alternative astronomical calibration of the lower Pleistocene timescale based on ODP Site 677. *Trans. R. Soc. Edinburgh: Earth Sci.,* 81:251–261.

Shackleton, N.J., Crowhurst, S., Hagelberg, T., Pisias, N.G., and Schneider, D.A., 1995. A new late Neogene time scale: application to Leg 138 sites. *In* Pisias, N.G., Mayer, L.A., Janecek, T.R., Palmer-Julson, A., and van Andel, T.H. (Eds.), *Proc. ODP, Sci. Results,* 138: College Station, TX (Ocean Drilling Program), 73–101.

Shafik, S., 1990. The Maastrichtian and early Tertiary record of the Great Australian Bight Basin and its onshore equivalents on the Australian southern margin: a nannofossil study. *BMR J. Australian Geol. Geophys.,* 11:473–497.

Stagg, H.M.J., Cockshell, C.D., Willcox, J.B., Hill, A.J., Needham, D.J.L., Thomas, B., O'Brien, G.W., and Hough, L.P., 1990. *Basins of the Great Australian Bight Region: Geology and Petroleum Potential*. Cont. Marg. Progr., Bur. Miner. Resour., Fol. 5.

Swart, P.K., and Guzikowski, M., 1988. Interstitial-water chemistry and diagenesis of periplatform sediments from the Bahamas, ODP Leg 101. *In* Austin, J.A., Jr., Schlager, W., Palmer, A.A., et al., *Proc. ODP, Sci. Results,* 101: College Station, TX (Ocean Drilling Program), 363–380.

van Morkhoven, F.P.C.M., Berggren, W.A., and Edwards, A.S., 1986. Cenozoic cosmopolitan deep-water benthic foraminifera. *Bull. Cent. Rech. Explor.—Prod. Elf-Aquitaine,* 11.

Figure F1. Map showing the location of Site 1130 on the upper continental slope in relation to other Leg 182 sites and the Australian Geological Survey Organisation Survey 169 (AGSO169) seismic lines.

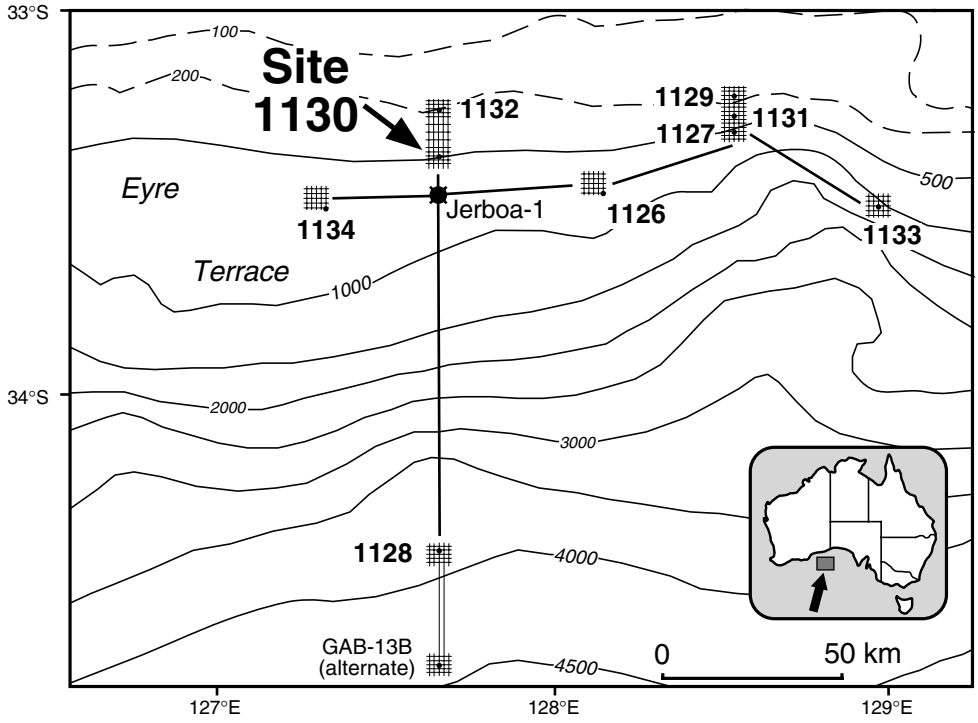

Figure F2. Portion of seismic Line AGSO169/13a showing the pre-drill seismic stratigraphic interpretation at Site 1130 and showing sequences planned (shown in white) and actually (shown in black) intersected at this site.

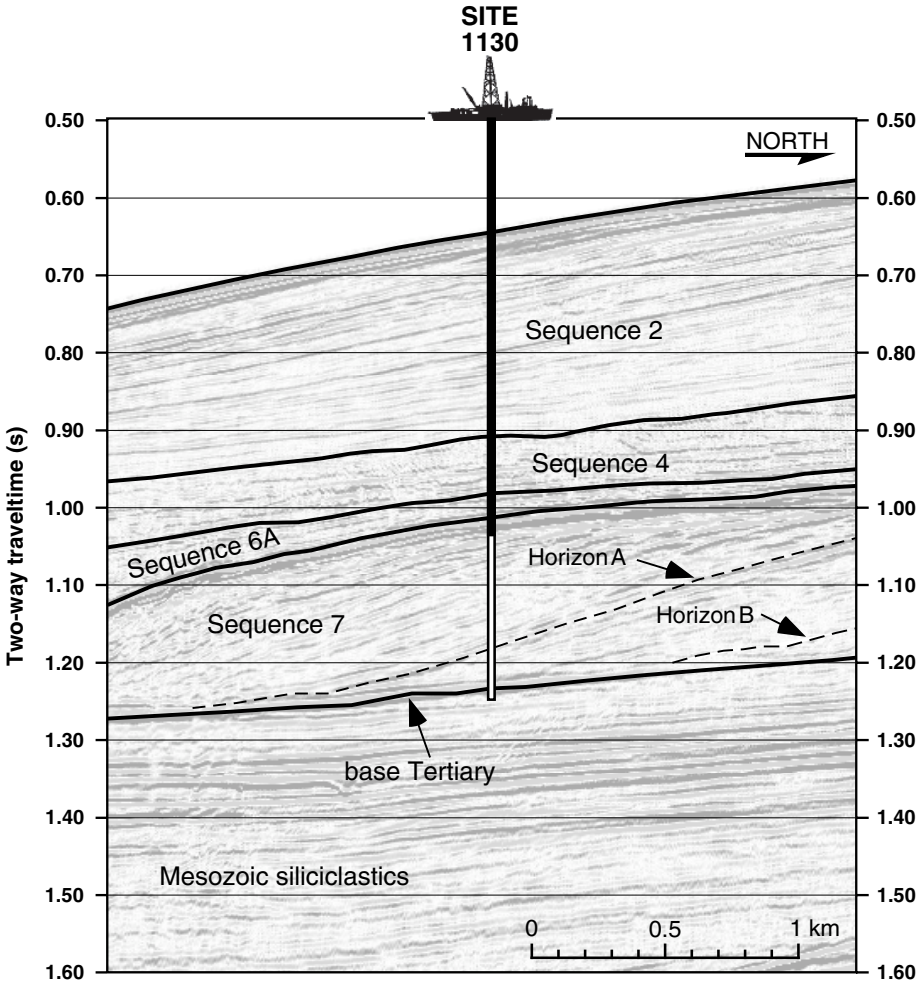

Figure F3. Summary of sediment lithostratigraphy at Site 1130. Ages are from **"Biostratigraphy,"** p. 10. (Continued on next page.)

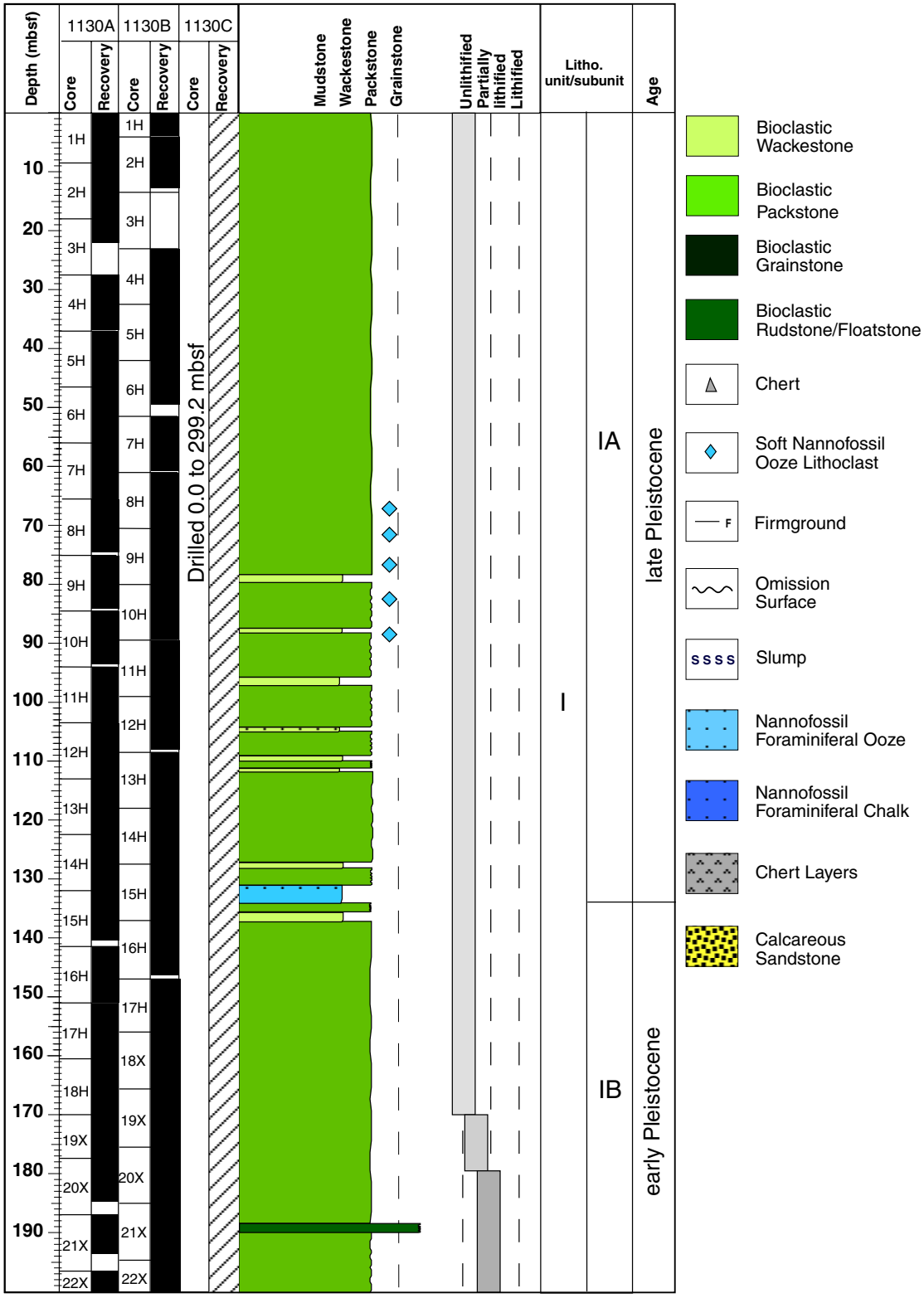

Figure F3 (continued).

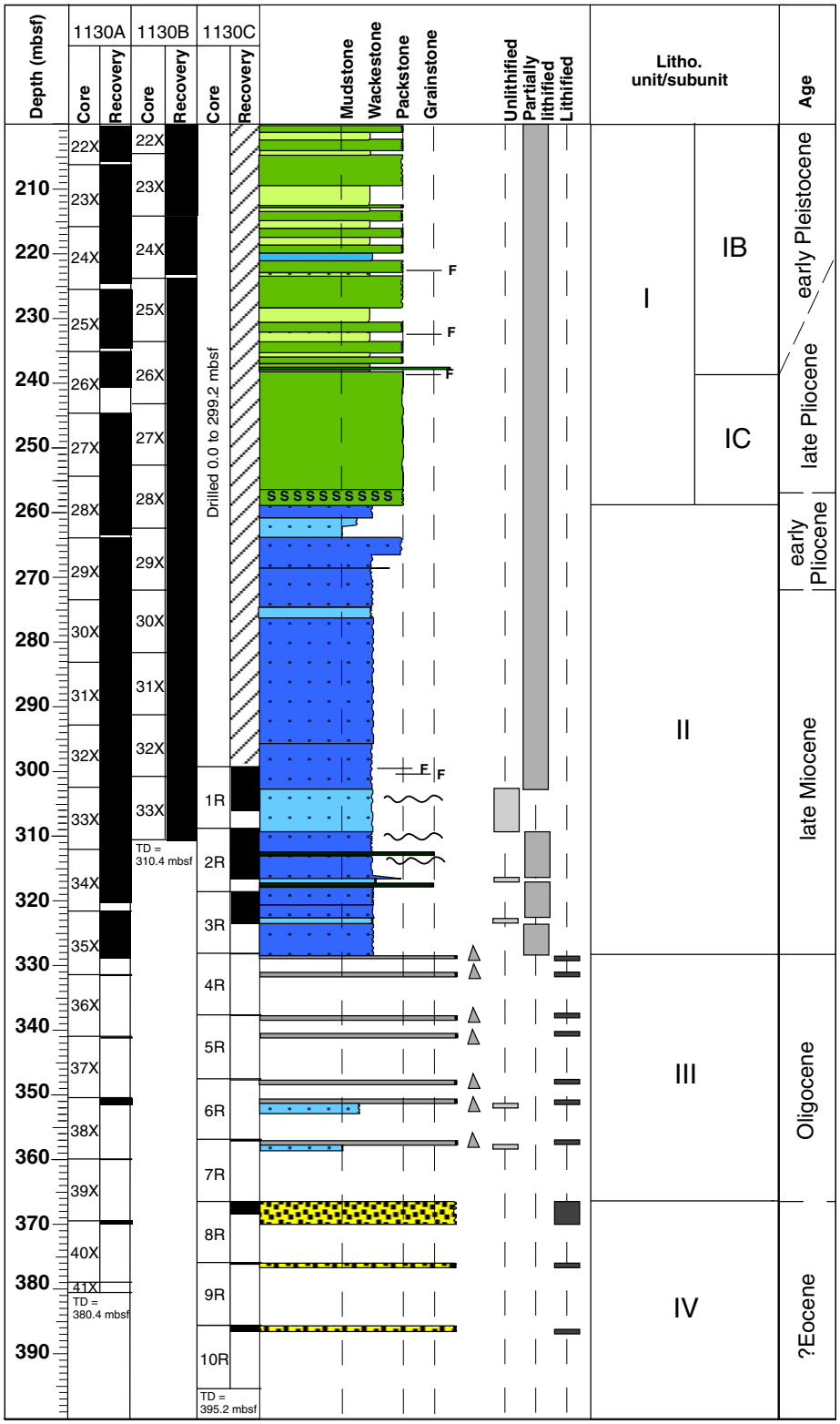

Figure F4. Turbidite (229.37–229.80 mbsf) from the lower part of Subunit IB containing pebble-sized gray bryozoan debris, blackened grains, and echinoid spines. It is characterized by an inverse to normal grading (interval 182-1130B-25X-4, 104–150 cm.).

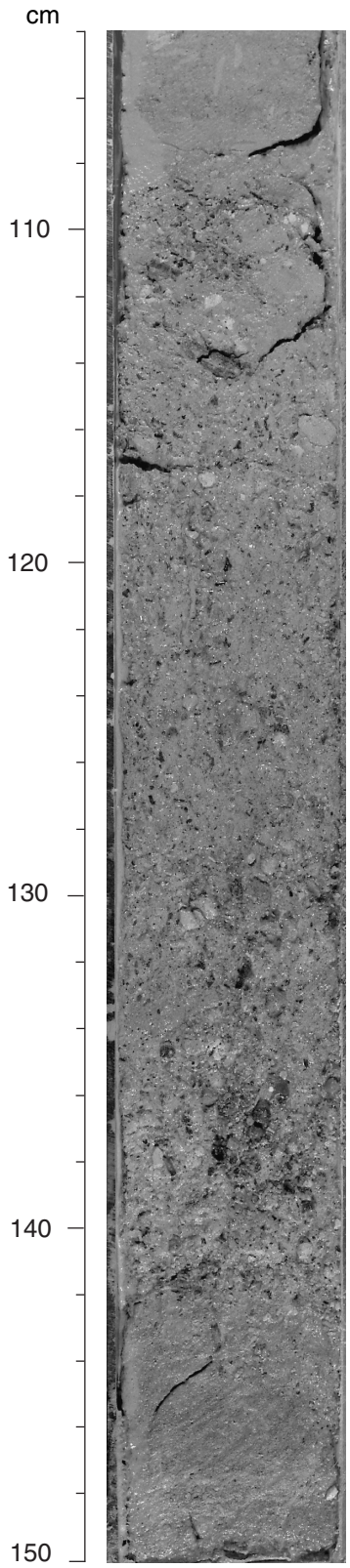

Figure F5. Lower part of the synsedimentary soft deformation (slump) marking the boundary between lithostratigraphic Units I and II (interval 182-1130A-28X-2, 100–135 cm.).

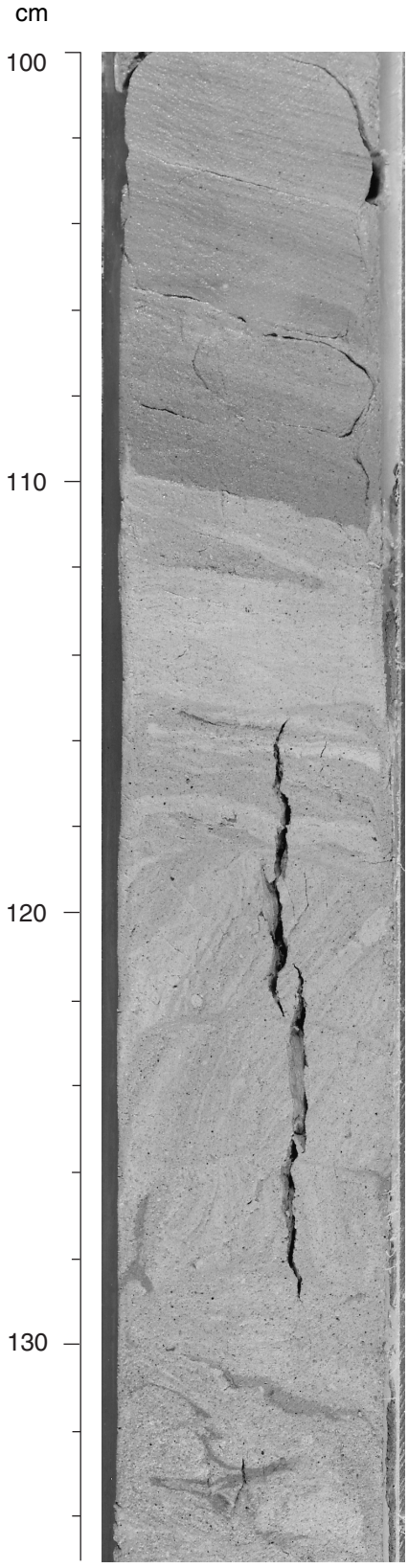

Figure F6. Stratigraphic position of calcareous nannofossil and planktonic foraminifer zones and benthic foraminifer assemblages at Site 1130. Dashed boundaries imply uncertainty.

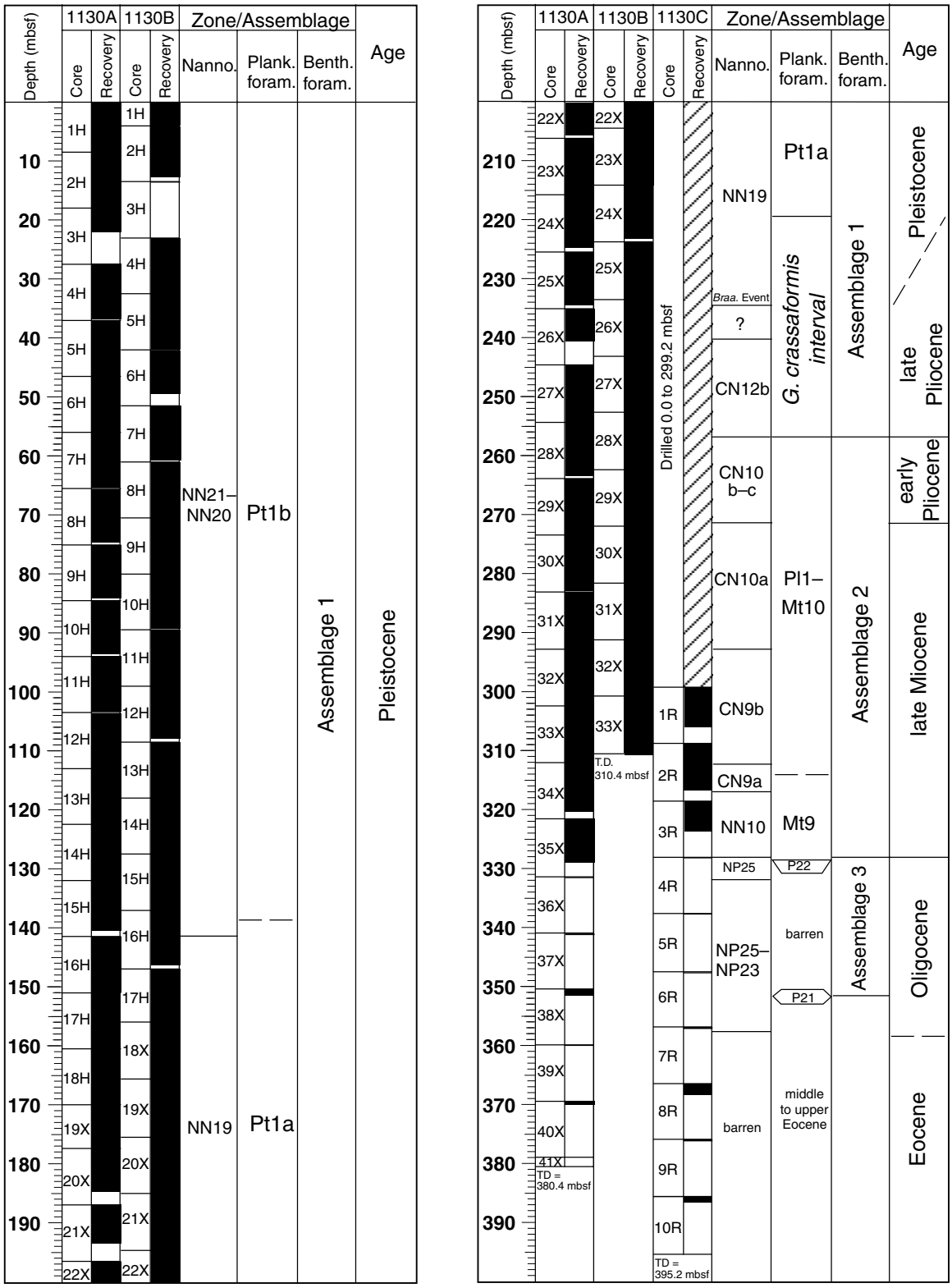

Figure F7. Sedimentation rate curve constructed from the datum levels listed in Table T2, p. 74. Stratigraphic error is indicated by the length of the error bars.

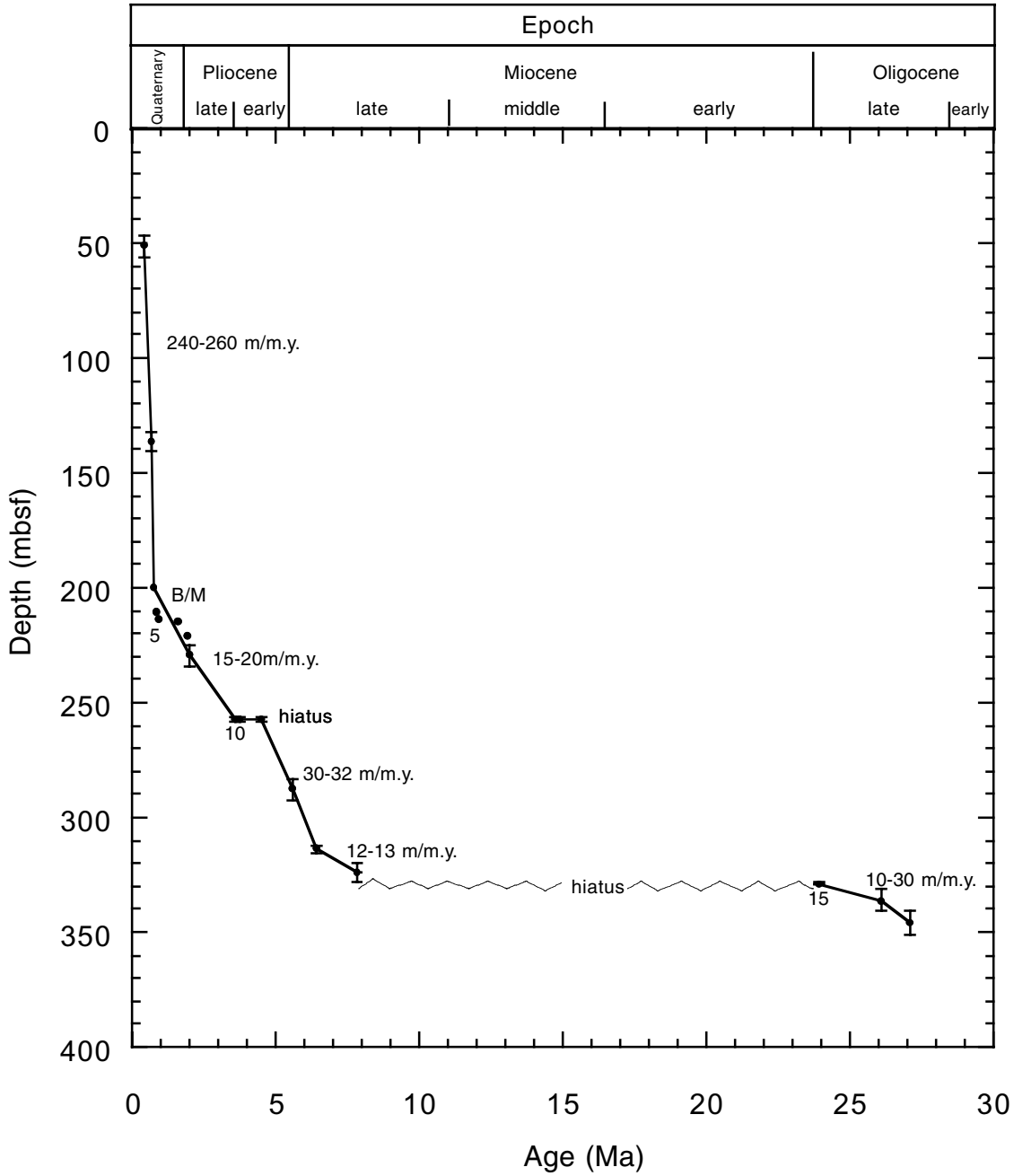

Figure F8. Hole 1130A (**A**) magnetic susceptibility and (**B**) intensity of magnetization downhole.

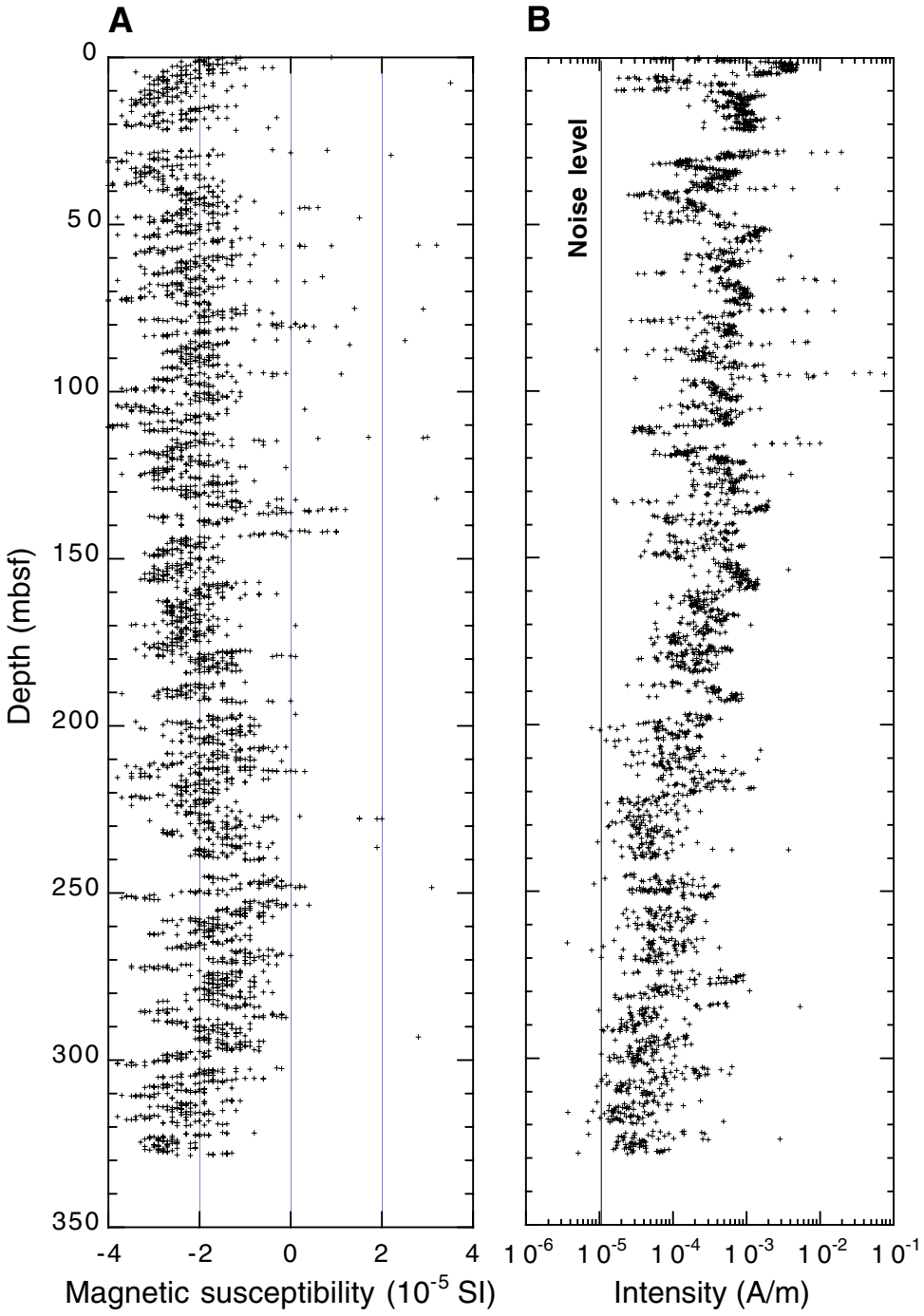

Figure F9. Demagnetization analysis for Sample 182-1130A-9H-5, 51–53 cm. On the left is a plot of intensity, in the center is a Zijderveld plot (solid symbols indicate north and east components of magnetization, open symbols indicate up and north components of magnetization), and on the right is a stereoplot of directions in which open symbols represent the upper hemisphere.

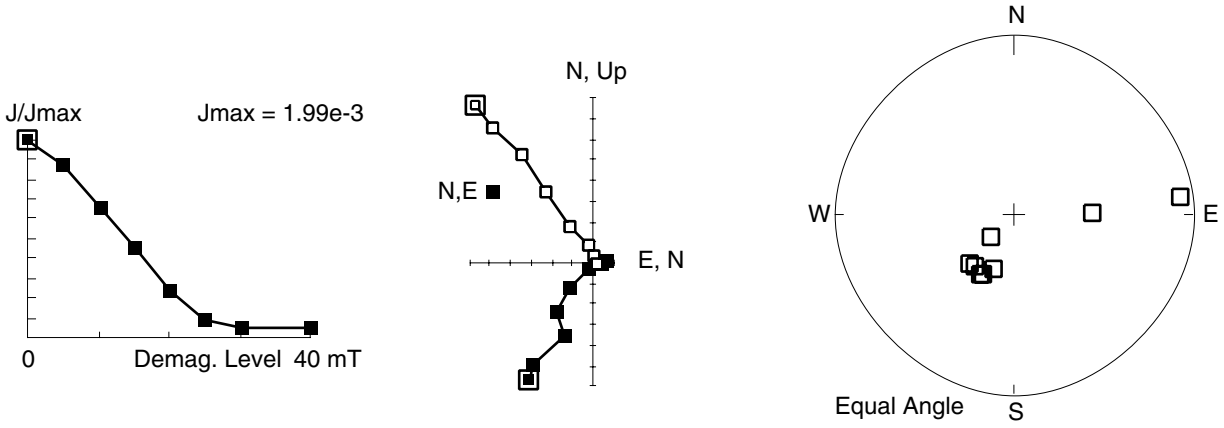

Figure F10. Plots of demagnetization of natural remanent magnetization (NRM), anhysteretic remanent magnetization (ARM), and isothermal remanent magnetization (IRM) and of the acquisition of IRM for (**A**) Section 182-1130A-6H-5 and (**B**) Section 182-1130A-27X-1. The plots summarize the magnetic characteristics of these samples. The ratio of IRM:ARM in (A) is indicative of single-domain behavior and suggests a magnetotactic origin of the magnetite. In (B), the ratio of ARM:IRM has fallen substantially, indicating increased dissolution with increasing depth.

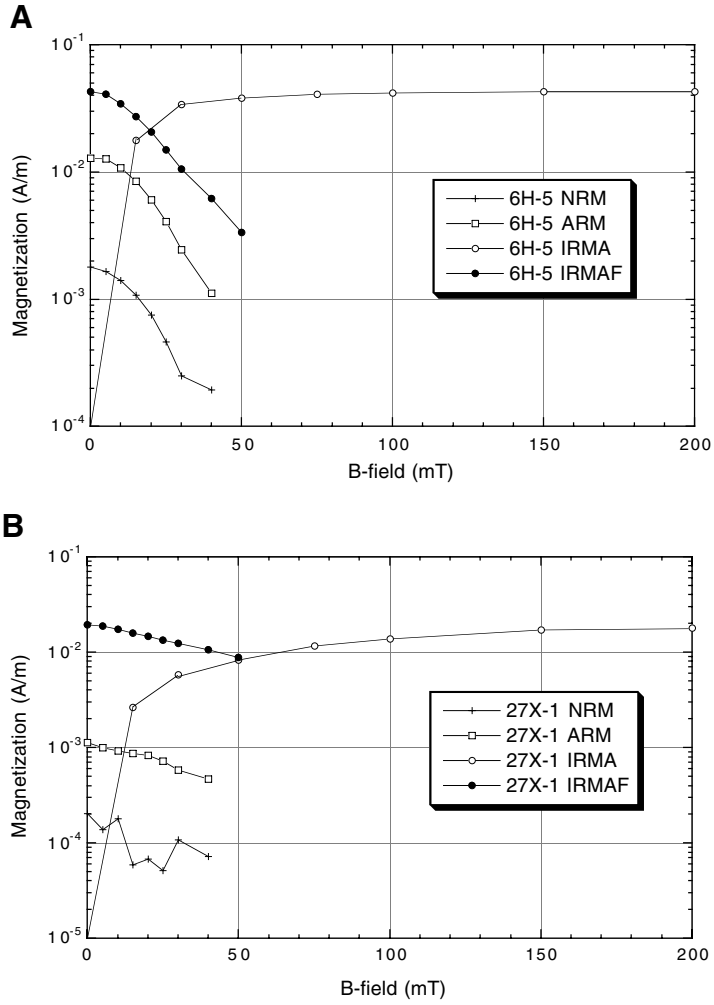

Figure F11. Magnetostratigraphy of Holes 1130A and 1130B showing similar stratigraphic depth of the Brunhes/Matuyama boundary with indeterminate magnetostratigraphy below.

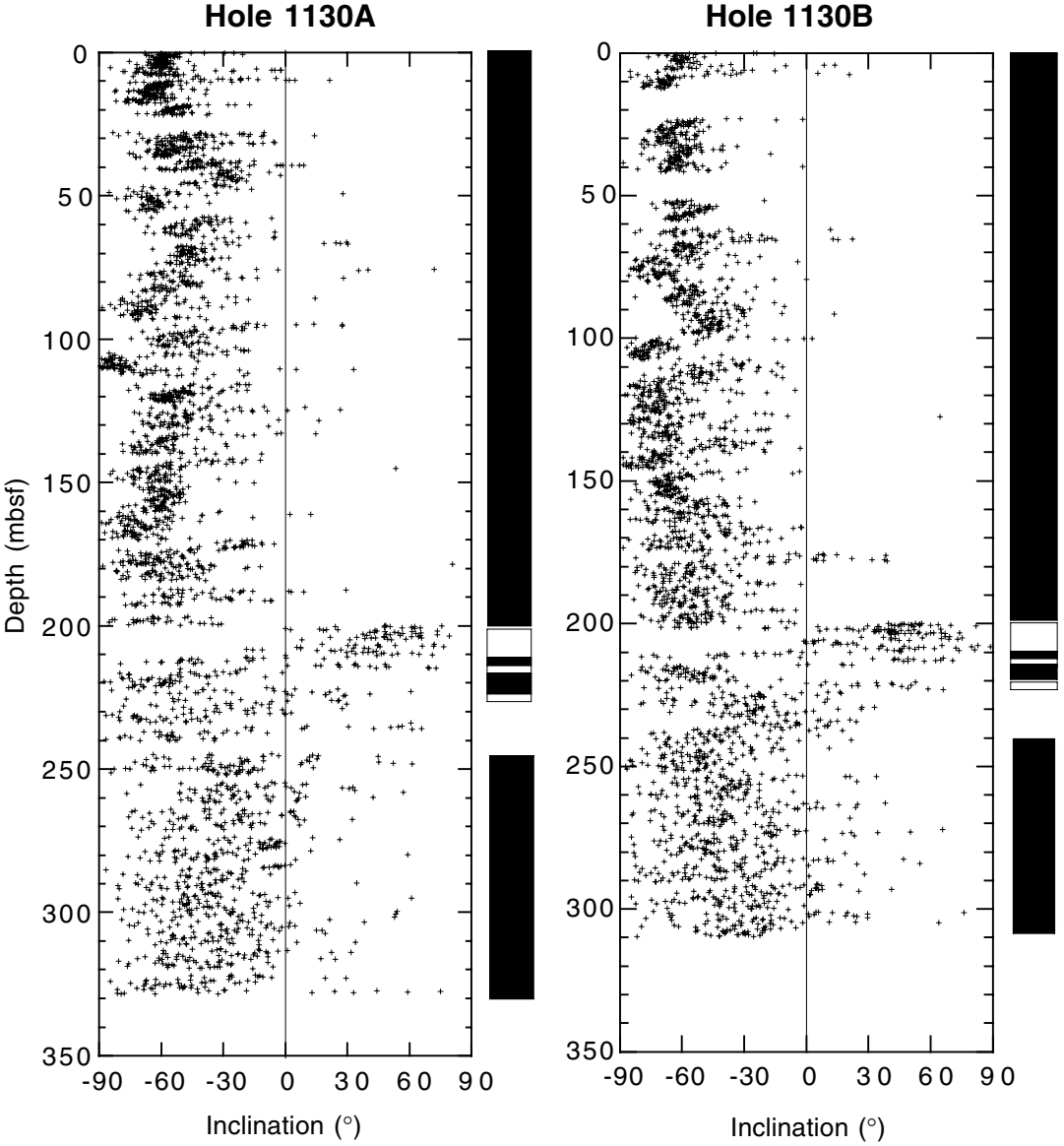

Figure F12. Composite depth section produced using the Splicer software. The black line is data from Hole 1130A, and the red line is data from Hole 1130B. NGR = natural gamma radiation. All depths use the meters composite depth (mcd) scale. For conversions from mcd to mbsf, see Table **T3,** p. 75. (Continued on next page.)

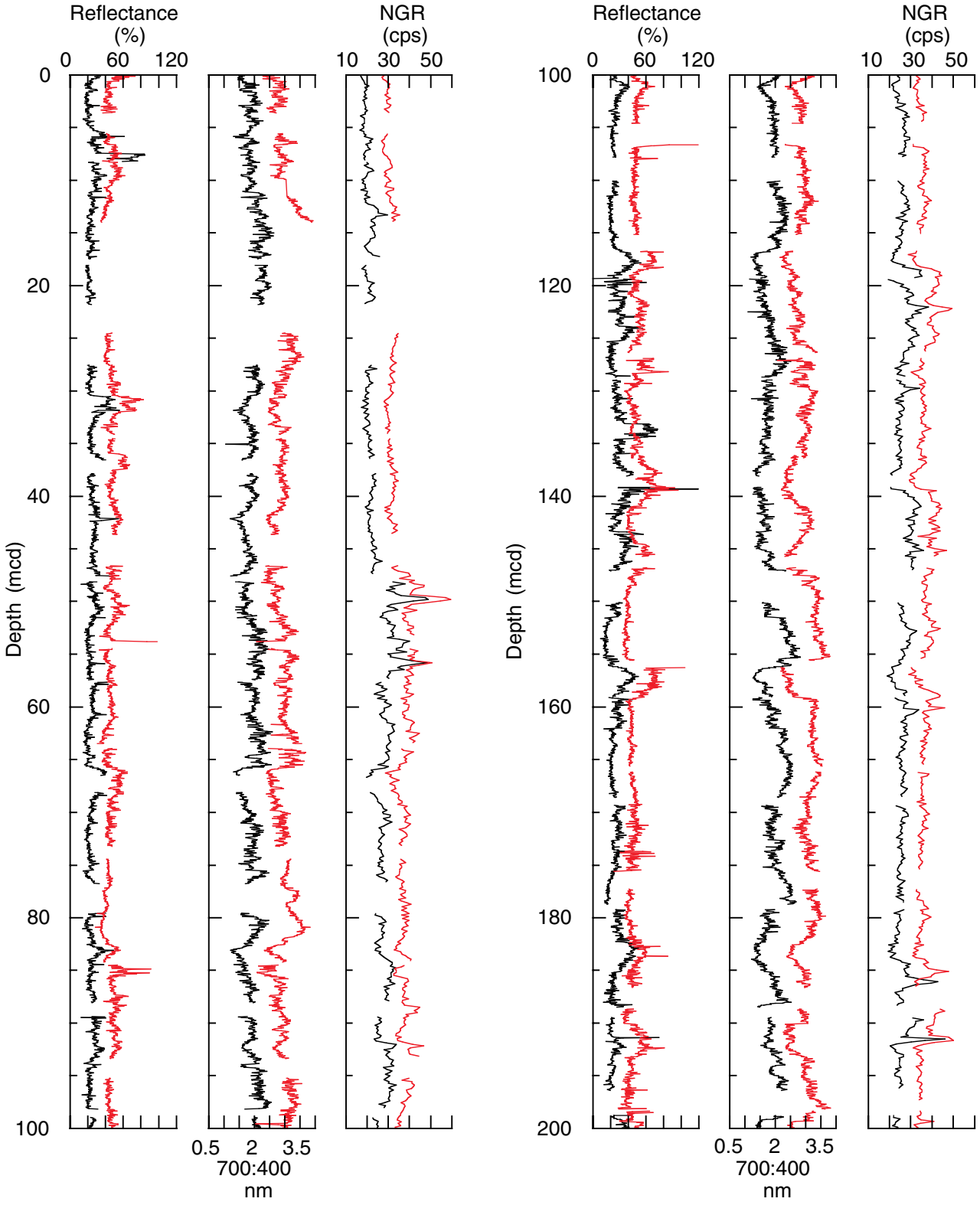

Figure F12 (continued).

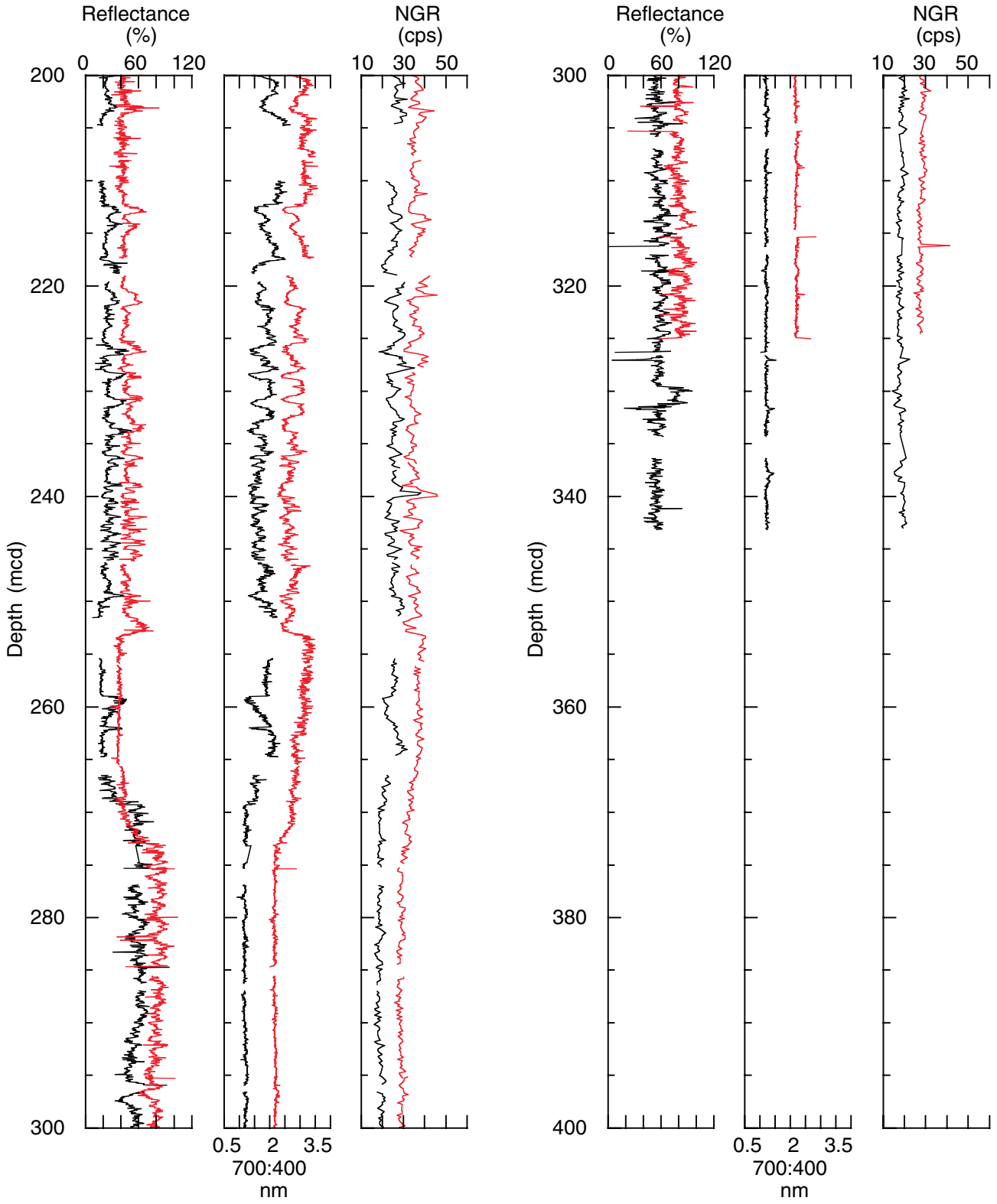

Figure F13. Spliced section of smoothed color reflectance ratio data (700:400 nm), smoothed 400-nm color reflectance data, and smoothed natural gamma radiation (NGR) data produced using the Splicer software. These data are a spliced composite of correlated data from Holes 1130A and 1130B. Ages are derived from biostratigraphic data. Lithostratigraphic units are described in "Lithostratigraphy," p. 3.

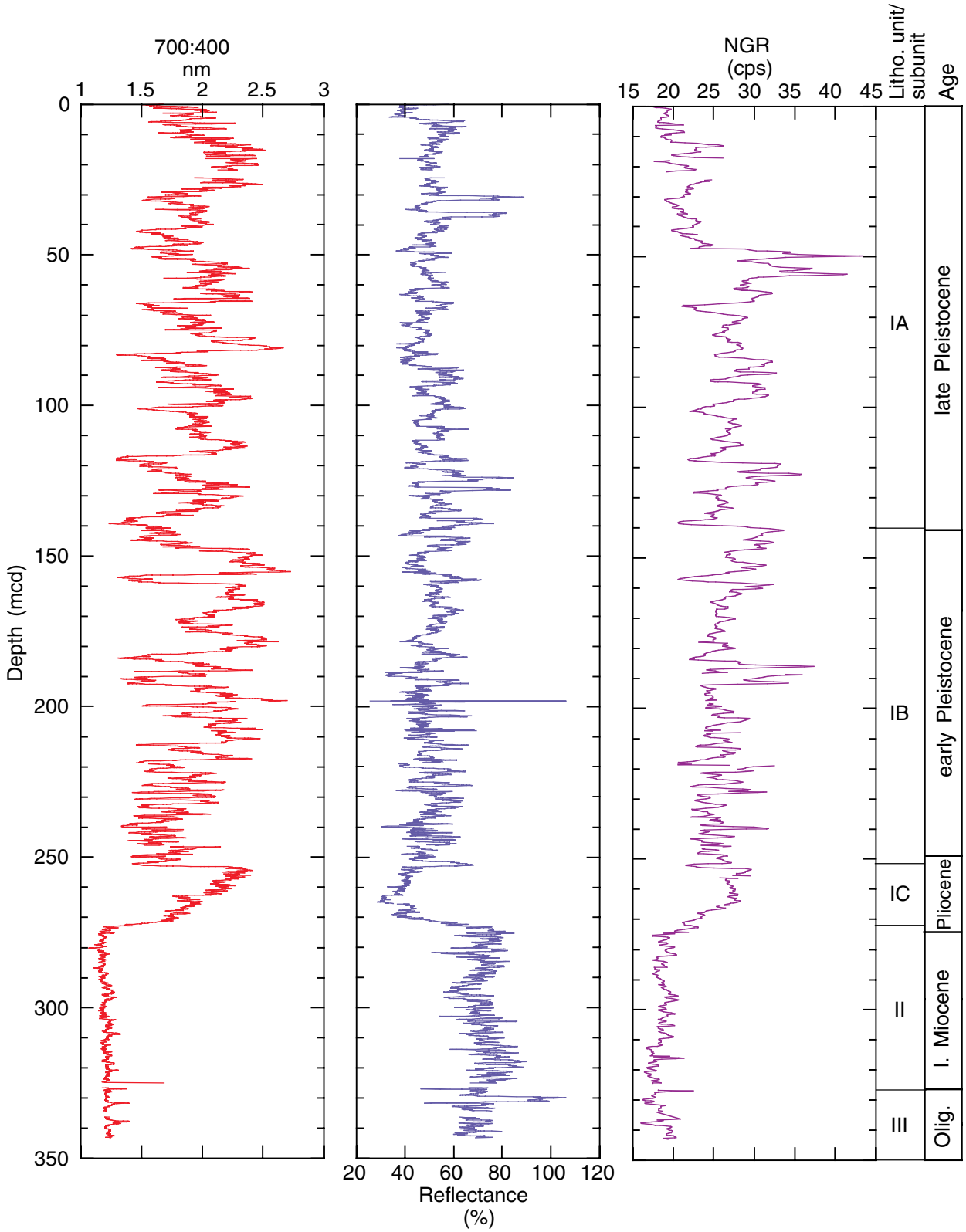

Figure F14. Spliced and tuned color reflectance record from Site 1130 compared to the composite seawater $\delta^{18}O$ curve from Site 656 (Raymo et al., 1989). The tuned record of the color reflectance ratio (700:400 nm) data is shown in black. The composite seawater $\delta^{18}O$ curve is shown in red.

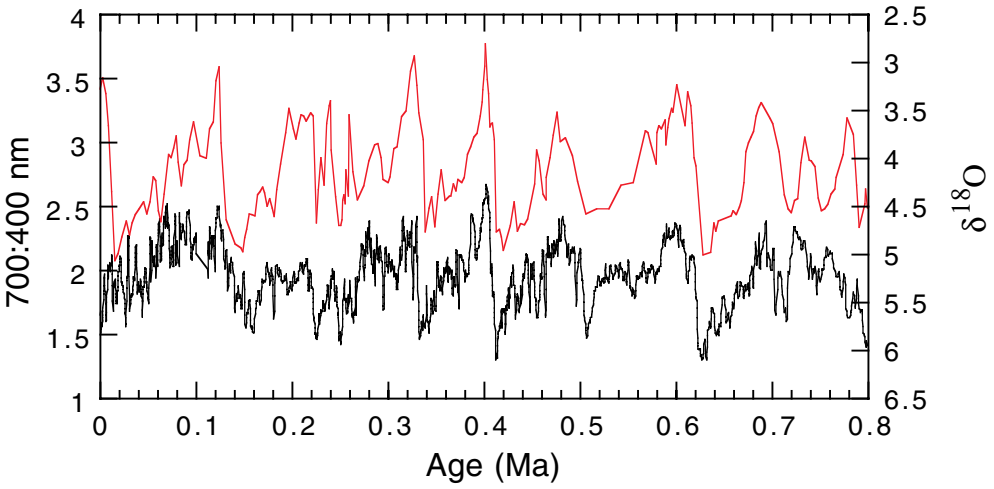

Figure F15. Calcium carbonate content of samples from Site 1130. Solid circles = Hole 1130A; open circles = Hole 1130C.

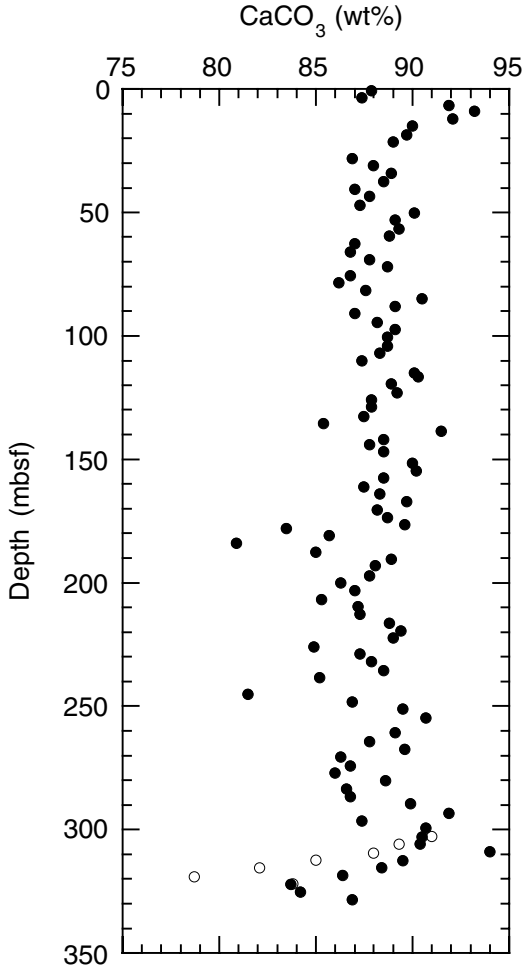

Figure F16. Depths vs. concentration profiles for (**A**) salinity, (**B**) Cl^-, (**C**) K^+, (**D**) Ca^{2+}, (**E**) Mg^{2+}, and (**F**) Sr^{2+}.

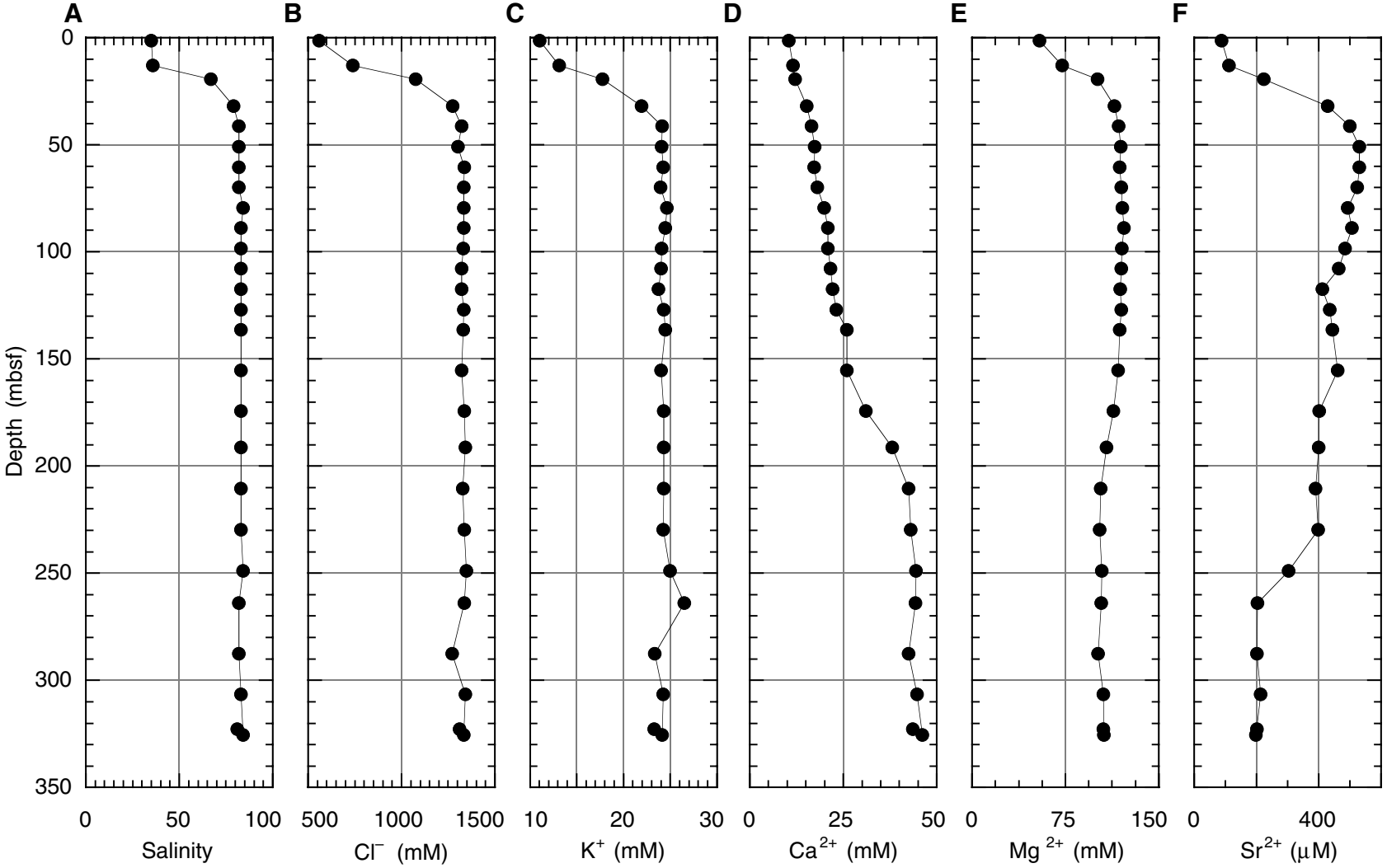

Figure F17. Depths vs. concentration profiles for (**A**) Li^+, (**B**) SO_4^{2-}, (**C**) H_4SiO_4, (**D**) NH_4^+, (**E**) Fe^{2+}, and (**F**) pH.

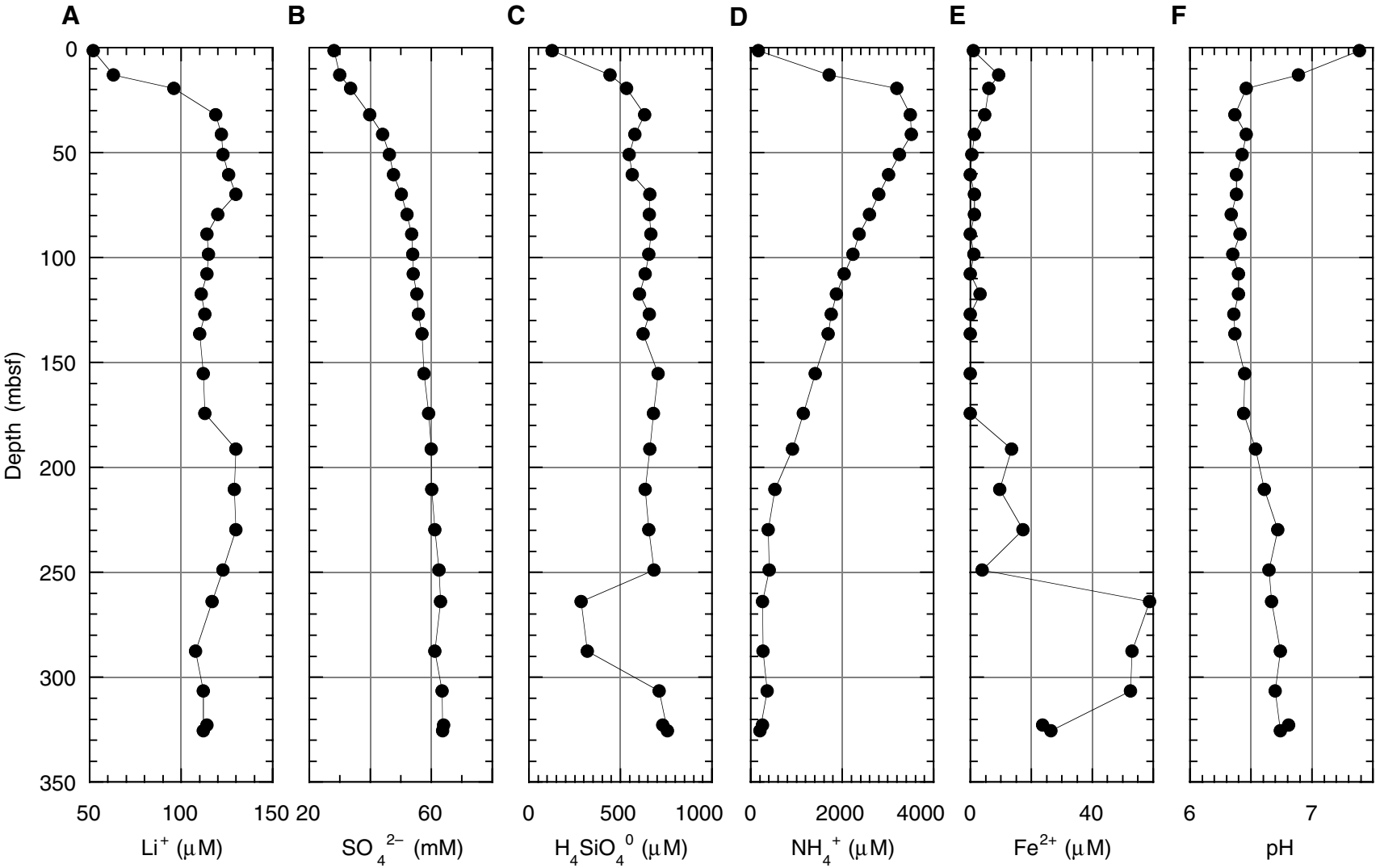

Figure F18. Depths vs. concentration profiles for (**A**) alkalinity, and depths vs. excess (with respect to seawater) concentrations for (**B**) Ca^{2+} and (**C**) Mg^{2+}. Because of the increase in salinity, the excess concentration was calculated as $(M/Cl^- - a) \times Cl^-$, where $M = Ca^{2+}$, Mg^{2+}, or Sr^{2+}, and $a = M/Cl^-$ of standard seawater (i.e., International Association for the Physical Sciences of the Ocean [IAPSO]). The concentrations of (**D**) silica and (**E**) lithium were normalized to chlorinity to compensate for the concentration increase with increasing salinity.

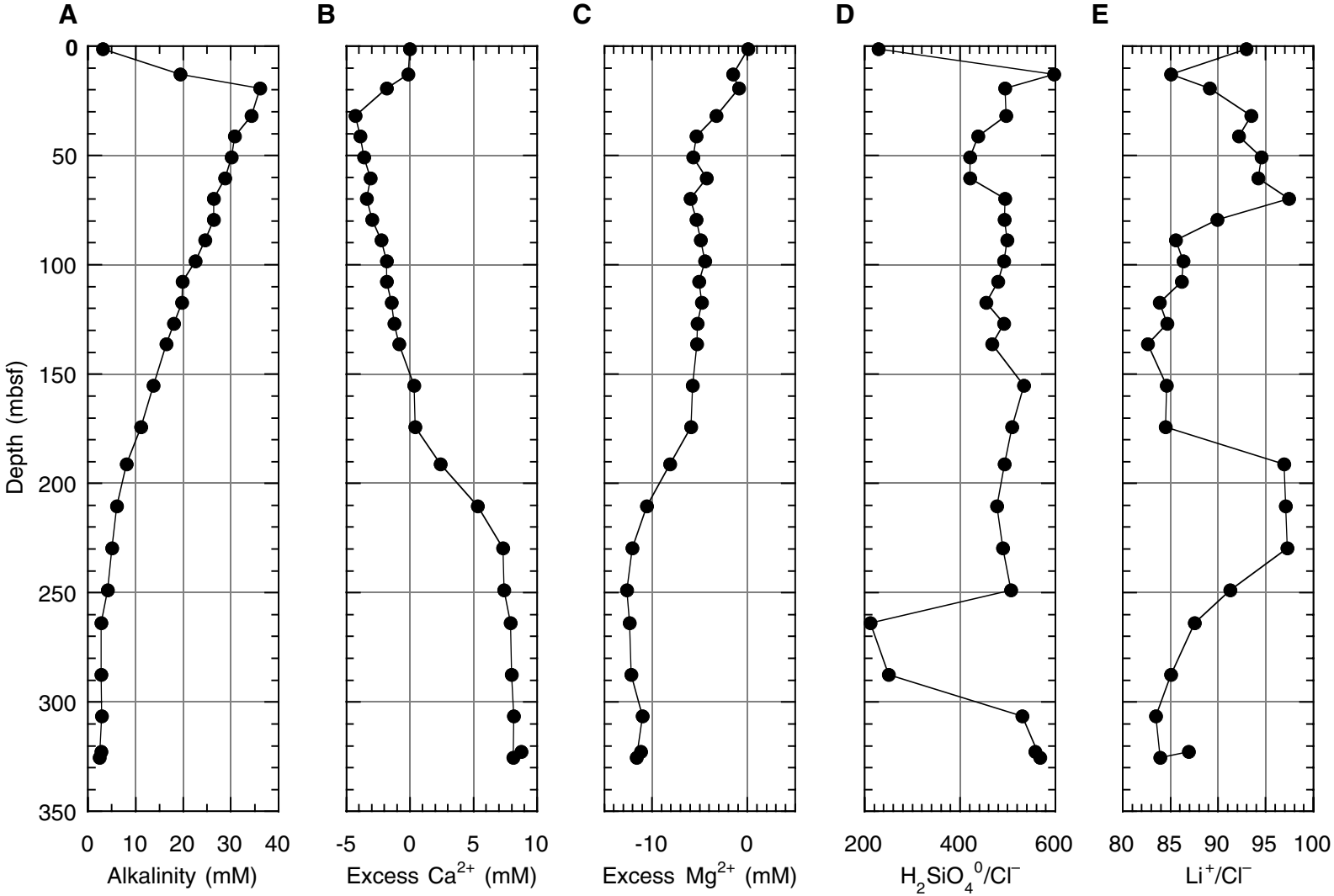

Figure F19. Variations in the concentration of aragonite (A), quartz (Q), low-Mg calcite (LMC), high-Mg calcite (HMC), and dolomite (D) at Site 1130 as derived from XRD analysis. Calculations assume that the sediment is composed solely of these minerals and make no allowance for the presence of insoluble minerals other than quartz (see "Organic Geochemistry," p. 23).

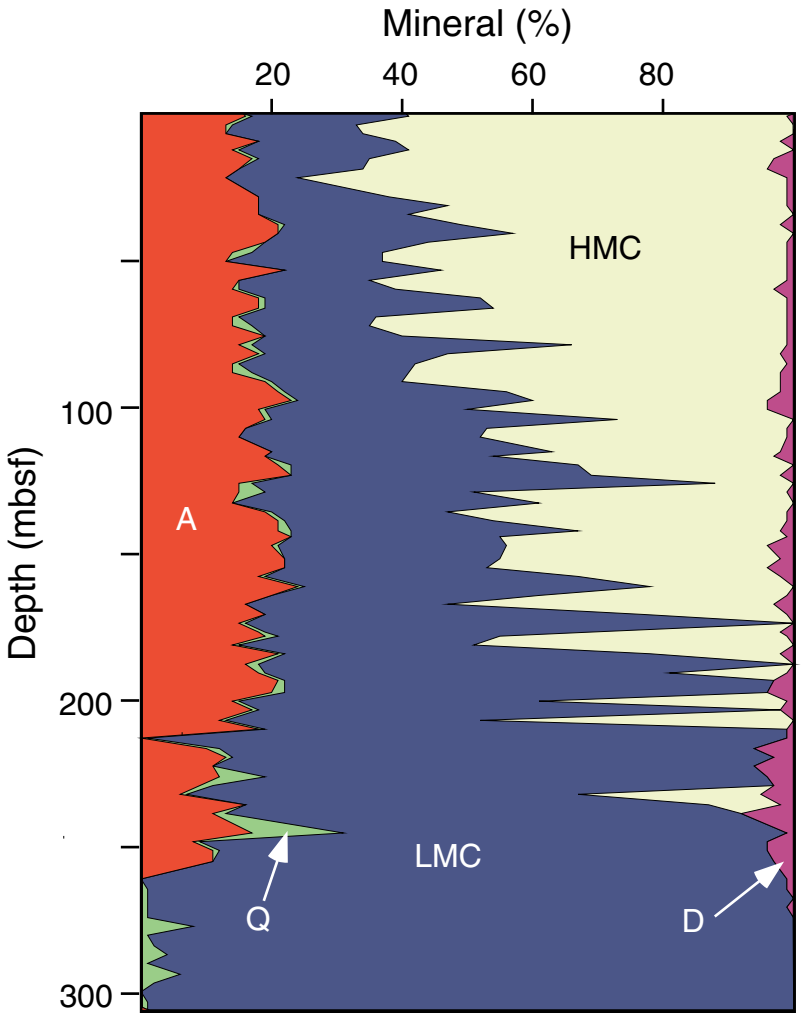

Figure F20. Combined plot of discrete *P*-wave velocities (PWS1 = red, PWS2 = blue, and PWS3 = green), bulk densities (multisensor track = blue; moisture and density = red), porosity, magnetic susceptibility, and natural gamma radiation (NGR). Physical properties units (PP units) are indicated on the right, and core recovery columns are on the left.

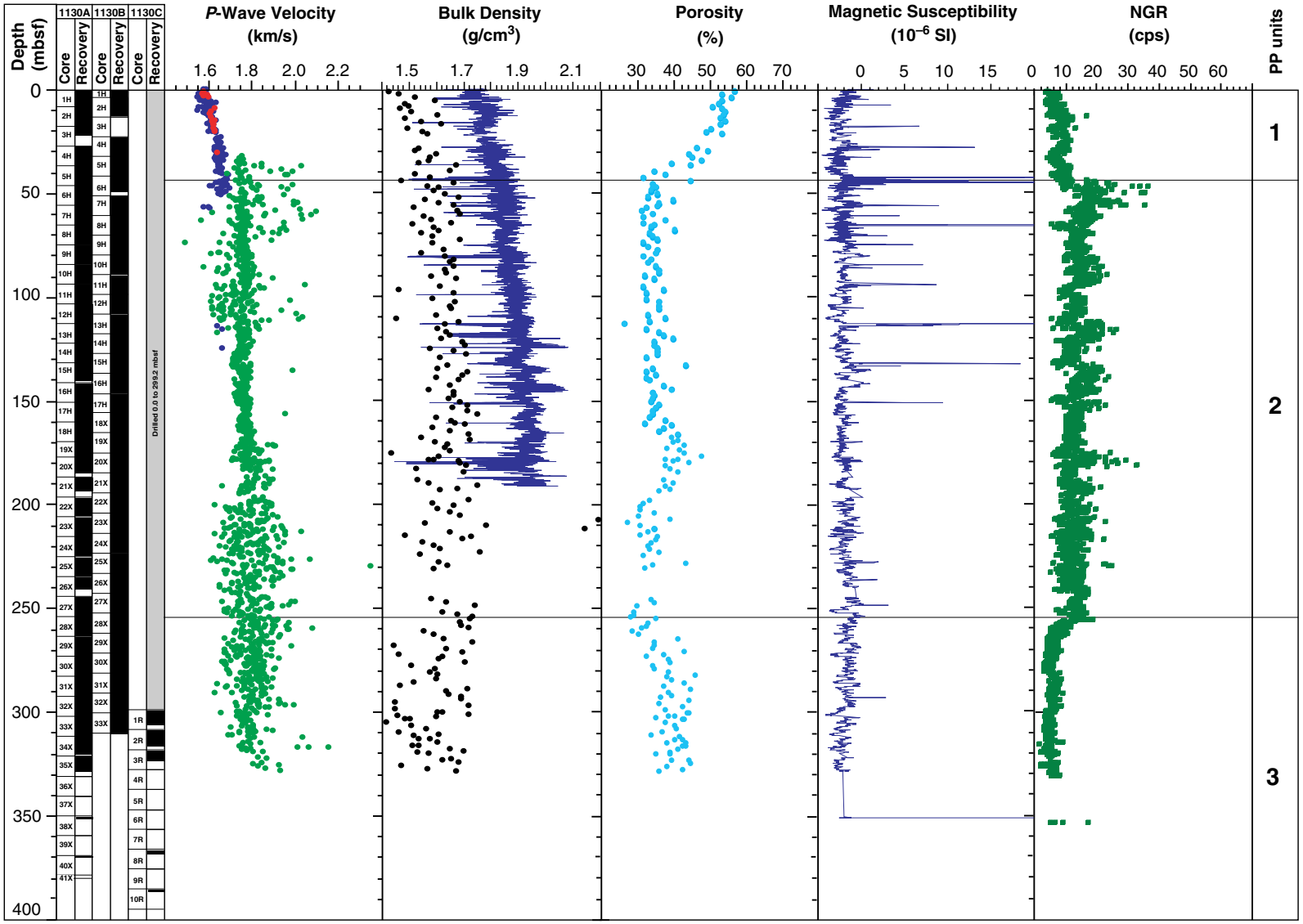

Figure F21. Comparison of downhole logging data and physical properties measurements on recovered sediments. **A.** Natural gamma-ray data (NGR) from the multisensor track (blue dots) and log data (red dots). **B.** Bulk density from GRA densiometry (blue dots) and downhole measurements (red dots). **C.** *P*-wave velocity from discrete measurements (blue dots) and sonic log (red dots). Physical properties units (PP units) are on the right.

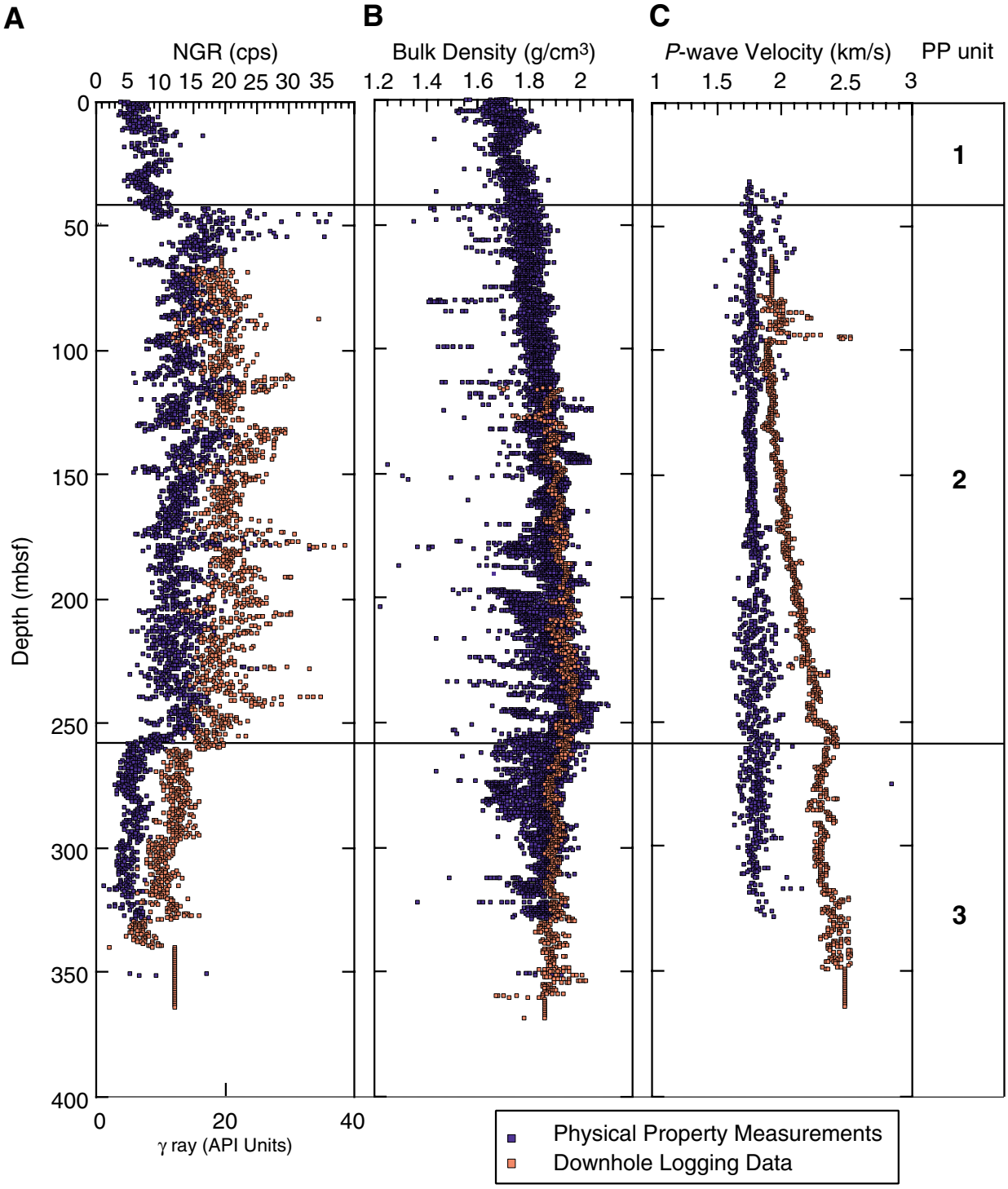

Figure F22. Shear strength measurements from Site 1130. Physical properties units (PP units) are indicated on the right.

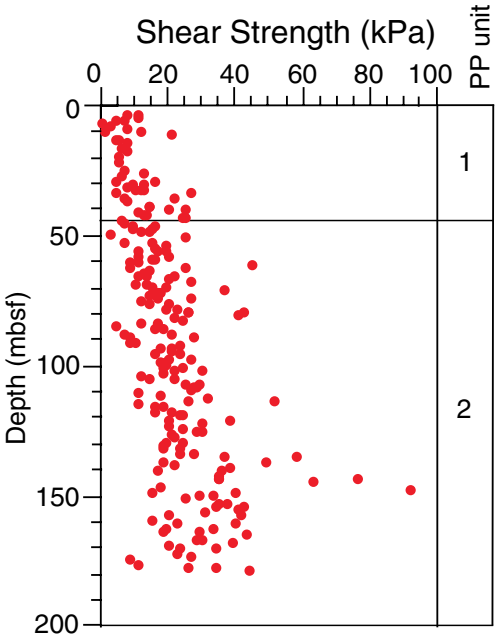

Figure F23. Thermal conductivity (blue squares) and bulk density (red squares) from Site 1130. Physical properties units (PP units) are indicated on the right.

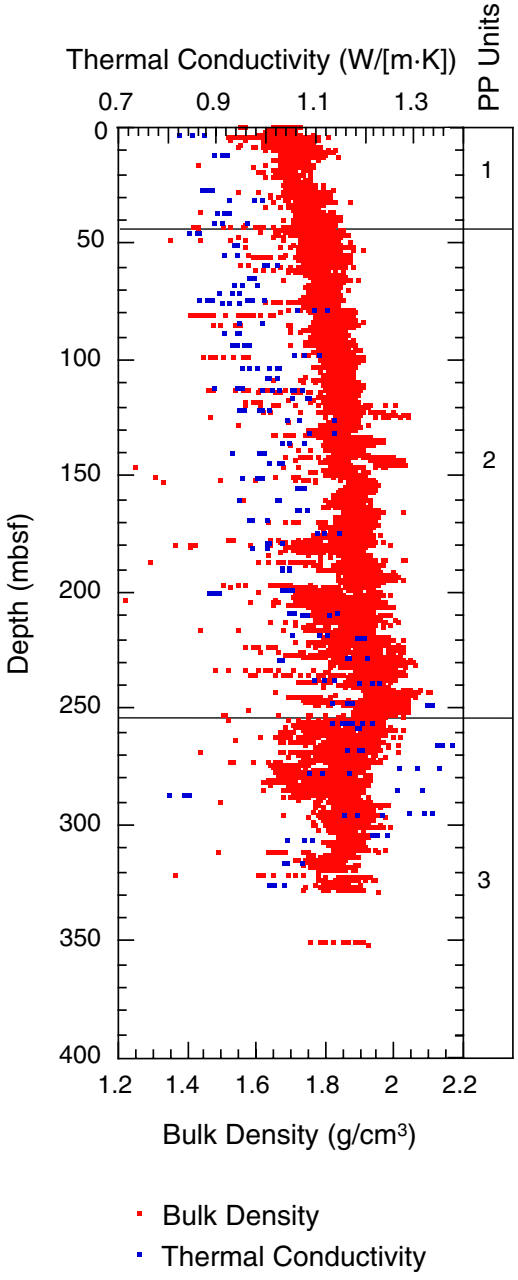

Figure F24. Variation of in situ formation temperature with depth at Site 1130. DVTP = Davis-Villinger temperature probe; Adara = Adara temperature tool.

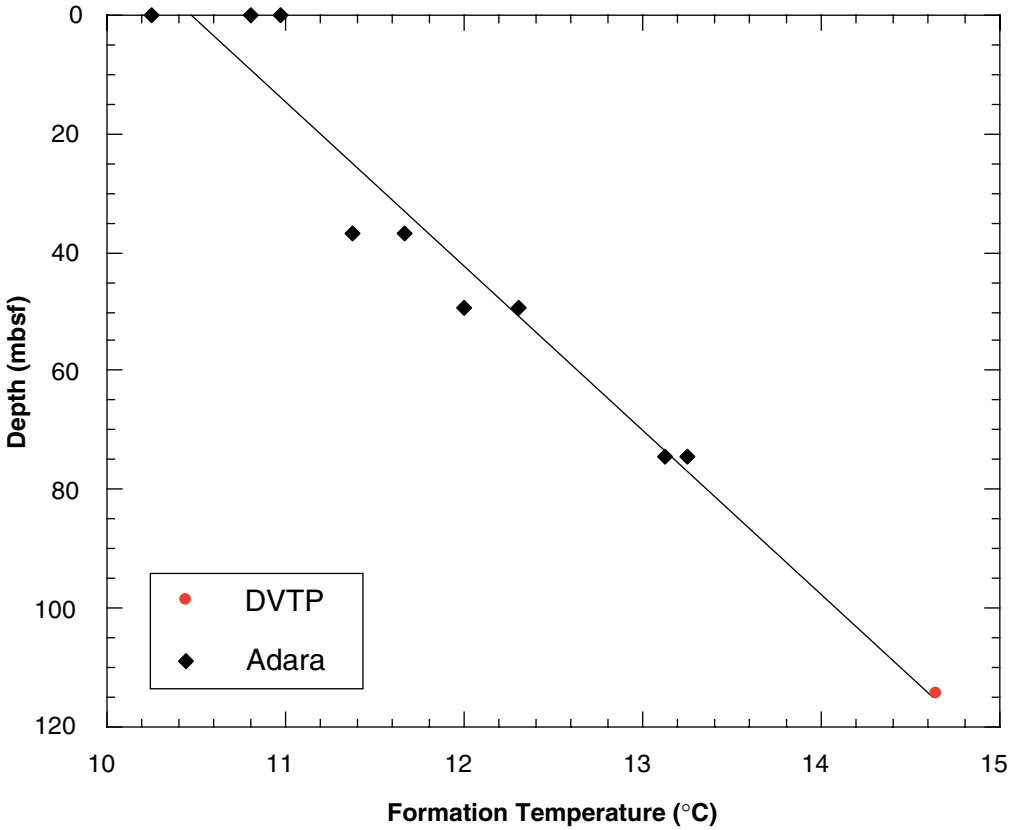

Figure F25. Summary of spectral gamma-ray logs from hostile environment natural gamma-ray sonde (HNGS vs. depth). From left to right, columns are core recovery, total gamma radiation (HSGR) and computed (uranium-free) gamma radiation (HCGR), uranium, thorium, potassium and caliper, logging units, lithostratigraphic units, and biostratigraphic ages.

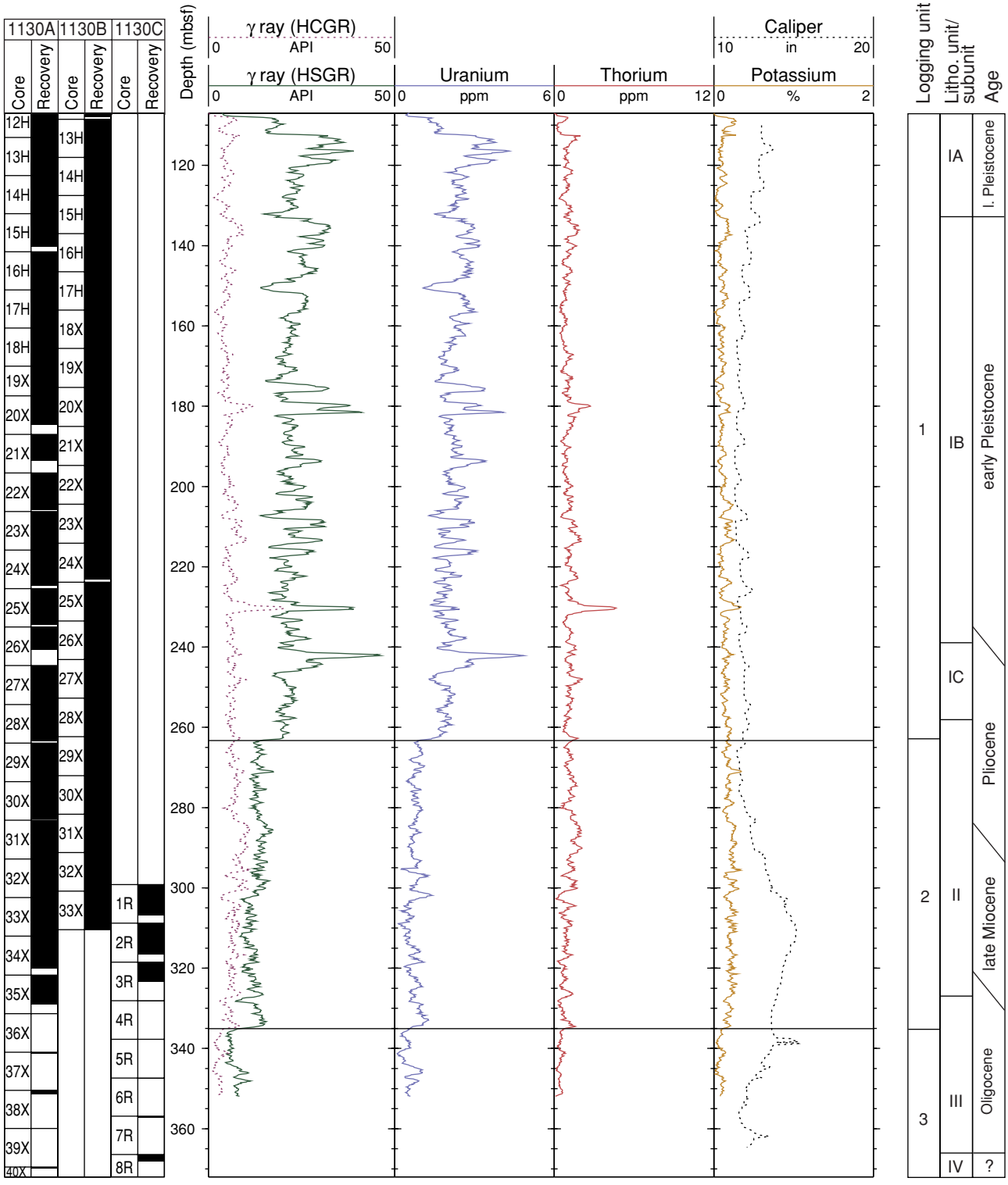

Figure F26. Summary of geophysical logs vs. depth. From left to right, columns are core recovery; gamma radiation (HSGR) and caliper; porosity and density; photoelectric effect (PEF); shallow, medium, and deep resistivity; sonic velocity; logging units; lithostratigraphic units; and biostratigraphic ages.

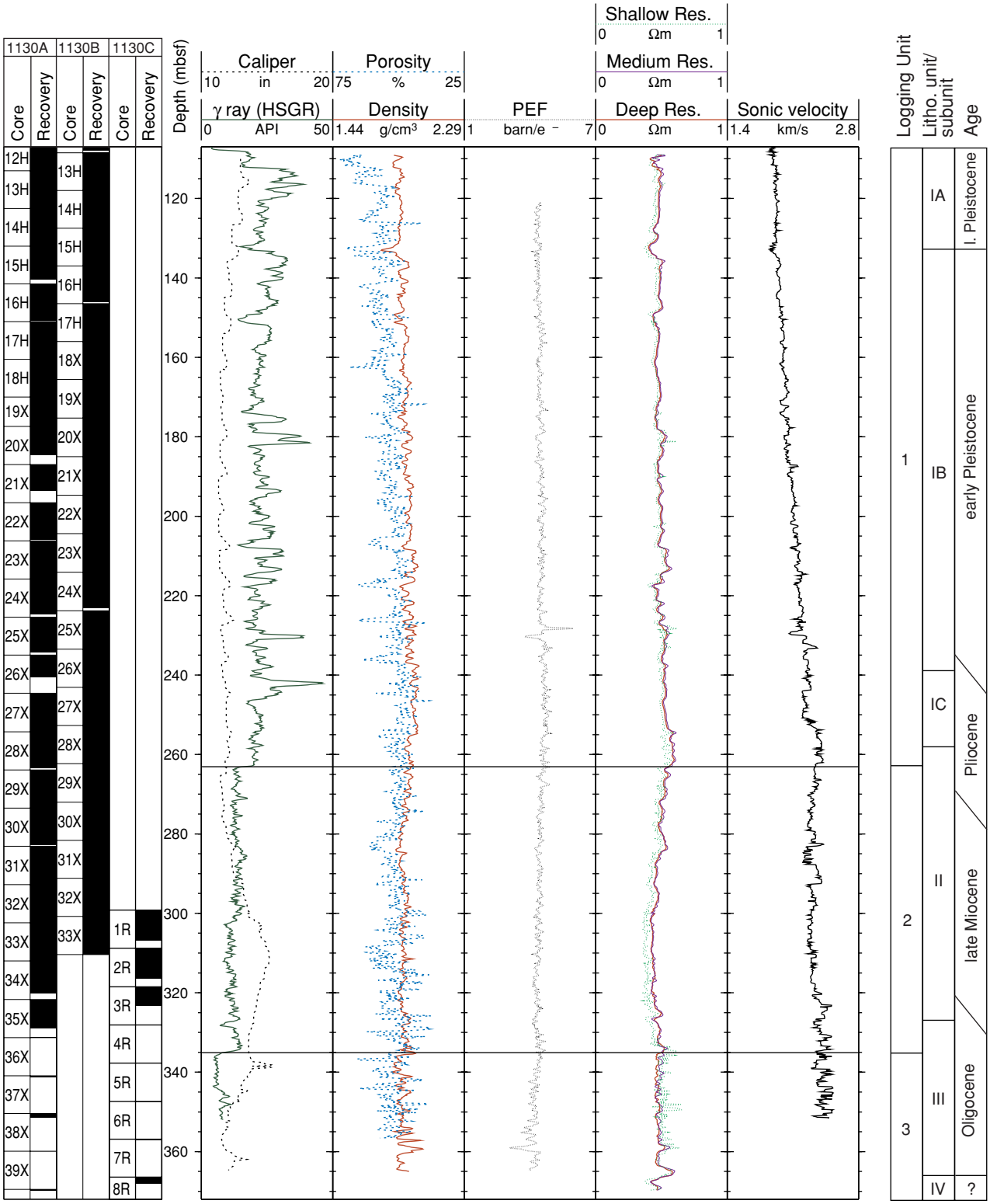

Figure F27. Comparison between geophysical logs and physical properties measured on the recovered cores. From left to right columns are core recovery, gamma radiation from logs (HSGR) and core (natural gamma radiation [NGR]), density from logs and core (gamma-ray attenuation [GRA]), *P*-wave velocity from logs and core, logging units, lithostratigraphic units, and biostratigraphic ages.

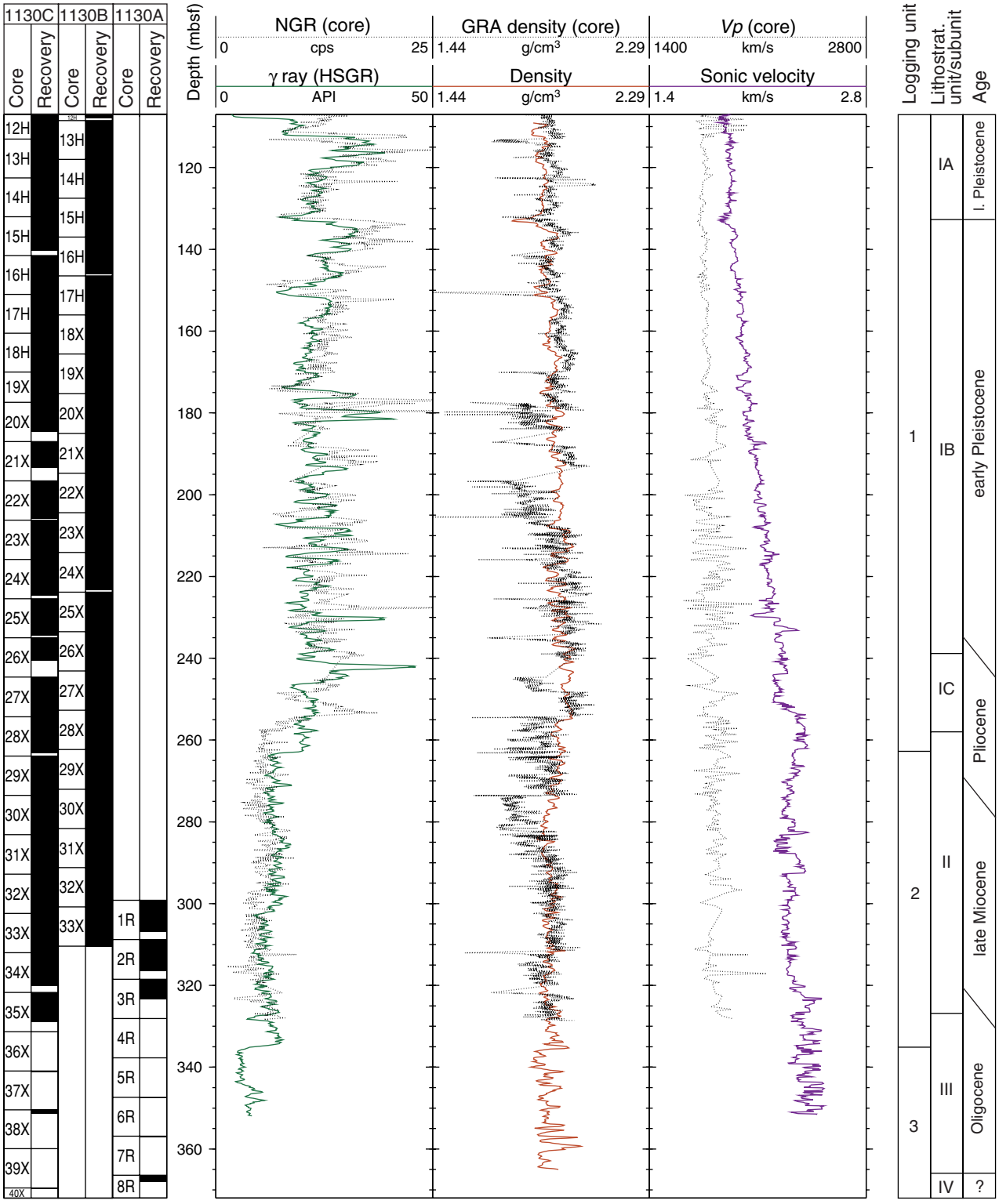

Figure F28. Summary of spectral gamma-ray logs from the hostile environment natural gamma-ray sonde vs. depth plotted on an expanded depth scale to highlight variations in the interval logged through pipe. From left to right, columns are core recovery, total gamma radiation (HSGR) and computed (uranium free) gamma radiation (HCGR), uranium, thorium, potassium, logging units, lithostratigraphic units, and biostratigraphic ages.

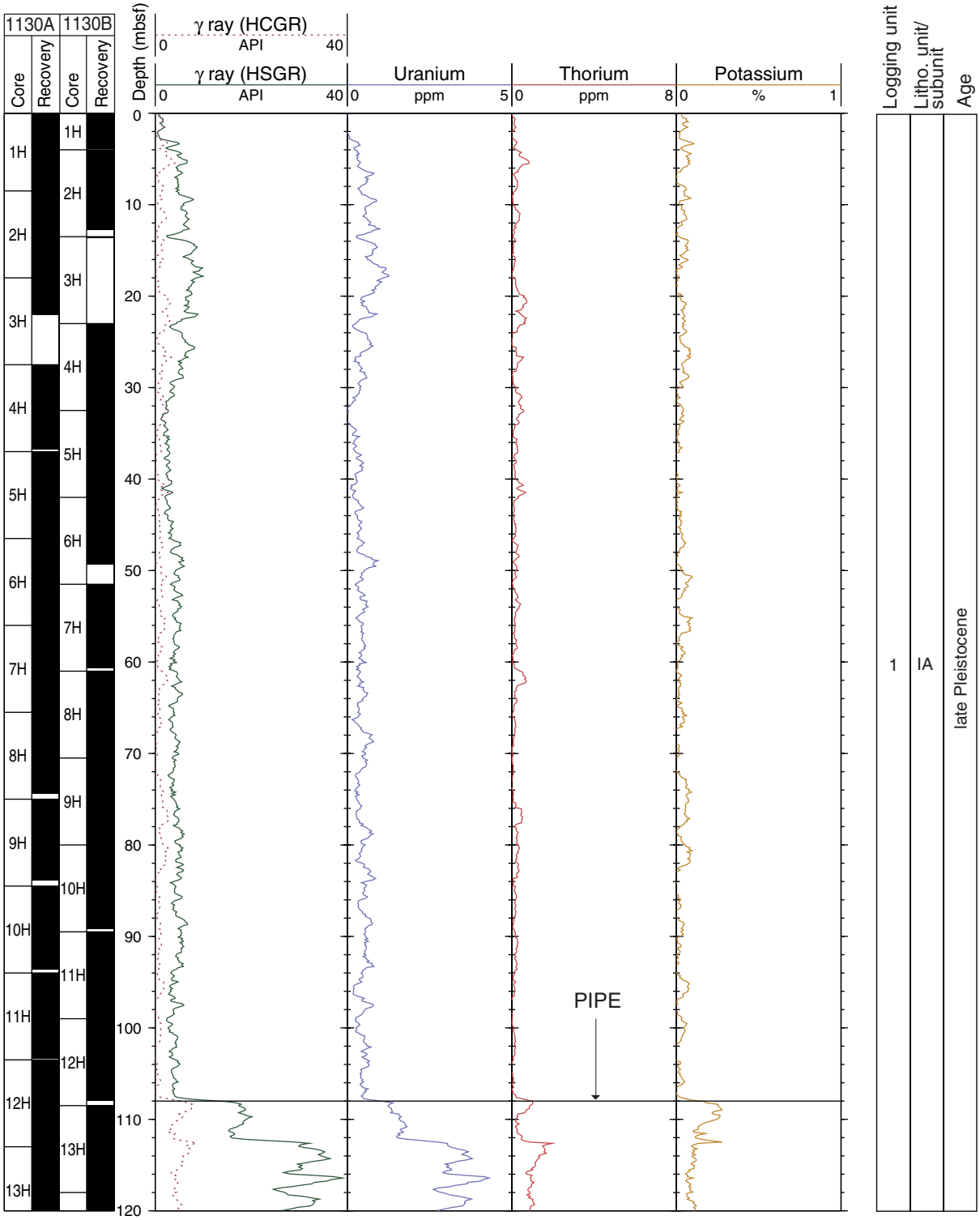

Figure F29. Formation MicroScanner (FMS) image showing the abrupt boundary between logging Units 2 and 3 at 329 mbsf, coinciding with the boundary between lithostratigraphic Units II and III. The depth of this boundary on the FMS images is slightly shallower than the depth measured using conventional logs. This may be an artifact of the triple combination logging tool being run without the wireline heave compensator in this interval. The thinly bedded succession below 329 mbsf represents a sequence of interbedded, thin chert layers (~20 cm) and chalk (1–3 m).

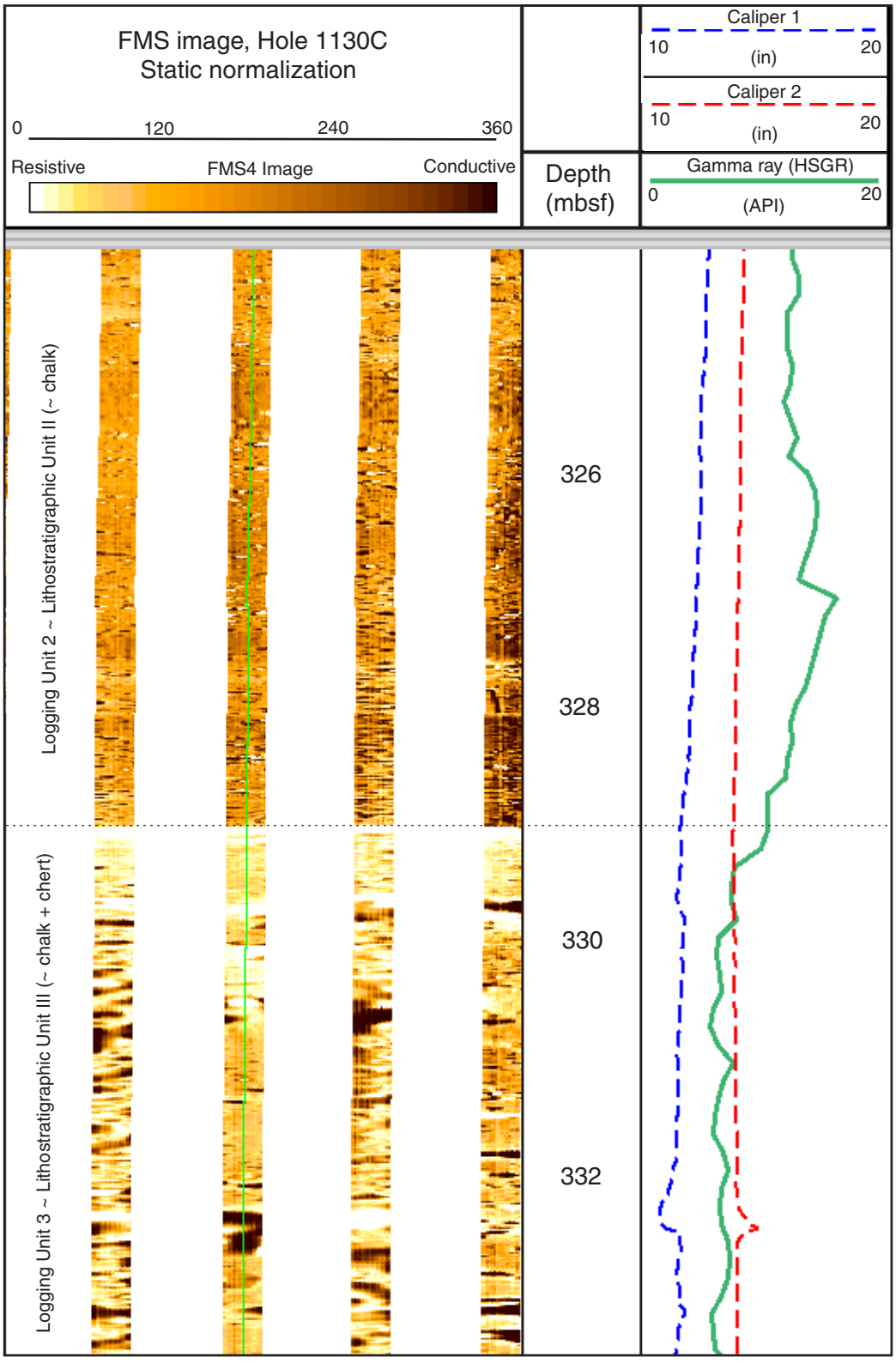

Figure F30. Seismic site-survey tracks for Site 1130 (Line AGSO169/13) in relation to other Leg 182 sites and the Australian Geological Survey Organisation Survey 169 (AGSO169) site-survey seismic lines. The bold trackline (part of AGSO169/13a) corresponds to the seismic line segment shown in Figure **F31,** p. 67.

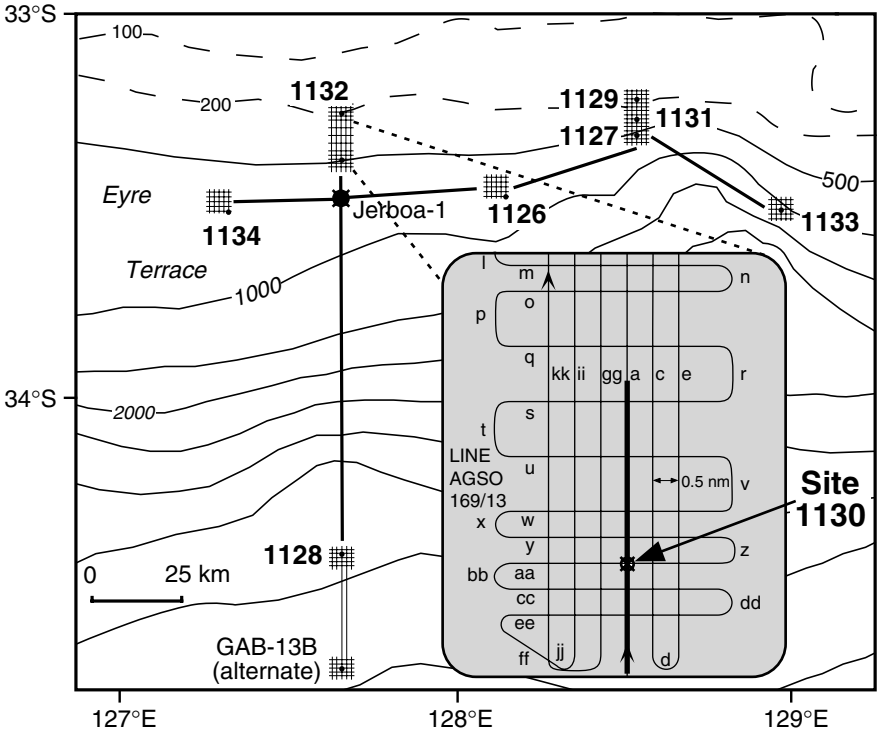

Figure F31. Portion of seismic Line AGSO169/13a showing interpreted seismic stratigraphic sequences planned (shown in white) and actually intersected (shown in black) at Site 1130.

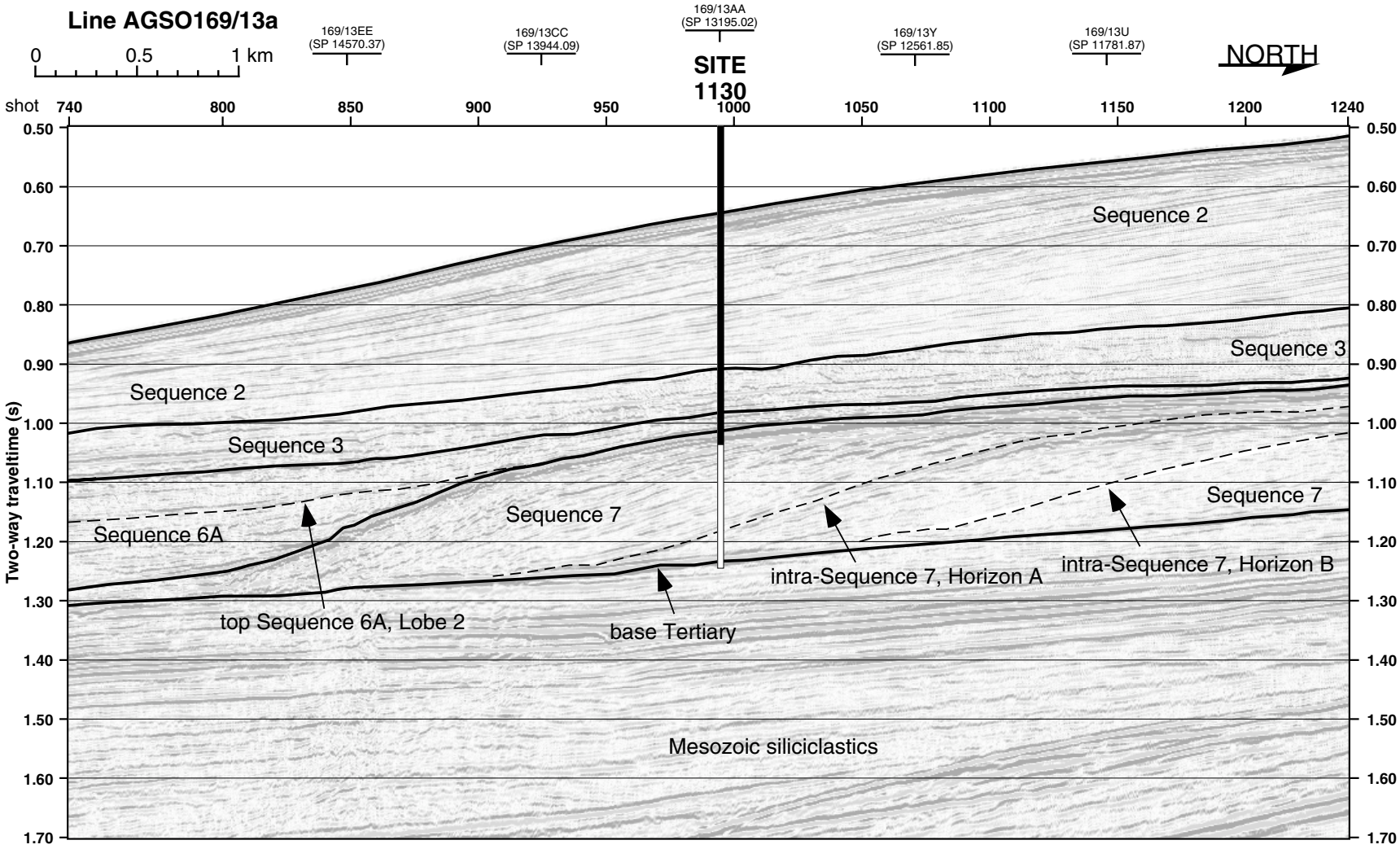

Figure F32. Check-shot stations and acquisition geometry for the well seismic tool (WST) survey at Hole 1130C, with corrected two-way traveltimes (TWT) and derived interval velocities. GI = generator-injector.

Depth (mbrf)	Depth (mbsl)	Transit time (ms)	True path length (m)	Corrected TWT (ms)	Interval velocity (ms)
640.0	628.5	401.92	628.7	805.36	1780.00
670.2	658.7	418.82	658.9	839.29	2041.31
699.9	688.4	433.31	688.6	868.39	2303.19
730.1	718.6	446.36	718.8	894.61	2102.69
760.0	748.5	460.53	748.7	923.05	2348.99
799.8	788.3	477.40	788.5	956.94	2505.43
830.1	818.6	489.45	818.8	981.13	2234.48
858.0	846.5	501.90	846.7	1006.10	

Corrected TWT is TWT from sea level to WST tool along a vertical path

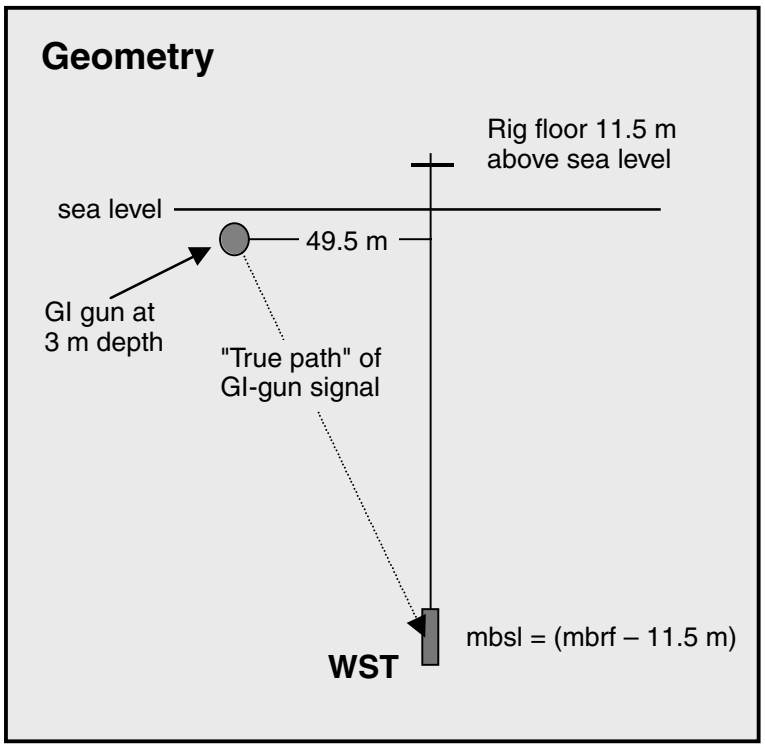

Figure F33. A. Plot showing relationship between predicted depths to key horizons and sequence boundaries (dashed) and corrected depths (arrowed) for Site 1130. Corrected depths are based on the check-shot survey data (heavy solid line), shown plotted immediately below the envelope of stacking velocity curves (derived from six common depth points from site-survey seismic data immediately adjacent to this site). The integrated sonic log, based on interval transit time data, is plotted as a heavy dashed line. **B.** Interval velocities derived from the eight check-shot stations are shown overlying the velocity log (derived from the compressional sonic trace).

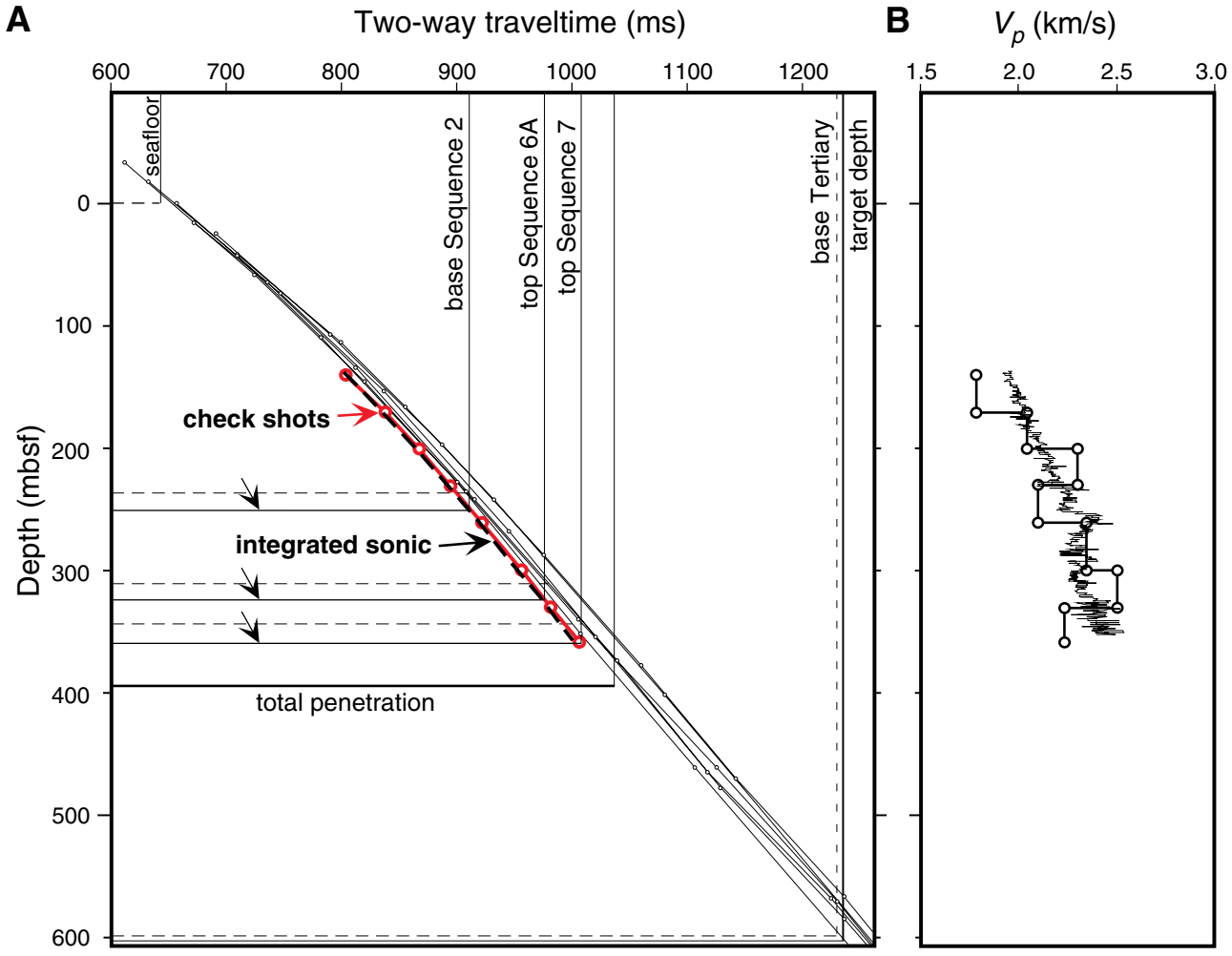

Figure F34. Tentative summary correlation between lithostratigraphic units, seismic sequences, biostratigraphic hiatuses, and ages for Site 1130. ? = seismic data shows missing section corresponding to these surfaces, although biostratigraphic data provide no constraint on the length of missing time.

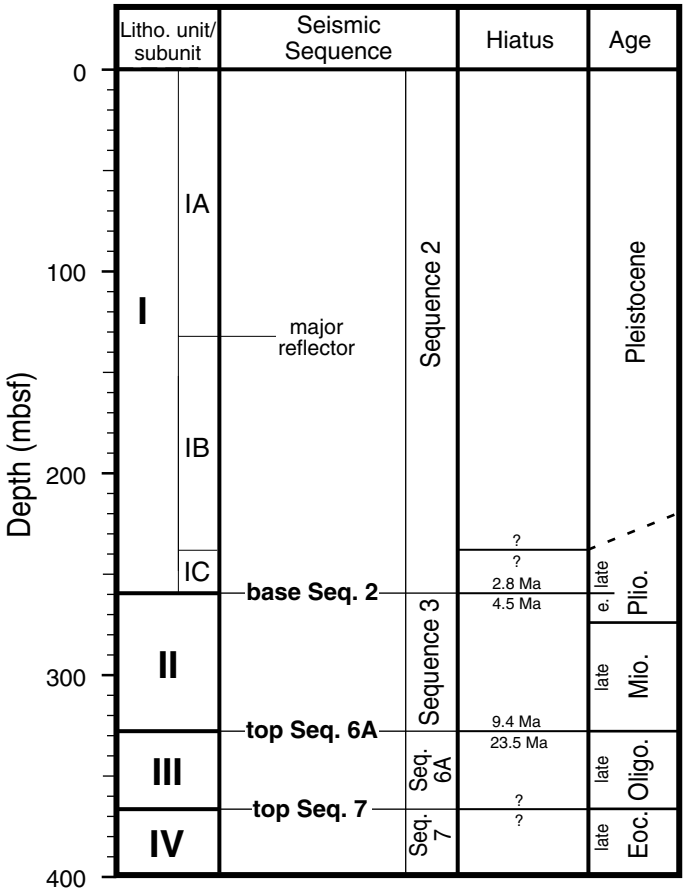

Table T1. Site 1130 coring summary. (See table note. Continued on next two pages.)

Hole 1130A

Latitude: –33.420190° (33°25.2114′S)
Longitude: 127.602330° (127°36.1398′E)
Seafloor (drill-pipe measurement from rig floor, mbrf): 498.0
Distance between rig floor and sea level (m): 11.3
Water depth (drill-pipe measurement from sea level, m): 486.7
Total depth (from rig floor, mbrf): 878.4
Penetration (mbsf): 380.4
Total number of cores: 41
Total length of cored section (m): 380.4
Total core recovered (m): 312.47
Core recovery (%): 82.1

Hole 1130B

Latitude: –33.4201517° (33°25.2091′S)
Longitude: 127.60208° (127°36.1248′E)
Seafloor (drill-pipe measurement from rig floor, mbrf): 499.5
Distance between rig floor and sea level (m): 11.4
Water depth (drill-pipe measurement from sea level, m): 488.1
Total depth (from rig floor, mbrf): 809.9
Penetration (mbsf): 310.4
Total number of cores: 33
Total length of cored section (m): 310.4
Total core recovered (m): 300.8
Core recovery (%): 96.9

Hole 1130C

Latitude: –33.419980° (33°25.1988′S)
Longitude: 127.602080° (127°36.1248′E)
Seafloor (drill-pipe measurement from rig floor, mbrf): 499.5
Distance between rig floor and sea level (m): 11.5
Water depth (drill-pipe measurement from sea level, m): 488.0
Total depth (from rig floor, mbrf): 894.7
Penetration (mbsf): 395.2
Total number of cores: 10
Total length of cored section (m): 96.0
Total number of drilled intervals: 1
Total length of drilled intervals (m): 299.2
Total core recovered (m): 23.3
Core recovery (%): 24.3

Core	Date (Nov 1998)	Time (UTC + 8 hr)	Depth (mbsf)	Length cored (m)	Length recovered (m)	Recovery (%)	Comment
180-1130A-							
1H	12	0215	0.00-8.50	8.5	8.48	99.8	
2H	12	0240	8.50-18.00	9.5	9.53	100.3	
3H	12	0345	18.00-27.50	9.5	3.99	42.0	Oriented
4H	12	0500	27.50-37.00	9.5	9.23	97.2	Oriented
5H	12	0600	37.00-46.50	9.5	10.06	105.9	Oriented
6H	12	0705	46.50-56.00	9.5	9.49	99.9	Oriented
7H	12	0800	56.00-65.50	9.5	9.45	99.5	Oriented
8H	12	0925	65.50-75.00	9.5	8.90	93.7	Oriented
9H	12	1000	75.00-84.50	9.5	8.90	93.7	Oriented
10H	12	1020	84.50-94.00	9.5	9.10	95.8	Oriented
11H	12	1115	94.00-103.50	9.5	9.37	98.6	Oriented
12H	12	1210	103.50-113.00	9.5	9.46	99.6	Oriented
13H	12	1420	113.00-122.50	9.5	9.57	100.7	Oriented; DVTP; top 50 cm maybe disturbed
14H	12	1500	122.50-132.00	9.5	9.44	99.4	Oriented
15H	12	1535	132.00-141.50	9.5	8.35	87.9	Oriented
16H	12	1650	141.50-151.00	9.5	9.41	99.1	Oriented; core liner broke between Sections 2 and 3; ~ 20 cm lost
17H	12	1720	151.00-160.50	9.5	9.83	103.5	Oriented
18H	12	2030	160.50-170.00	9.5	9.91	104.3	Drill over
19X	12	2125	170.00-177.40	7.4	9.73	131.5	
20X	12	2150	177.40-187.00	9.6	7.20	75.0	
21X	12	2220	187.00-196.60	9.6	6.54	68.1	
22X	12	2245	196.60-206.20	9.6	9.28	96.7	
23X	12	2310	206.20-215.80	9.6	9.76	101.7	
24X	12	2340	215.80-225.40	9.6	8.93	93.0	

Table T1 (continued).

Core	Date (Nov 1998)	Time (UTC + 8 hr)	Depth (mbsf)	Length cored (m)	Length recovered (m)	Recovery (%)	Comment
25X	13	0015	225.40-235.00	9.6	8.96	93.3	
26X	13	0045	235.00-244.60	9.6	5.62	58.5	
27X	13	0110	244.60-254.30	9.7	9.70	100.0	
28X	13	0140	254.30-263.90	9.6	8.99	93.7	
29X	13	0215	263.90-273.50	9.6	9.84	102.5	
30X	13	0240	273.50-283.10	9.6	9.38	97.7	
31X	13	0310	283.10-292.80	9.7	9.68	99.8	
32X	13	0345	292.80-302.40	9.6	9.64	100.4	
33X	13	0415	302.40-312.00	9.6	9.70	101.0	
34X	13	0540	312.00-321.70	9.7	8.15	84.0	
35X	13	0720	321.70-331.30	9.6	7.22	75.2	
36X	13	0930	331.30-340.90	9.6	0.06	0.6	
37X	13	1030	340.90-350.40	9.5	0.22	2.3	
38X	13	1135	350.40-359.90	9.5	1.00	10.5	
39X	13	1320	359.90-369.50	9.6	0.03	0.3	
40X	13	1440	369.50-379.10	9.6	0.37	3.9	
41X	13	1645	379.10-380.40	1.3	0.00	0.0	No recovery
Totals:				380.4	312.47	82.1	
180-1130B-							
1H	13	1920	0.00-4.00	4.0	3.93	98.3	
2H	13	1945	4.00-13.50	9.5	8.75	92.1	
3H	13	2030	13.50-23.00	9.5	0.10	1.1	Oriented
4H	13	2100	23.00-32.50	9.5	9.95	104.7	Oriented
5H	13	2130	32.50-42.00	9.5	9.45	99.5	Oriented
6H	13	2240	42.00-51.50	9.5	7.33	77.2	Oriented; extremely disturbed; liner completely destroyed; entire core transferred section by section; liner replaced
7H	13	2345	51.50-61.00	9.5	9.17	96.5	Oriented
8H	14	0035	61.00-70.50	9.5	9.63	101.4	Oriented
9H	14	0120	70.50-80.00	9.5	9.94	104.6	Oriented
10H	14	0150	80.00-89.50	9.5	9.16	96.4	Oriented
11H	14	0220	89.50-99.00	9.5	9.61	101.2	Oriented
12H	14	0255	99.00-108.50	9.5	8.94	94.1	Oriented
13H	14	0325	108.50-118.00	9.5	9.96	104.8	Oriented
14H	14	0350	118.00-127.50	9.5	9.87	103.9	Oriented
15H	14	0420	127.50-137.00	9.5	9.86	103.8	Oriented
16H	14	0455	137.00-146.50	9.5	9.14	96.2	Oriented; liner split at top and bottom; bottom section liner patched; Section 2 patched in new liner
17H	14	0525	146.50-156.00	9.5	9.73	102.4	Oriented
18X	14	0620	156.00-165.60	9.6	9.89	103.0	
19X	14	0645	165.60-175.30	9.7	9.84	101.4	
20X	14	0710	175.30-185.00	9.7	9.66	99.6	
21X	14	0730	185.00-194.70	9.7	9.86	101.7	
22X	14	0755	194.70-204.40	9.7	9.79	100.9	
23X	14	0815	204.40-214.10	9.7	9.66	99.6	
24X	14	0840	214.10-223.80	9.7	9.10	93.8	
25X	14	0855	223.80-233.50	9.7	9.75	100.5	
26X	14	0925	233.50-243.10	9.6	9.78	101.9	
27X	14	0950	243.10-252.70	9.6	9.88	102.9	
28X	14	1020	252.70-262.30	9.6	9.86	102.7	
29X	14	1045	262.30-272.00	9.7	9.85	101.6	
30X	14	1115	272.00-281.60	9.6	9.83	102.4	
31X	14	1150	281.60-291.20	9.6	9.89	103.0	
32X	14	1220	291.20-300.80	9.6	9.88	102.9	
33X	14	1255	300.80-310.40	9.6	9.76	101.7	
Totals:				310.4	300.80	96.9	
180-1130C-							
		*****Drilled from 0 to 299.2 mbsf*****					
1R	15	0340	299.20-308.80	9.6	7.66	79.8	
2R	15	0405	308.80-318.50	9.7	7.65	78.9	
3R	15	0435	318.50-328.10	9.6	4.87	50.7	
4R	15	0510	328.10-337.70	9.6	0.09	0.9	
5R	15	0535	337.70-347.40	9.7	0.04	0.4	
6R	15	0625	347.40-356.90	9.5	0.12	1.3	
7R	15	0700	356.90-366.40	9.5	0.23	2.4	
8R	15	0920	366.40-376.00	9.6	1.63	17.0	
9R	15	1130	376.00-385.60	9.6	0.10	1.0	

Table T1 (continued).

Core	Date (Nov 1998)	Time (UTC + 8 hr)	Depth (mbsf)	Length cored (m)	Length recovered (m)	Recovery (%)	Comment
10R	15	1525	385.60-395.20	9.6	0.91	9.5	
Coring totals:				96.0	23.30	24.3	
Drilled total:				299.2			
Total:				395.2			

Note: UTC = Universal Time Coordinated; DVTP = Davis-Villinger temperature probe.

Table T2. Datum levels used for the calculation of the Site 1130 sedimentation rate.

Datum type	Datum level	Age (Ma)	Midpoint (mbsf)	Stratigraphic error (m)	Fossil group	Datum level code	Upper sample		Lower sample	
							Core, section, interval (cm)	Depth (mbsf)	Core, section, interval (cm)	Depth (mbsf)
							182-1130A-		182-1130A-	
B	*G. hirsuta*	0.45	51.46	4.5	4	1	5H-CC, 9-11	46.96	6H-CC, 0-4	55.95
T	*G. tosaensis*	0.65	136.15	4.2	4	2	14H-CC, 17-20	131.91	15H-CC, 22-25	140.32
	Brunhes/Matuyama	0.78	199.9			3	22X-3, 90	199.9		
B	*G. truncatulinoides*	2	229.52	4.8	4	8	24X-CC, 17-20	224.7	25X-CC, 24-26	234.34
T	*Sphenolithus* spp.	3.62	257.5	1.1	1	9	28X-2, 58-62	256.38	28X-3, 124-128	258.54
T	*R. pseudoumbilicus*	3.75	257.5	1.1	1	10	28X-2, 58-62	256.38	28X-3, 124-128	258.54
T	*Amaurolithus* spp.	4.5	257.5	1.1	1	11	28X-2, 58-62	256.38	28X-3, 124-128	258.54
B	*G. pliozea*	5.6	287.82	4.95	4	12	30X-CC, 31-34	282.88	31X-CC, 31-34	292.75
B	*G. margaritae*	6.4	313.79	1.7	4	13	33X-CC, 29-32	312.07	34X-3, 51-52	315.51
B	*G.* cf. *cibaoensis*	7.8	324.35	4.2	4	14	34X-CC, 36-39	320.12	35X-5, 87-92	328.57
T	*D. bisectus*	23.9	328.77	0.15	1	15	35X-5, 87-92	328.57	35X-CC, 27-30	328.89
T	*C. altus*	26.1	336.21	4.9	1	16	36X-CC, 0-0.1	331.3	37X-CC, 21-22	341.11
T	*Z. labiacrassata*	27.1	346.26	5.14	4	17	37X-CC, 21-22	341.11	38X-CC, 17-20	351.37

Notes: T = top of taxon stratigraphic range, B = bottom of taxon stratigraphic range. Midpoint = is the middle depth between the sample where the taxon occurs and the adjacent sample where it does not occur. Stratigraphic error = one-half the distance between these two samples. Datum level code = the number assigned to the datum level on Figure F7, p. 42. Fossil groups = calcareous nannofossils (1) and planktonic foraminifers (4).

Table T3. Core and section depths in mcd and mbsf, Site 1130. (See table notes. Continued on next six pages.)

Leg	Site	Hole	Core	Type	Section	Depth (mbsf)	Offset	Depth (mcd)
182	1130	A	1	H	1	0.00	0.00	0.00
182	1130	A	1	H	2	1.50	0.00	1.50
182	1130	A	1	H	3	3.00	0.00	3.00
182	1130	A	1	H	4	4.50	0.00	4.50
182	1130	A	1	H	5	6.00	0.00	6.00
182	1130	A	1	H	6	7.50	0.00	7.50
182	1130	A	2	H	1	8.50	–0.30	8.20
182	1130	A	2	H	2	10.00	–0.30	9.70
182	1130	A	2	H	3	11.50	–0.30	11.20
182	1130	A	2	H	4	13.00	–0.30	12.70
182	1130	A	2	H	5	14.50	–0.30	14.20
182	1130	A	2	H	6	16.00	–0.30	15.70
182	1130	A	2	H	7	17.00	–0.30	16.70
182	1130	A	3	H	1	18.00	0.00	18.00
182	1130	A	3	H	2	19.50	0.00	19.50
182	1130	A	3	H	3	21.00	0.00	21.00
182	1130	A	4	H	1	27.50	0.00	27.50
182	1130	A	4	H	2	29.00	0.00	29.00
182	1130	A	4	H	3	30.50	0.00	30.50
182	1130	A	4	H	4	32.00	0.00	32.00
182	1130	A	4	H	5	33.50	0.00	33.50
182	1130	A	4	H	6	35.00	0.00	35.00
182	1130	A	4	H	7	36.00	0.00	36.00
182	1130	A	5	H	1	37.00	0.78	37.78
182	1130	A	5	H	2	38.50	0.78	39.28
182	1130	A	5	H	3	40.00	0.78	40.78
182	1130	A	5	H	4	41.50	0.78	42.28
182	1130	A	5	H	5	43.00	0.78	43.78
182	1130	A	5	H	6	44.50	0.78	45.28
182	1130	A	5	H	7	46.00	0.78	46.78
182	1130	A	6	H	1	46.50	1.55	48.05
182	1130	A	6	H	2	48.00	1.55	49.55
182	1130	A	6	H	3	49.50	1.55	51.05
182	1130	A	6	H	4	51.00	1.55	52.55
182	1130	A	6	H	5	52.50	1.55	54.05
182	1130	A	6	H	6	54.00	1.55	55.55
182	1130	A	6	H	7	55.50	1.55	57.05
182	1130	A	7	H	1	56.00	1.6	57.60
182	1130	A	7	H	2	57.50	1.6	59.10
182	1130	A	7	H	3	59.00	1.6	60.60
182	1130	A	7	H	4	60.50	1.6	62.10
182	1130	A	7	H	5	62.00	1.6	63.60
182	1130	A	7	H	6	63.50	1.6	65.10
182	1130	A	8	H	1	65.50	2.56	68.06
182	1130	A	8	H	2	67.00	2.56	69.56
182	1130	A	8	H	3	68.50	2.56	71.06
182	1130	A	8	H	4	70.00	2.56	72.56
182	1130	A	8	H	5	71.50	2.56	74.06
182	1130	A	8	H	6	73.00	2.56	75.56
182	1130	A	9	H	1	75.00	4.53	79.53
182	1130	A	9	H	2	76.50	4.53	81.03
182	1130	A	9	H	3	78.00	4.53	82.53
182	1130	A	9	H	4	79.50	4.53	84.03
182	1130	A	9	H	5	81.00	4.53	85.53
182	1130	A	9	H	6	82.50	4.53	87.03
182	1130	A	10	H	1	84.50	4.82	89.32
182	1130	A	10	H	2	86.00	4.82	90.82
182	1130	A	10	H	3	87.50	4.82	92.32
182	1130	A	10	H	4	89.00	4.82	93.82
182	1130	A	10	H	5	90.50	4.82	95.32
182	1130	A	10	H	6	92.00	4.82	96.82
182	1130	A	11	H	1	94.00	4.91	98.91
182	1130	A	11	H	2	95.50	4.91	100.41
182	1130	A	11	H	3	97.00	4.91	101.91
182	1130	A	11	H	4	98.50	4.91	103.41
182	1130	A	11	H	5	100.00	4.91	104.91
182	1130	A	11	H	6	101.50	4.91	106.41
182	1130	A	12	H	1	103.50	6.51	110.01

Table T3 (continued).

Leg	Site	Hole	Core	Type	Section	Depth (mbsf)	Offset	Depth (mcd)
182	1130	A	12	H	2	105.00	6.51	111.51
182	1130	A	12	H	3	106.50	6.51	113.01
182	1130	A	12	H	4	108.00	6.51	114.51
182	1130	A	12	H	5	109.50	6.51	116.01
182	1130	A	12	H	6	111.00	6.51	117.51
182	1130	A	12	H	7	112.50	6.51	119.01
182	1130	A	13	H	1	113.00	6.33	119.33
182	1130	A	13	H	2	114.50	6.33	120.83
182	1130	A	13	H	3	116.00	6.33	122.33
182	1130	A	13	H	4	117.50	6.33	123.83
182	1130	A	13	H	5	119.00	6.33	125.33
182	1130	A	13	H	6	120.50	6.33	126.83
182	1130	A	13	H	7	122.00	6.33	128.33
182	1130	A	14	H	1	122.50	6.38	128.88
182	1130	A	14	H	2	123.70	6.38	130.08
182	1130	A	14	H	3	125.20	6.38	131.58
182	1130	A	14	H	4	126.70	6.38	133.08
182	1130	A	14	H	5	128.20	6.38	134.58
182	1130	A	14	H	6	129.70	6.38	136.08
182	1130	A	14	H	7	131.20	6.38	137.58
182	1130	A	15	H	1	132.00	7.07	139.07
182	1130	A	15	H	2	133.50	7.07	140.57
182	1130	A	15	H	3	135.00	7.07	142.07
182	1130	A	15	H	4	136.50	7.07	143.57
182	1130	A	15	H	5	138.00	7.07	145.07
182	1130	A	15	H	6	139.50	7.07	146.57
182	1130	A	16	H	1	141.50	8.54	150.04
182	1130	A	16	H	2	143.00	8.54	151.54
182	1130	A	16	H	3	143.48	8.54	152.02
182	1130	A	16	H	4	144.98	8.54	153.52
182	1130	A	16	H	5	146.48	8.54	155.02
182	1130	A	16	H	6	147.98	8.54	156.52
182	1130	A	16	H	7	149.48	8.54	158.02
182	1130	A	17	H	1	151.00	8.07	159.07
182	1130	A	17	H	2	152.50	8.07	160.57
182	1130	A	17	H	3	154.00	8.07	162.07
182	1130	A	17	H	4	155.50	8.07	163.57
182	1130	A	17	H	5	157.00	8.07	165.07
182	1130	A	17	H	6	158.50	8.07	166.57
182	1130	A	17	H	7	160.00	8.07	168.07
182	1130	A	18	H	1	160.50	8.79	169.29
182	1130	A	18	H	2	162.00	8.79	170.79
182	1130	A	18	H	3	163.50	8.79	172.29
182	1130	A	18	H	4	165.00	8.79	173.79
182	1130	A	18	H	5	166.50	8.79	175.29
182	1130	A	18	H	6	168.00	8.79	176.79
182	1130	A	18	H	7	169.50	8.79	178.29
182	1130	A	19	X	1	170.00	9.17	179.17
182	1130	A	19	X	2	171.50	9.17	180.67
182	1130	A	19	X	3	173.00	9.17	182.17
182	1130	A	19	X	4	174.50	9.17	183.67
182	1130	A	19	X	5	176.00	9.17	185.17
182	1130	A	19	X	6	177.50	9.17	186.67
182	1130	A	19	X	7	178.60	9.17	187.77
182	1130	A	20	X	1	177.40	12.05	189.45
182	1130	A	20	X	2	178.90	12.05	190.95
182	1130	A	20	X	3	180.40	12.05	192.45
182	1130	A	20	X	4	181.90	12.05	193.95
182	1130	A	20	X	5	183.40	12.05	195.45
182	1130	A	21	X	1	187.00	11.71	198.71
182	1130	A	21	X	2	188.50	11.71	200.21
182	1130	A	21	X	3	190.00	11.71	201.71
182	1130	A	21	X	4	191.50	11.71	203.21
182	1130	A	21	X	5	192.50	11.71	204.21
182	1130	A	22	X	1	196.60	13.37	209.97
182	1130	A	22	X	2	198.10	13.37	211.47
182	1130	A	22	X	3	199.60	13.37	212.97
182	1130	A	22	X	4	201.10	13.37	214.47
182	1130	A	22	X	5	202.60	13.37	215.97

Table T3 (continued).

Leg	Site	Hole	Core	Type	Section	Depth (mbsf)	Offset	Depth (mcd)
182	1130	A	22	X	6	204.10	13.37	217.47
182	1130	A	23	X	1	206.20	13.37	219.57
182	1130	A	23	X	2	207.70	13.37	221.07
182	1130	A	23	X	3	209.20	13.37	222.57
182	1130	A	23	X	4	210.70	13.37	224.07
182	1130	A	23	X	5	212.20	13.37	225.57
182	1130	A	23	X	6	213.70	13.37	227.07
182	1130	A	23	X	7	215.20	13.37	228.57
182	1130	A	24	X	1	215.80	12.97	228.77
182	1130	A	24	X	2	217.30	12.97	230.27
182	1130	A	24	X	3	218.80	12.97	231.77
182	1130	A	24	X	4	220.30	12.97	233.27
182	1130	A	24	X	5	221.80	12.97	234.77
182	1130	A	24	X	6	223.30	12.97	236.27
182	1130	A	25	X	1	225.40	12.03	237.43
182	1130	A	25	X	2	226.90	12.03	238.93
182	1130	A	25	X	3	228.40	12.03	240.43
182	1130	A	25	X	4	229.90	12.03	241.93
182	1130	A	25	X	5	231.40	12.03	243.43
182	1130	A	25	X	6	232.90	12.03	244.93
182	1130	A	26	X	1	235.00	11.25	246.25
182	1130	A	26	X	2	236.50	11.25	247.75
182	1130	A	26	X	3	238.00	11.25	249.25
182	1130	A	26	X	4	239.50	11.25	250.75
182	1130	A	27	X	1	244.60	10.73	255.33
182	1130	A	27	X	2	246.10	10.73	256.83
182	1130	A	27	X	3	247.60	10.73	258.33
182	1130	A	27	X	4	249.10	10.73	259.83
182	1130	A	27	X	5	250.60	10.73	261.33
182	1130	A	27	X	6	252.10	10.73	262.83
182	1130	A	27	X	7	253.60	10.73	264.33
182	1130	A	28	X	1	254.30	12.11	266.41
182	1130	A	28	X	2	255.80	12.11	267.91
182	1130	A	28	X	3	257.30	12.11	269.41
182	1130	A	28	X	4	258.80	12.11	270.91
182	1130	A	28	X	5	260.30	12.11	272.41
182	1130	A	28	X	CC	262.67	12.11	274.78
182	1130	A	29	X	1	263.90	12.97	276.87
182	1130	A	29	X	2	265.40	12.97	278.37
182	1130	A	29	X	3	266.90	12.97	279.87
182	1130	A	29	X	4	268.40	12.97	281.37
182	1130	A	29	X	5	269.90	12.97	282.87
182	1130	A	29	X	6	271.40	12.97	284.37
182	1130	A	29	X	7	272.90	12.97	285.87
182	1130	A	30	X	1	273.50	13.43	286.93
182	1130	A	30	X	2	275.00	13.43	288.43
182	1130	A	30	X	3	276.50	13.43	289.93
182	1130	A	30	X	4	278.00	13.43	291.43
182	1130	A	30	X	5	279.50	13.43	292.93
182	1130	A	30	X	6	281.00	13.43	294.43
182	1130	A	30	X	7	282.00	13.43	295.43
182	1130	A	31	X	1	283.10	13.43	296.53
182	1130	A	31	X	2	284.60	13.43	298.03
182	1130	A	31	X	3	286.10	13.43	299.53
182	1130	A	31	X	4	287.60	13.43	301.03
182	1130	A	31	X	5	289.10	13.43	302.53
182	1130	A	31	X	6	290.60	13.43	304.03
182	1130	A	31	X	7	291.80	13.43	305.23
182	1130	A	32	X	1	292.80	14.13	306.93
182	1130	A	32	X	2	294.30	14.13	308.43
182	1130	A	32	X	3	295.80	14.13	309.93
182	1130	A	32	X	4	297.30	14.13	311.43
182	1130	A	32	X	5	298.80	14.13	312.93
182	1130	A	32	X	6	300.30	14.13	314.43
182	1130	A	32	X	7	301.80	14.13	315.93
182	1130	A	33	X	1	302.40	14.59	316.99
182	1130	A	33	X	2	303.90	14.59	318.49
182	1130	A	33	X	3	305.40	14.59	319.99
182	1130	A	33	X	4	306.90	14.59	321.49

Table T3 (continued).

Leg	Site	Hole	Core	Type	Section	Depth (mbsf)	Offset	Depth (mcd)
182	1130	A	33	X	5	308.40	14.59	322.99
182	1130	A	33	X	6	309.90	14.59	324.49
182	1130	A	33	X	7	311.40	14.59	325.99
182	1130	A	34	X	1	312.00	14.59	326.59
182	1130	A	34	X	2	313.50	14.59	328.09
182	1130	A	34	X	3	315.00	14.59	329.59
182	1130	A	34	X	4	316.50	14.59	331.09
182	1130	A	34	X	5	318.00	14.59	332.59
182	1130	A	34	X	6	319.00	14.59	333.59
182	1130	A	35	X	1	321.70	14.59	336.29
182	1130	A	35	X	2	323.20	14.59	337.79
182	1130	A	35	X	3	324.70	14.59	339.29
182	1130	A	35	X	4	326.20	14.59	340.79
182	1130	A	35	X	5	327.70	14.59	342.29
182	1130	B	1	H	1	0.00	0.00	0.00
182	1130	B	1	H	2	1.50	0.00	1.50
182	1130	B	1	H	3	3.00	0.00	3.00
182	1130	B	2	H	1	4.00	1.52	5.52
182	1130	B	2	H	2	5.50	1.52	7.02
182	1130	B	2	H	3	7.00	1.52	8.52
182	1130	B	2	H	4	8.50	1.52	10.02
182	1130	B	2	H	5	10.00	1.52	11.52
182	1130	B	2	H	6	11.50	1.52	13.02
182	1130	B	4	H	1	23.00	1.46	24.46
182	1130	B	4	H	2	24.50	1.46	25.96
182	1130	B	4	H	3	26.00	1.46	27.46
182	1130	B	4	H	4	27.50	1.46	28.96
182	1130	B	4	H	5	29.00	1.46	30.46
182	1130	B	4	H	6	30.50	1.46	31.96
182	1130	B	4	H	7	32.00	1.46	33.46
182	1130	B	5	H	1	32.50	1.98	34.48
182	1130	B	5	H	2	34.00	1.98	35.98
182	1130	B	5	H	3	35.50	1.98	37.48
182	1130	B	5	H	4	37.00	1.98	38.98
182	1130	B	5	H	5	38.50	1.98	40.48
182	1130	B	5	H	6	40.00	1.98	41.98
182	1130	B	5	H	7	41.00	1.98	42.98
182	1130	B	6	H	1	42.00	4.54	46.54
182	1130	B	6	H	2	43.19	4.54	47.73
182	1130	B	6	H	3	44.69	4.54	49.23
182	1130	B	6	H	4	46.19	4.54	50.73
182	1130	B	6	H	5	47.57	4.54	52.11
182	1130	B	6	H	CC	48.80	4.54	53.34
182	1130	B	7	H	1	51.50	2.93	54.43
182	1130	B	7	H	2	53.00	2.93	55.93
182	1130	B	7	H	3	54.50	2.93	57.43
182	1130	B	7	H	4	56.00	2.93	58.93
182	1130	B	7	H	5	57.50	2.93	60.43
182	1130	B	7	H	6	59.00	2.93	61.93
182	1130	B	7	H	7	60.20	2.93	63.13
182	1130	B	8	H	1	61.00	2.88	63.88
182	1130	B	8	H	2	62.50	2.88	65.38
182	1130	B	8	H	3	64.00	2.88	66.88
182	1130	B	8	H	4	65.50	2.88	68.38
182	1130	B	8	H	5	67.00	2.88	69.88
182	1130	B	8	H	6	68.50	2.88	71.38
182	1130	B	8	H	7	70.00	2.88	72.88
182	1130	B	9	H	1	70.50	3.88	74.38
182	1130	B	9	H	2	72.00	3.88	75.88
182	1130	B	9	H	3	73.50	3.88	77.38
182	1130	B	9	H	4	75.00	3.88	78.88
182	1130	B	9	H	5	76.50	3.88	80.38
182	1130	B	9	H	6	78.00	3.88	81.88
182	1130	B	9	H	7	79.50	3.88	83.38
182	1130	B	10	H	1	80.00	4.45	84.45
182	1130	B	10	H	2	81.50	4.45	85.95
182	1130	B	10	H	3	83.00	4.45	87.45
182	1130	B	10	H	4	84.50	4.45	88.95
182	1130	B	10	H	5	86.00	4.45	90.45

Table T3 (continued).

Leg	Site	Hole	Core	Type	Section	Depth (mbsf)	Offset	Depth (mcd)
182	1130	B	10	H	6	87.50	4.45	91.95
182	1130	B	11	H	1	89.50	5.67	95.17
182	1130	B	11	H	2	91.00	5.67	96.67
182	1130	B	11	H	3	92.50	5.67	98.17
182	1130	B	11	H	4	94.00	5.67	99.67
182	1130	B	11	H	5	95.50	5.67	101.17
182	1130	B	11	H	6	97.00	5.67	102.67
182	1130	B	11	H	7	98.50	5.67	104.17
182	1130	B	12	H	1	99.00	7.53	106.53
182	1130	B	12	H	2	100.50	7.53	108.03
182	1130	B	12	H	3	102.00	7.53	109.53
182	1130	B	12	H	4	103.50	7.53	111.03
182	1130	B	12	H	5	105.00	7.53	112.53
182	1130	B	12	H	6	106.50	7.53	114.03
182	1130	B	13	H	1	108.50	8.16	116.66
182	1130	B	13	H	2	110.00	8.16	118.16
182	1130	B	13	H	3	111.50	8.16	119.66
182	1130	B	13	H	4	113.00	8.16	121.16
182	1130	B	13	H	5	114.50	8.16	122.66
182	1130	B	13	H	6	116.00	8.16	124.16
182	1130	B	13	H	7	117.50	8.16	125.66
182	1130	B	14	H	1	118.00	8.84	126.84
182	1130	B	14	H	2	119.50	8.84	128.34
182	1130	B	14	H	3	121.00	8.84	129.84
182	1130	B	14	H	4	122.50	8.84	131.34
182	1130	B	14	H	5	124.00	8.84	132.84
182	1130	B	14	H	6	125.50	8.84	134.34
182	1130	B	14	H	7	127.00	8.84	135.84
182	1130	B	15	H	1	127.50	8.58	136.08
182	1130	B	15	H	2	129.00	8.58	137.58
182	1130	B	15	H	3	130.50	8.58	139.08
182	1130	B	15	H	4	132.00	8.58	140.58
182	1130	B	15	H	5	133.50	8.58	142.08
182	1130	B	15	H	6	135.00	8.58	143.58
182	1130	B	15	H	7	136.50	8.58	145.08
182	1130	B	16	H	1	137.00	9.73	146.73
182	1130	B	16	H	2	137.81	9.73	147.54
182	1130	B	16	H	3	138.91	9.73	148.64
182	1130	B	16	H	4	140.41	9.73	150.14
182	1130	B	16	H	5	141.61	9.73	151.34
182	1130	B	16	H	6	143.11	9.73	152.84
182	1130	B	16	H	7	144.61	9.73	154.34
182	1130	B	17	H	1	146.50	9.69	156.19
182	1130	B	17	H	2	148.00	9.69	157.69
182	1130	B	17	H	3	149.50	9.69	159.19
182	1130	B	17	H	4	151.00	9.69	160.69
182	1130	B	17	H	5	152.50	9.69	162.19
182	1130	B	17	H	6	154.00	9.69	163.69
182	1130	B	17	H	7	155.50	9.69	165.19
182	1130	B	18	X	1	156.00	10.13	166.13
182	1130	B	18	X	2	157.50	10.13	167.63
182	1130	B	18	X	3	159.00	10.13	169.13
182	1130	B	18	X	4	160.50	10.13	170.63
182	1130	B	18	X	5	162.00	10.13	172.13
182	1130	B	18	X	6	163.50	10.13	173.63
182	1130	B	18	X	7	165.00	10.13	175.13
182	1130	B	19	X	1	165.60	11.63	177.23
182	1130	B	19	X	2	167.10	11.63	178.73
182	1130	B	19	X	3	168.60	11.63	180.23
182	1130	B	19	X	4	170.10	11.63	181.73
182	1130	B	19	X	5	171.60	11.63	183.23
182	1130	B	19	X	6	173.10	11.63	184.73
182	1130	B	19	X	7	174.60	11.63	186.23
182	1130	B	20	X	1	175.30	13.31	188.61
182	1130	B	20	X	2	176.80	13.31	190.11
182	1130	B	20	X	3	178.30	13.31	191.61
182	1130	B	20	X	4	179.80	13.31	193.11
182	1130	B	20	X	5	181.30	13.31	194.61
182	1130	B	20	X	6	182.80	13.31	196.11

Table T3 (continued).

Leg	Site	Hole	Core	Type	Section	Depth (mbsf)	Offset	Depth (mcd)
182	1130	B	20	X	7	184.30	13.31	197.61
182	1130	B	20	X	CC	184.62	13.31	197.93
182	1130	B	21	X	1	185.00	13.31	198.31
182	1130	B	21	X	2	186.50	13.31	199.81
182	1130	B	21	X	3	188.00	13.31	201.31
182	1130	B	21	X	4	189.50	13.31	202.81
182	1130	B	21	X	5	191.00	13.31	204.31
182	1130	B	21	X	6	192.50	13.31	205.81
182	1130	B	21	X	7	194.00	13.31	207.31
182	1130	B	22	X	1	194.70	13.31	208.01
182	1130	B	22	X	2	196.20	13.31	209.51
182	1130	B	22	X	3	197.70	13.31	211.01
182	1130	B	22	X	4	199.20	13.31	212.51
182	1130	B	22	X	5	200.70	13.31	214.01
182	1130	B	22	X	6	202.20	13.31	215.51
182	1130	B	22	X	7	203.70	13.31	217.01
182	1130	B	23	X	1	204.40	14.59	218.99
182	1130	B	23	X	2	205.90	14.59	220.49
182	1130	B	23	X	3	207.40	14.59	221.99
182	1130	B	23	X	4	208.90	14.59	223.49
182	1130	B	23	X	5	210.40	14.59	224.99
182	1130	B	23	X	6	211.90	14.59	226.49
182	1130	B	23	X	7	213.40	14.59	227.99
182	1130	B	24	X	1	214.10	14.05	228.15
182	1130	B	24	X	2	215.60	14.05	229.65
182	1130	B	24	X	3	217.10	14.05	231.15
182	1130	B	24	X	4	218.60	14.05	232.65
182	1130	B	24	X	5	220.10	14.05	234.15
182	1130	B	24	X	6	221.60	14.05	235.65
182	1130	B	25	X	1	223.80	12.91	236.71
182	1130	B	25	X	2	225.30	12.91	238.21
182	1130	B	25	X	3	226.80	12.91	239.71
182	1130	B	25	X	4	228.30	12.91	241.21
182	1130	B	25	X	5	229.80	12.91	242.71
182	1130	B	25	X	6	231.30	12.91	244.21
182	1130	B	25	X	7	232.80	12.91	245.71
182	1130	B	26	X	1	233.50	12.91	246.41
182	1130	B	26	X	2	235.00	12.91	247.91
182	1130	B	26	X	3	236.50	12.91	249.41
182	1130	B	26	X	4	238.00	12.91	250.91
182	1130	B	26	X	5	239.50	12.91	252.41
182	1130	B	26	X	6	241.00	12.91	253.91
182	1130	B	26	X	7	242.50	12.91	255.41
182	1130	B	27	X	1	243.10	12.91	256.01
182	1130	B	27	X	2	244.60	12.91	257.51
182	1130	B	27	X	3	246.10	12.91	259.01
182	1130	B	27	X	4	247.60	12.91	260.51
182	1130	B	27	X	5	249.10	12.91	262.01
182	1130	B	27	X	6	250.60	12.91	263.51
182	1130	B	27	X	7	252.10	12.91	265.01
182	1130	B	28	X	1	252.70	12.91	265.61
182	1130	B	28	X	2	254.20	12.91	267.11
182	1130	B	28	X	3	255.70	12.91	268.61
182	1130	B	28	X	4	257.20	12.91	270.11
182	1130	B	28	X	5	258.70	12.91	271.61
182	1130	B	28	X	6	260.20	12.91	273.11
182	1130	B	28	X	7	261.70	12.91	274.61
182	1130	B	28	X	CC	262.16	12.91	275.07
182	1130	B	29	X	1	262.30	12.91	275.21
182	1130	B	29	X	2	263.80	12.91	276.71
182	1130	B	29	X	3	265.30	12.91	278.21
182	1130	B	29	X	4	266.80	12.91	279.71
182	1130	B	29	X	5	268.30	12.91	281.21
182	1130	B	29	X	6	269.80	12.91	282.71
182	1130	B	29	X	7	271.30	12.91	284.21
182	1130	B	30	X	1	272.00	13.55	285.55
182	1130	B	30	X	2	273.50	13.55	287.05
182	1130	B	30	X	3	275.00	13.55	288.55
182	1130	B	30	X	4	276.50	13.55	290.05

Table T3 (continued).

Leg	Site	Hole	Core	Type	Section	Depth (mbsf)	Offset	Depth (mcd)
182	1130	B	30	X	5	278.00	13.55	291.55
182	1130	B	30	X	6	279.50	13.55	293.05
182	1130	B	30	X	7	281.00	13.55	294.55
182	1130	B	30	X	CC	281.42	13.55	294.97
182	1130	B	31	X	1	281.60	13.47	295.07
182	1130	B	31	X	2	283.10	13.47	296.57
182	1130	B	31	X	3	284.60	13.47	298.07
182	1130	B	31	X	4	286.10	13.47	299.57
182	1130	B	31	X	5	287.60	13.47	301.07
182	1130	B	31	X	6	289.10	13.47	302.57
182	1130	B	31	X	7	290.60	13.47	304.07
182	1130	B	32	X	1	291.20	14.03	305.23
182	1130	B	32	X	2	292.70	14.03	306.73
182	1130	B	32	X	3	294.20	14.03	308.23
182	1130	B	32	X	4	295.70	14.03	309.73
182	1130	B	32	X	5	297.20	14.03	311.23
182	1130	B	32	X	6	298.70	14.03	312.73
182	1130	B	32	X	7	300.20	14.03	314.23
182	1130	B	33	X	1	300.80	14.49	315.29
182	1130	B	33	X	2	302.30	14.49	316.79
182	1130	B	33	X	3	303.80	14.49	318.29
182	1130	B	33	X	4	305.30	14.49	319.79
182	1130	B	33	X	5	306.80	14.49	321.29
182	1130	B	33	X	6	308.30	14.49	322.79
182	1130	B	33	X	7	309.80	14.49	324.29
182	1130	B	33	X	CC	310.16	14.49	324.65

Notes: Depths are measured at the top of each section. This table is also available in **ASCII format.**

Table T4. Biostratigraphic data used for correlations, Site 1130.

Datum	Taxon	Age (Ma)	Leg, hole, core, section, interval (cm)	Depth (mbsf)	Leg, hole, core, section, interval (cm)	Depth (mbsf)
FAD	*Globorotalia hirsuta*	0.45	182-1130A-5H-CC, 9	46.96	182-1130A-6H-CC, 0	55.95
FAD	*G. hirsuta*	0.45	182-1130B-5H-CC, 18	41.92	182-1130B-6H-CC, 50	49.30
LAD	*Globorotalia tosaensis*	0.65	182-1130A-14H-CC, 17	131.91	182-1130A-15H-CC, 22	140.32
LAD	*G. tosaensis*	0.65	182-1130B-15H-CC, 12	137.33	182-1130B-16H-CC, 18	146.12
FAD	*Globorotalia truncatulinoides*	2	182-1130A-24X-CC, 17	224.70	182-1130A-25X-CC, 24	234.34
FAD	*G. truncatulinoides*	2	182-1130B-23X-CC, 28	214.03	182-1130B-24X-CC, 15	223.17
LAD	*Reticulofenestra pseudoumbilicus*	3.75	182-1130A-28X-2, 58	256.38	182-1130A-28X-CC, 124	258.54
LAD	*R. pseudoumbilicus*	3.75	182-1130B-27X-CC, 35	252.95	182-1130B-28X-CC, 37	262.53
LAD	*Globorotalia margaritae*	3.58	182-1130A-28X-3, 124	258.54	182-1130A-28X-CC, 59	263.26
LAD	*G. margaritae*	3.58	182-1130B-27X-CC, 35	252.95	182-1130B-28X-CC, 37	262.53
LAD	*Zeagloborotalia nepenthes*	4.2	182-1130A-28X-CC, 59	263.26	182-1130A-29X-CC, 36	273.71
LAD	*Z. nepenthes*	4.2	182-1130B-29X-CC, 32	272.12	182-1130B-30X-CC, 37	281.79
LAD	*Globorotalia pliozea*	5.6	182-1130A-35X-5, 87	328.57	182-1130A-35X-CC, 27	328.89
LAD	*G. pliozea*	5.6	182-1130B-32X-CC, 37	301.05	182-1130B-33X-CC, 37	310.53

Note: FAD = first appearance datum, LAD = last appearance datum.

Table T5. Site 1130 splice tie points.

Site	Hole	Core	Type	Section	Interval (cm)	Depth (mbsf)	Depth (mcd)		Site	Hole	Core	Type	Section	Interval (cm)	Depth (mbsf)	Depth (mcd)
1130	A	1	H	5	36	6.36	6.36	Tie to	1130	B	2	H	1	84	4.84	6.36
1130	B	2	H	3	104	8.04	9.56	Tie to	1130	A	2	H	1	136	9.86	9.56
1130	A	2	H	7	80	17.80	17.50	Append to	1130	A	3	H	1	0	18.00	18.00
1130	A	3	H	3	84	21.84	21.84	Append to	1130	B	4	H	1	0	23.00	24.46
1130	B	4	H	6	91	31.41	32.87	Tie to	1130	A	4	H	4	85	32.87	32.87
1130	A	4	H	6	84	35.84	35.84	Tie to	1130	B	5	H	1	136	33.86	35.84
1130	B	5	H	6	84	40.84	42.82	Tie to	1130	A	5	H	4	53	42.04	42.82
1130	A	5	H	7	64	46.64	47.42	Tie to	1130	B	6	H	1	88	42.88	47.42
1130	B	6	H	3	43	45.12	49.66	Tie to	1130	A	6	H	2	11	48.11	49.66
1130	A	6	H	6	123	55.23	56.78	Tie to	1130	B	7	H	2	82	53.85	56.78
1130	B	7	H	5	75	58.25	61.18	Tie to	1130	A	7	H	3	57.5	59.58	61.18
1130	A	7	H	6	40	63.90	65.50	Tie to	1130	B	8	H	2	12	62.62	65.50
1130	B	8	H	6	123	69.73	72.61	Tie to	1130	A	8	H	4	2	70.05	72.61
1130	A	8	H	5	91	72.41	74.97	Tie to	1130	B	9	H	1	59	71.09	74.97
1130	B	9	H	6	43	78.43	82.31	Tie to	1130	A	9	H	2	122.5	77.78	82.31
1130	A	9	H	6	32	82.82	87.35	Tie to	1130	B	10	H	2	140	82.90	87.35
1130	B	10	H	5	107	87.07	91.52	Tie to	1130	A	10	H	2	67.5	86.70	91.52
1130	A	10	H	6	11	92.11	96.93	Tie to	1130	B	11	H	2	25.5	91.26	96.93
1130	B	11	H	5	4	95.54	101.21	Tie to	1130	A	11	H	2	80	96.30	101.21
1130	A	11	H	6	64	102.14	107.05	Tie to	1130	B	12	H	1	52	99.52	107.05
1130	B	12	H	4	59	104.09	111.62	Tie to	1130	A	12	H	2	11	105.11	111.62
1130	A	12	H	6	27	111.27	117.78	Tie to	1130	B	13	H	1	106.5	109.62	117.78
1130	B	13	H	5	75	115.25	123.41	Tie to	1130	A	13	H	3	100.5	117.08	123.41
1130	A	13	H	6	43	120.93	127.26	Tie to	1130	B	14	H	1	41.5	118.42	127.26
1130	B	14	H	6	100	126.50	135.34	Tie to	1130	A	14	H	5	76	128.96	135.34
1130	A	14	H	6	136	131.06	137.44	Tie to	1130	B	15	H	1	136	128.86	137.44
1130	B	15	H	3	75	131.25	139.83	Tie to	1130	A	15	H	1	68.5	132.76	139.83
1130	A	15	H	6	40	139.90	146.97	Tie to	1130	B	16	H	1	24	137.24	146.97
1130	B	16	H	7	80	145.41	155.14	Tie to	1130	A	16	H	5	12	146.60	155.14
1130	A	16	H	6	123	149.21	157.75	Tie to	1130	B	17	H	2	3.5	148.06	157.75
1130	B	17	H	6	44	154.44	164.13	Tie to	1130	A	17	H	4	56	156.06	164.13
1130	A	17	H	6	44	158.94	167.01	Tie to	1130	B	18	X	1	88	156.88	167.01
1130	B	18	X	3	107	160.07	170.20	Tie to	1130	A	18	H	1	91	161.41	170.20
1130	A	18	H	7	28	169.78	178.57	Tie to	1130	B	19	X	1	133	166.94	178.57
1130	B	19	X	5	43	172.03	183.66	Tie to	1130	A	19	X	3	149	174.49	183.66
1130	A	19	X	7	76	179.36	188.53	Append to	1130	B	20	X	1	0	175.30	188.61
1130	B	20	X	CC	28	184.90	198.21	Append to	1130	B	21	X	1	0	185.00	198.31
1130	B	21	X	7	48	194.48	207.79	Append to	1130	B	22	X	1	0	194.70	208.01
1130	B	22	X	4	40	199.60	212.91	Tie to	1130	A	22	X	2	144	199.54	212.91
1130	A	22	X	7	11	205.61	218.98	Append to	1130	B	23	X	1	0	204.40	218.99
1130	B	23	X	6	116	213.06	227.65	Tie to	1130	A	23	X	6	57	214.28	227.65
1130	A	23	X	6	120	214.90	228.27	Tie to	1130	B	24	X	1	12	214.22	228.27
1130	B	24	X	6	60	222.20	236.25	Tie to	1130	A	24	X	5	148	223.28	236.25
1130	A	24	X	6	96	224.26	237.23	Tie to	1130	B	25	X	1	52	224.32	237.23
1130	B	25	X	7	44	233.24	246.15	Append to	1130	B	26	X	1	0	233.50	246.41
1130	B	26	X	7	44	242.94	255.85	Append to	1130	B	27	X	1	0	243.10	256.01
1130	B	27	X	8	11	252.71	265.62	Append to	1130	B	28	X	1	0	252.70	265.61
1130	B	28	X	CC	28	262.44	275.35	Tie to	1130	B	29	X	1	13	262.44	275.35
1130	B	29	X	5	107	269.37	282.28	Tie to	1130	A	29	X	4	91	269.31	282.28
1130	A	29	X	7	32	273.22	286.19	Tie to	1130	B	30	X	1	64	272.64	286.19
1130	B	30	X	5	16	278.16	291.71	Tie to	1130	A	30	X	4	26	278.28	291.71
1130	A	30	X	7	4	282.04	295.47	Tie to	1130	B	31	X	1	38	282.00	295.47
1130	B	31	X	6	112	290.22	303.69	Tie to	1130	A	31	X	5	116	290.26	303.69
1130	A	31	X	7	28	292.08	305.51	Tie to	1130	B	32	X	1	28	291.48	305.51
1130	B	32	X	6	96	299.66	313.69	Tie to	1130	A	32	X	5	76	299.56	313.69
1130	A	32	X	6	120	301.50	315.63	Tie to	1130	B	33	X	1	33	301.14	315.63
1130	B	33	X	CC	36	310.52	325.01	Append to	1130	A	34	X	1	0	312.00	326.59
1130	A	34	X	6	72	319.72	334.31	Append to	1130	A	35	X	1	0	321.70	336.29
1130	A	35	X	5	88	328.58	343.17									

Note: This table is also available in **ASCII format.**

Table T6. Composition of headspace gases, Site 1130.

Core, section	Depth (mbsf)	C_1 (ppmv)
182-1130A-		
1H-4	4.50	1
2H-4	13.00	5
3H-2	19.50	11
4H-4	32.00	7
5H-4	41.50	6
6H-4	51.00	10
7H-4	60.50	8
8H-4	70.00	9
9H-4	79.50	6
10H-4	89.00	9
11H-4	98.50	5
12H-4	108.00	6
13H-4	117.50	5
14H-4	126.70	5
15H-4	136.50	4
16H-7	150.50	3
17H-4	155.50	3
18H-4	165.00	8
19X-4	174.50	11
20X-3	180.40	8
21X-3	190.00	2
22X-4	201.10	8
23X-4	210.70	3
24X-5	221.80	4
25X-4	229.90	4
26X-2	236.50	3
27X-4	249.10	3
28X-4	258.80	2
29X-4	268.40	2
30X-4	278.00	3
31X-4	287.60	2
32X-4	297.30	2
33X-4	306.90	2
34X-4	316.50	2
35X-4	326.20	2
38X-1	351.20	2
40X-CC	369.80	2
182-1130C-		
1R-4	303.70	3
2R-4	313.30	2
7R-CC	356.90	2

Table T7. Calcium carbonate ($CaCO_3$) content of samples, Site 1130.

Core, section, interval (cm)	Depth (mbsf)	$CaCO_3$ (wt%)
182-1130A-		
1H-1, 60-61	0.60	87.9
1H-3, 60-61	3.60	87.4
1H-5, 60-61	6.60	91.9
2H-1, 60-61	9.10	93.2
2H-3, 60-61	12.10	92.1
2H-5, 60-61	15.10	90.0
3H-1, 60-61	18.60	89.7
3H-3, 60-61	21.60	89.0
4H-1, 60-61	28.10	86.9
4H-3, 60-61	31.10	88.0
4H-5, 60-61	34.10	88.9
5H-1, 60-61	37.60	88.5
5H-3, 60-61	40.60	87.0
5H-5, 60-61	43.60	87.8
6H-1, 61-62	47.11	87.3
6H-3, 61-62	50.11	90.1
6H-5, 61-62	53.11	89.1
7H-1, 60-61	56.60	89.3
7H-3, 60-61	59.60	88.8
7H-5, 60-61	62.60	87.0
8H-1, 60-61	66.10	86.8
8H-3, 60-61	69.10	87.8
8H-5, 60-61	72.10	88.7
9H-1, 60-61	75.60	86.8
9H-3, 60-61	78.60	86.2
9H-5, 61-62	81.61	87.6
10H-1, 60-61	85.10	90.5
10H-3, 60-61	88.10	89.1
10H-5, 60-61	91.10	87.0
11H-1, 60-61	94.60	88.2
11H-3, 60-61	97.60	89.1
11H-5, 60-61	100.60	88.7
12H-1, 60-61	104.10	88.7
12H-3, 60-61	107.10	88.3
12H-5, 60-61	110.10	87.4
13H-2, 60-61	115.10	90.1
13H-3, 60-61	116.60	90.3
13H-5, 60-61	119.60	88.9
14H-1, 60-61	123.10	89.2
14H-3, 60-61	125.80	87.9
14H-5, 60-61	128.80	87.9
15H-1, 60-61	132.60	87.5
15H-3, 60-61	135.60	85.4
15H-5, 60-61	138.60	91.5
16H-1, 60-61	142.10	88.5
16H-3, 60-61	144.08	87.8
16H-5, 60-61	147.08	88.5
17H-1, 60-61	151.60	90.0
17H-3, 60-61	154.60	90.2
17H-5, 60-61	157.60	88.5
18H-1, 60-62	161.10	87.5
18H-3, 60-62	164.10	88.3
18H-5, 60-62	167.10	89.7
19X-1, 60-61	170.60	88.2
19X-3, 60-61	173.60	88.7
19X-5, 60-61	176.60	89.6
20X-1, 60-61	178.00	83.5
20X-3, 60-61	181.00	85.7
20X-5, 60-61	184.00	80.9
21X-1, 60-61	187.60	85.0
21X-3, 60-61	190.60	88.9
21X-5, 60-61	193.10	88.1
22X-1, 60-61	197.20	87.8
22X-3, 60-61	200.20	86.3
22X-5, 60-61	203.20	87.0
23X-1, 60-61	206.80	85.3
23X-3, 60-61	209.80	87.2
23X-5, 60-61	212.80	87.3
24X-1, 60-61	216.40	88.8
24X-3, 60-61	219.40	89.4
24X-5, 60-61	222.40	89.0
25X-1, 60-61	226.00	84.9
25X-3, 60-61	229.00	87.3
25X-5, 60-61	232.00	87.9
26X-1, 60-61	235.60	88.5
26X-3, 60-61	238.60	85.2
27X-1, 60-61	245.20	81.5
27X-3, 60-61	248.20	86.9
27X-5, 60-61	251.20	89.5
28X-1, 60-61	254.90	90.7
28X-5, 62-63	260.92	89.1
29X-1, 60-61	264.50	87.8
29X-3, 60-61	267.50	89.6
29X-5, 60-61	270.50	86.3
30X-1, 60-61	274.10	86.8
30X-3, 60-61	277.10	86.0
30X-5, 60-61	280.10	88.6
31X-1, 60-61	283.70	86.6
31X-3, 60-61	286.70	86.8
31X-5, 60-61	289.70	89.9
32X-1, 60-61	293.40	91.9
32X-3, 60-61	296.40	87.4
32X-5, 60-61	299.40	90.7
33X-1, 60-61	303.00	90.5
33X-3, 60-61	306.00	90.4
33X-5, 60-61	309.00	94.0
34X-1, 62-63	312.62	89.5
34X-3, 60-61	315.60	88.4
34X-5, 60-61	318.60	86.4
35X-1, 60-61	322.30	83.7
35X-3, 60-61	325.30	84.2
35X-5, 60-61	328.30	86.9
182-1130C-		
1R-3, 60-61	302.80	91.0
1R-5, 60-61	305.80	89.3
2R-1, 60-61	309.40	88.0
2R-3, 60-61	312.40	85.0
2R-5, 60-61	315.40	82.1
3R-1, 60-61	319.10	78.7
3R-3, 60-61	322.10	83.8

Table T8. Interstitial water geochemistry, Site 1130.

Core, section	Depth (mbsf)	Ca^{2+} (mM)	Mg^{2+} (mM)	K^{+} (mM)	Li^{+} (µM)	$H_4SiO_4^0$ (µM)	Sr^{2+} (µM)	NH_4^{+} (µM)	Fe^{2+} (µM)	SO_4^{2-} (mM)	Alkalinity (mM)	pH	ppH	Salinity	Cl^{-} (mM)
182-1130A-															
1H-3	4.45	10.5	54.1	11.1	52	128	88	171	0.9	28.1	3.17	7.39	7.78	35	559
2H-3	12.95	11.6	72.4	13.2	63	442	112	1715	9.4	30.0	19.39	6.89	7.03	36	740
3H-1	19.40	12.2	100.7	17.8	96	533	223	3193	6.2	33.5	36.10	6.46	6.50	67	1077
4H-3	31.90	15.2	114.3	21.9	119	633	429	3493	4.7	39.8	34.31	6.37	6.65	79	1273
5H-3	41.40	16.5	118.0	24.1	122	580	500	3508	1.4	44.0	30.82	6.46	6.52	82	1323
6H-3	50.90	17.4	119.2	24.1	123	547	530	3248	0.5	46.3	30.21	6.43	6.57	82	1301
7H-3	60.40	17.2	118.5	24.3	126	564	530	3019	0.0	47.6	28.75	6.38	6.43	82	1337
8H-3	69.90	18.1	119.8	24.0	130	661	524	2802	1.3	50.2	26.40	6.38	6.55	82	1334
9H-3	79.40	19.9	120.8	24.6	120	659	494	2596	1.3	51.9	26.45	6.34	6.55	84	1334
10H-3	88.90	20.8	121.8	24.5	114	666	507	2377	0.0	53.5	24.63	6.41	6.55	83	1332
11H-3	98.40	20.8	120.2	24.1	115	656	485	2237	1.1	53.9	22.60	6.35	6.53	83	1331
12H-3	107.90	21.6	120.1	24.0	114	635	465	2047	0.0	54.1	19.89	6.40	6.53	83	1322
13H-3	117.40	22.1	119.1	23.8	111	603	412	1868	3.2	55.2	19.71	6.40	6.55	83	1323
14H-3	126.60	23.2	120.0	24.3	113	658	436	1763	0.0	55.8	18.05	6.36	6.51	83	1334
15H-3	136.40	26.0	118.6	24.5	110	623	444	1693	0.0	57.0	16.51	6.37		83	1331
17H-3	155.40	26.0	117.5	24.1	112	707	460	1418	0.0	57.5	13.75	6.45		83	1323
19X-3	174.40	31.0	113.4	24.3	113	681	402	1150	0.0	59.1	11.17	6.44	6.60	83	1337
21X-2	189.90	38.2	108.0	24.3	130	662	400	912	13.6	59.9	8.13	6.54		83	1341
23X-3	210.60	42.5	103.2	24.3	129	635	390	525	9.7	60.2	6.15	6.61		83	1328
25X-3	229.80	43.0	102.5	24.3	130	654	398	380	17.3	61.1	5.12	6.72		83	1336
27X-3	249.00	44.5	104.0	25.0	123	684	303	410	3.8	62.6	4.13	6.65		84	1347
29X-3	268.30	44.4	103.6	26.5	117	284	204	254	58.8	63.0	2.78	6.67		82	1336
31X-3	287.50	42.5	101.2	23.4	108	319	202	273	53.0	61.2	2.77	6.74		82	1270
33X-3	306.80	44.8	105.5	24.3	112	712	213	362	52.5	63.6	2.95	6.70		83	1341
35X-3	326.10	46.2	106.0	24.1	112	758	198	198	26.4	63.7	2.49	6.74		84	1334
182-1130C-															
3R-2	321.40	43.7	105.4	23.3	114	732	201	257	23.8	64.0	2.79	6.81		81	1311

Table T9. Summary of X-ray diffraction analysis, Site 1130. (See table note. Continued on next page.)

Leg	Site	Hole	Core	Type	Section	Top (cm)	Bottom (cm)	Depth (mbsf)	Aragonite (wt%)	Quartz (wt%)	LMC (wt%)	HMC (wt%)	Dolerite (wt%)
182	1130	A	1	H	1	60	61	0.60	16	1	24	59	1
182	1130	A	1	H	3	60	61	3.60	13	1	19	67	0
182	1130	A	1	H	5	60	61	6.60	13	0	21	65	0
182	1130	A	2	H	1	60	61	9.10	18	0	21	59	2
182	1130	A	2	H	3	60	61	12.10	14	1	26	59	0
182	1130	A	2	H	5	60	61	15.10	17	1	17	62	3
182	1130	A	3	H	1	60	61	18.60	15	0	19	62	4
182	1130	A	3	H	3	60	61	21.60	13	0	11	75	1
182	1130	A	4	H	1	60	61	28.10	18	0	20	61	1
182	1130	A	4	H	3	60	61	31.10	18	0	29	52	1
182	1130	A	4	H	5	60	61	34.10	18	0	23	59	0
182	1130	A	5	H	1	60	61	37.60	21	0	28	48	2
182	1130	A	5	H	3	60	61	40.60	21	0	36	42	0
182	1130	A	5	H	5	60	61	43.60	19	0	24	55	1
182	1130	A	6	H	1	61	62	47.11	14	3	20	63	1
182	1130	A	6	H	3	61	62	50.11	13	0	24	62	1
182	1130	A	6	H	5	61	62	53.11	22	1	23	53	1
182	1130	A	7	H	1	60	61	56.60	15	0	21	64	1
182	1130	A	7	H	3	60	61	59.60	14	1	24	59	3
182	1130	A	7	H	5	60	61	62.60	18	1	33	47	1
182	1130	A	8	H	1	60	61	66.10	18	1	35	46	1
182	1130	A	8	H	3	60	61	69.10	14	1	21	63	1
182	1130	A	8	H	5	60	61	72.10	14	3	18	64	1
182	1130	A	9	H	1	60	61	75.60	19	0	21	59	1
182	1130	A	9	H	3	60	61	78.60	15	1	49	34	1
182	1130	A	9	H	5	61	62	81.61	18	1	28	51	2
182	1130	A	10	H	1	60	61	85.10	14	0	28	56	1
182	1130	A	10	H	3	60	61	88.10	14	2	24	57	2
182	1130	A	10	H	5	60	61	91.10	19	1	20	57	2
182	1130	A	11	H	1	60	61	94.60	21	1	34	42	2
182	1130	A	11	H	3	60	61	97.60	23	0	36	36	4
182	1130	A	11	H	5	60	61	100.60	18	2	31	46	4
182	1130	A	12	H	1	60	61	104.10	19	1	52	27	0
182	1130	A	12	H	3	60	61	107.10	16	0	37	45	1
182	1130	A	12	H	5	60	61	110.10	15	0	36	48	1
182	1130	A	13	H	2	60	61	115.10	20	1	43	35	2
182	1130	A	13	H	3	60	61	116.60	19	0	34	43	3
182	1130	A	13	H	5	60	61	119.60	21	2	43	33	0
182	1130	A	14	H	1	60	61	123.10	23	1	46	29	2
182	1130	A	14	H	3	60	61	125.80	15	2	71	12	0
182	1130	A	14	H	5	60	61	128.80	15	4	32	48	1
182	1130	A	15	H	1	60	61	132.60	14	1	46	39	0
182	1130	A	15	H	3	60	61	135.60	19	0	27	52	1
182	1130	A	15	H	5	60	61	138.60	21	1	32	45	1
182	1130	A	16	H	1	60	61	142.10	21	2	45	31	2
182	1130	A	16	H	3	60	61	144.08	23	1	32	43	1
182	1130	A	16	H	5	60	61	147.08	20	1	35	41	4
182	1130	A	17	H	1	60	61	151.60	22	0	32	44	2
182	1130	A	17	H	3	60	61	154.60	22	1	31	43	4
182	1130	A	17	X	5	60	61	157.60	18	0	49	31	2
182	1130	A	18	X	1	60	62	161.10	24	1	53	22	0
182	1130	A	18	X	3	60	62	164.10	20	0	41	39	1
182	1130	A	18	X	5	60	62	167.10	16	0	32	49	3
182	1130	A	19	X	1	60	61	170.60	19	1	58	21	1
182	1130	A	19	X	3	60	61	173.60	15	1	84	0	0
182	1130	A	19	X	5	60	61	176.60	18	1	50	29	2
182	1130	A	20	X	1	60	61	178.00	19	2	33	44	1
182	1130	A	20	X	3	60	61	181.00	14	1	36	48	0
182	1130	A	20	X	5	60	61	184.00	21	0	56	20	2
182	1130	A	21	X	1	60	61	187.60	16	2	82	0	0
182	1130	A	21	X	3	60	61	190.60	18	1	62	18	1
182	1130	A	21	X	5	60	61	193.10	21	1	76	0	3
182	1130	A	22	X	1	60	61	197.20	20	2	74	0	4
182	1130	A	22	X	3	60	61	200.20	14	1	46	38	1
182	1130	A	22	X	5	60	61	203.20	17	1	79	0	2
182	1130	A	23	X	1	60	61	206.80	12	1	40	47	0
182	1130	A	23	X	3	60	61	209.80	18	1	80	0	1
182	1130	A	23	X	5	60	61	212.80	0	1	98	0	1

Table T9 (continued).

Leg	Site	Hole	Core	Type	Section	Top (cm)	Bottom (cm)	Depth (mbsf)	Aragonite (wt%)	Quartz (wt%)	LMC (wt%)	HMC (wt%)	Dolerite (wt%)
182	1130	A	24	X	1	60	61	216.40	10	2	81	0	6
182	1130	A	24	X	3	60	61	219.40	13	1	83	0	3
182	1130	A	24	X	5	60	61	222.40	11	1	83	0	6
182	1130	A	25	X	1	60	61	226.00	12	7	77	0	4
182	1130	A	25	X	3	60	61	229.00	9	1	86	0	3
182	1130	A	25	X	5	60	61	232.00	6	1	59	28	5
182	1130	A	26	X	1	60	61	235.60	16	1	70	12	2
182	1130	A	26	X	3	60	61	238.60	11	2	79	0	8
182	1130	A	27	X	1	60	61	245.20	17	14	68	0	1
182	1130	A	27	X	3	60	61	248.20	8	1	87	0	4
182	1130	A	27	X	5	60	61	251.20	11	0	85	0	4
182	1130	A	28	X	1	60	61	254.90	11	0	85	0	3
182	1130	A	28	X	5	62	63	260.92	0	0	98	0	1
182	1130	A	29	X	1	60	61	264.50	0	1	99	0	1
182	1130	A	29	X	3	60	61	267.50	0	1	99	0	0
182	1130	A	29	X	5	60	61	270.50	0	1	99	0	1
182	1130	A	30	X	1	60	61	274.10	0	1	99	0	0
182	1130	A	30	X	3	60	61	277.10	0	8	92	0	0
182	1130	A	30	X	5	60	61	280.10	0	1	99	0	0
182	1130	A	31	X	1	60	61	283.70	0	2	98	0	0
182	1130	A	31	X	3	60	61	286.70	0	4	96	0	0
182	1130	A	31	X	5	60	61	289.70	0	1	99	0	0
182	1130	A	32	X	1	60	61	293.40	0	6	94	0	0
182	1130	A	32	X	3	60	61	296.40	0	2	98	0	0
182	1130	A	32	X	5	60	61	299.40	0	0	100	0	0
182	1130	A	33	X	1	60	61	303.00	0	1	99	0	0
182	1130	A	33	X	3	60	61	306.00	0	1	99	0	0
182	1130	A	33	X	5	60	61	309.00	0	0	100	0	0
182	1130	A	34	X	1	62	63	312.62	0	1	98	0	1
182	1130	A	34	X	3	60	61	315.60	0	0	99	0	1
182	1130	A	34	X	5	60	61	318.60	0	1	98	0	1
182	1130	A	35	X	1	60	61	322.30	0	1	99	0	0
182	1130	A	35	X	3	60	61	325.30	0	1	98	0	1
182	1130	A	35	X	5	60	61	328.30	0	1	99	0	0

Note: This table is also available in **ASCII format.**

Table T10. *P*-wave velocity measurements from the multisensor track, Site 1130.

Leg	Site	Hole	Core	Type	Section	Interval (cm)	Depth (mbsf)	V_p (km/s)
182	1130	A	1	H	1	3.0	0.03	3.0265
182	1130	A	1	H	1	7.0	0.07	3.8854
182	1130	A	1	H	1	15.0	0.15	3.8478
182	1130	A	1	H	1	19.0	0.19	3.8501
182	1130	A	1	H	1	23.0	0.23	3.8591
182	1130	A	1	H	1	27.0	0.27	3.8546
182	1130	A	1	H	1	31.0	0.31	3.8568
182	1130	A	1	H	1	35.0	0.35	3.8523
182	1130	A	1	H	1	39.0	0.39	3.8433
182	1130	A	1	H	1	43.0	0.43	3.8523
182	1130	A	1	H	1	51.0	0.51	3.8411
182	1130	A	1	H	1	55.0	0.55	3.8122
182	1130	A	1	H	1	59.0	0.59	3.8411
182	1130	A	1	H	1	63.0	0.63	3.8321
182	1130	A	1	H	1	67.0	0.67	3.8144
182	1130	A	1	H	1	71.0	0.71	3.8210
182	1130	A	1	H	1	75.0	0.75	3.8109
182	1130	A	1	H	1	79.0	0.79	3.8065
182	1130	A	1	H	1	83.0	0.83	3.8309
182	1130	A	1	H	1	87.0	0.87	3.8242
182	1130	A	1	H	1	91.0	0.91	3.8109
182	1130	A	1	H	1	95.0	0.95	3.8198
182	1130	A	1	H	1	99.0	0.99	3.8153
182	1130	A	1	H	1	103.0	1.03	3.8264
182	1130	A	1	H	1	107.0	1.07	3.8242
182	1130	A	1	H	1	111.0	1.11	3.8131
182	1130	A	1	H	1	115.0	1.15	3.8264
182	1130	A	1	H	1	119.0	1.19	3.8176
182	1130	A	1	H	1	123.0	1.23	3.8109
182	1130	A	1	H	1	127.0	1.27	3.8053
182	1130	A	1	H	1	131.0	1.31	3.8230
182	1130	A	1	H	1	135.0	1.35	3.7002
182	1130	A	1	H	1	139.0	1.39	3.8399
182	1130	A	1	H	1	143.0	1.43	3.8267
182	1130	A	1	H	1	147.0	1.47	3.6289
182	1130	A	1	H	2	3.0	1.53	1.4846
182	1130	A	1	H	2	7.0	1.57	3.8763
182	1130	A	1	H	2	11.0	1.61	3.8637
182	1130	A	1	H	2	15.0	1.65	3.8546
182	1130	A	1	H	2	19.0	1.69	3.8466
182	1130	A	1	H	2	23.0	1.73	3.8466
182	1130	A	1	H	2	27.0	1.77	3.8198
182	1130	A	1	H	2	31.0	1.81	3.8331
182	1130	A	1	H	2	35.0	1.85	3.8255
182	1130	A	1	H	2	39.0	1.89	3.7902
182	1130	A	1	H	2	43.0	1.93	3.7837
182	1130	A	1	H	2	47.0	1.97	3.8255
182	1130	A	1	H	2	51.0	2.01	3.8344
182	1130	A	1	H	2	55.0	2.05	3.8366
182	1130	A	1	H	2	59.0	2.09	3.8188
182	1130	A	1	H	2	63.0	2.13	3.7837
182	1130	A	1	H	2	67.0	2.17	3.8100
182	1130	A	1	H	2	71.0	2.21	3.8078
182	1130	A	1	H	2	75.0	2.25	3.7968
182	1130	A	1	H	2	79.0	2.29	3.8122
182	1130	A	1	H	2	83.0	2.33	1.6649
182	1130	A	1	H	2	87.0	2.37	3.8065
182	1130	A	1	H	2	91.0	2.41	3.7911
182	1130	A	1	H	2	95.0	2.45	1.9337
182	1130	A	1	H	2	99.0	2.49	3.7943
182	1130	A	1	H	2	103.0	2.53	3.4118
182	1130	A	1	H	2	107.0	2.57	3.7987
182	1130	A	1	H	2	111.0	2.61	3.7803
182	1130	A	1	H	2	115.0	2.65	3.7933

Note: Only a portion of this table appears here. The complete table is available in **ASCII format.**

Table T11. Gamma-ray attenuation densiometry measurements from the multisensor track, Site 1130.

Leg	Site	Hole	Core	Type	Section	Interval (cm)	Depth (mbsf)	Density (g/cm^3)	Corrected density (g/cm^3)
182	1130	A	1	H	1	3.0	0.03	1.63	1.55
182	1130	A	1	H	1	7.0	0.07	1.72	1.65
182	1130	A	1	H	1	11.0	0.11	1.74	1.67
182	1130	A	1	H	1	15.0	0.15	1.76	1.70
182	1130	A	1	H	1	19.0	0.19	1.76	1.69
182	1130	A	1	H	1	23.0	0.23	1.77	1.70
182	1130	A	1	H	1	27.0	0.27	1.77	1.71
182	1130	A	1	H	1	31.0	0.31	1.77	1.71
182	1130	A	1	H	1	35.0	0.35	1.79	1.73
182	1130	A	1	H	1	39.0	0.39	1.77	1.71
182	1130	A	1	H	1	43.0	0.43	1.74	1.67
182	1130	A	1	H	1	47.0	0.47	1.72	1.66
182	1130	A	1	H	1	51.0	0.51	1.75	1.69
182	1130	A	1	H	1	55.0	0.55	1.74	1.67
182	1130	A	1	H	1	59.0	0.59	1.75	1.69
182	1130	A	1	H	1	63.0	0.63	1.72	1.66
182	1130	A	1	H	1	67.0	0.67	1.75	1.69
182	1130	A	1	H	1	71.0	0.71	1.72	1.65
182	1130	A	1	H	1	75.0	0.75	1.71	1.64
182	1130	A	1	H	1	79.0	0.79	1.73	1.66
182	1130	A	1	H	1	83.0	0.83	1.72	1.66
182	1130	A	1	H	1	87.0	0.87	1.70	1.64
182	1130	A	1	H	1	91.0	0.91	1.73	1.67
182	1130	A	1	H	1	95.0	0.95	1.70	1.64
182	1130	A	1	H	1	99.0	0.99	1.74	1.68
182	1130	A	1	H	1	103.0	1.03	1.73	1.67
182	1130	A	1	H	1	107.0	1.07	1.73	1.67
182	1130	A	1	H	1	111.0	1.11	1.71	1.64
182	1130	A	1	H	1	115.0	1.15	1.74	1.67
182	1130	A	1	H	1	119.0	1.19	1.71	1.64
182	1130	A	1	H	1	123.0	1.23	1.71	1.64
182	1130	A	1	H	1	127.0	1.27	1.73	1.66
182	1130	A	1	H	1	131.0	1.31	1.71	1.65
182	1130	A	1	H	1	135.0	1.35	1.72	1.65
182	1130	A	1	H	1	139.0	1.39	1.71	1.64
182	1130	A	1	H	1	143.0	1.43	1.72	1.65
182	1130	A	1	H	1	147.0	1.47	1.73	1.67
182	1130	A	1	H	2	3.0	1.53	1.74	1.68
182	1130	A	1	H	2	7.0	1.57	1.71	1.65
182	1130	A	1	H	2	11.0	1.61	1.72	1.66
182	1130	A	1	H	2	15.0	1.65	1.72	1.66
182	1130	A	1	H	2	19.0	1.69	1.71	1.65
182	1130	A	1	H	2	23.0	1.73	1.73	1.66
182	1130	A	1	H	2	27.0	1.77	1.74	1.67
182	1130	A	1	H	2	31.0	1.81	1.74	1.67
182	1130	A	1	H	2	35.0	1.85	1.72	1.65
182	1130	A	1	H	2	39.0	1.89	1.74	1.68
182	1130	A	1	H	2	43.0	1.93	1.70	1.64
182	1130	A	1	H	2	47.0	1.97	1.78	1.72
182	1130	A	1	H	2	51.0	2.01	1.72	1.66
182	1130	A	1	H	2	55.0	2.05	1.70	1.64
182	1130	A	1	H	2	59.0	2.09	1.72	1.66
182	1130	A	1	H	2	63.0	2.13	1.74	1.68
182	1130	A	1	H	2	67.0	2.17	1.72	1.66
182	1130	A	1	H	2	71.0	2.21	1.73	1.67
182	1130	A	1	H	2	75.0	2.25	1.73	1.66
182	1130	A	1	H	2	79.0	2.29	1.74	1.68
182	1130	A	1	H	2	83.0	2.33	1.74	1.68
182	1130	A	1	H	2	87.0	2.37	1.75	1.69
182	1130	A	1	H	2	91.0	2.41	1.72	1.66
182	1130	A	1	H	2	95.0	2.45	1.76	1.70
182	1130	A	1	H	2	99.0	2.49	1.74	1.68
182	1130	A	1	H	2	103.0	2.53	1.72	1.66

Note: Only a portion of this table appears here. The complete table is available in **ASCII format.**

Table T12. Magnetic susceptibility measurements from the multisensor track, Site 1130.

Leg	Site	Hole	Core	Type	Section	Interval (cm)	Depth (mbsf)	Magnetic susceptibility (10^{-6}; SI units)	Corrected susceptibility (10^{-6}; SI units)
182	1130	A	1	H	1	3.0	0.03	0.9	0.9
182	1130	A	1	H	1	11.0	0.11	–1.1	–1.1
182	1130	A	1	H	1	19.0	0.19	–1.2	–1.2
182	1130	A	1	H	1	27.0	0.27	–1.5	–1.5
182	1130	A	1	H	1	35.0	0.35	–1.8	–1.8
182	1130	A	1	H	1	43.0	0.43	–1.8	–1.8
182	1130	A	1	H	1	51.0	0.51	–1.6	–1.6
182	1130	A	1	H	1	59.0	0.59	–2.0	–2.0
182	1130	A	1	H	1	67.0	0.67	–1.2	–1.2
182	1130	A	1	H	1	75.0	0.75	–1.6	–1.6
182	1130	A	1	H	1	83.0	0.83	–1.9	–1.9
182	1130	A	1	H	1	91.0	0.91	–2.0	–2.0
182	1130	A	1	H	1	99.0	0.99	–2.1	–2.1
182	1130	A	1	H	1	107.0	1.07	–1.9	–1.9
182	1130	A	1	H	1	115.0	1.15	–1.9	–1.9
182	1130	A	1	H	1	123.0	1.23	–2.4	–2.4
182	1130	A	1	H	1	131.0	1.31	–2.0	–2.0
182	1130	A	1	H	1	139.0	1.39	–2.1	–2.1
182	1130	A	1	H	1	147.0	1.47	–1.9	–1.9
182	1130	A	1	H	2	3.0	1.53	–1.2	–1.2
182	1130	A	1	H	2	11.0	1.61	–1.4	–1.4
182	1130	A	1	H	2	19.0	1.69	–1.4	–1.4
182	1130	A	1	H	2	27.0	1.77	–1.3	–1.3
182	1130	A	1	H	2	35.0	1.85	–1.8	–1.8
182	1130	A	1	H	2	43.0	1.93	–1.7	–1.7
182	1130	A	1	H	2	51.0	2.01	–1.6	–1.6
182	1130	A	1	H	2	59.0	2.09	–1.5	–1.5
182	1130	A	1	H	2	67.0	2.17	–1.6	–1.6
182	1130	A	1	H	2	75.0	2.25	–1.9	–1.9
182	1130	A	1	H	2	83.0	2.33	–1.8	–1.8
182	1130	A	1	H	2	91.0	2.41	–2.2	–2.2
182	1130	A	1	H	2	99.0	2.49	–2.3	–2.3
182	1130	A	1	H	2	107.0	2.57	–1.8	–1.8
182	1130	A	1	H	2	115.0	2.65	–2.5	–2.5
182	1130	A	1	H	2	123.0	2.73	–2.6	–2.6
182	1130	A	1	H	2	131.0	2.81	–2.4	–2.4
182	1130	A	1	H	2	139.0	2.89	–2.4	–2.4
182	1130	A	1	H	3	3.0	3.03	–0.4	–0.4
182	1130	A	1	H	3	11.0	3.11	–0.6	–0.6
182	1130	A	1	H	3	19.0	3.19	–1.0	–1.0
182	1130	A	1	H	3	27.0	3.27	–1.1	–1.1
182	1130	A	1	H	3	35.0	3.35	–1.5	–1.5
182	1130	A	1	H	3	43.0	3.43	–1.7	–1.7
182	1130	A	1	H	3	51.0	3.51	–1.8	–1.8
182	1130	A	1	H	3	59.0	3.59	–1.8	–1.8
182	1130	A	1	H	3	67.0	3.67	–1.7	–1.7
182	1130	A	1	H	3	75.0	3.75	–2.1	–2.1
182	1130	A	1	H	3	83.0	3.83	–2.3	–2.3
182	1130	A	1	H	3	91.0	3.91	–1.8	–1.8
182	1130	A	1	H	3	99.0	3.99	–2.4	–2.4
182	1130	A	1	H	3	107.0	4.07	–2.1	–2.1
182	1130	A	1	H	3	115.0	4.15	–2.8	–2.8
182	1130	A	1	H	3	123.0	4.23	–2.7	–2.7
182	1130	A	1	H	3	131.0	4.31	–2.8	–2.8
182	1130	A	1	H	3	139.0	4.39	–3.4	–3.4
182	1130	A	1	H	4	3.0	4.53	–1.4	–1.4
182	1130	A	1	H	4	11.0	4.61	–1.5	–1.5
182	1130	A	1	H	4	19.0	4.69	–1.7	–1.7
182	1130	A	1	H	4	27.0	4.77	–1.5	–1.5
182	1130	A	1	H	4	35.0	4.85	–1.8	–1.8
182	1130	A	1	H	4	43.0	4.93	–2.0	–2.0
182	1130	A	1	H	4	51.0	5.01	–2.2	–2.2
182	1130	A	1	H	4	59.0	5.09	–2.3	–2.3
182	1130	A	1	H	4	67.0	5.17	–2.3	–2.3

Note: Only a portion of this table appears here. The complete table is available in **ASCII format.**

Table T13. Natural gamma-ray measurements from the multisensor track, Site 1130.

Leg	Site	Hole	Core	Type	Section	Interval (cm)	Depth (mbsf)	NGR (cps)
182	1130	A	1	H	1	11.0	0.11	3.69
182	1130	A	1	H	1	27.0	0.27	4.27
182	1130	A	1	H	1	43.0	0.43	4.69
182	1130	A	1	H	1	59.0	0.59	5.35
182	1130	A	1	H	1	75.0	0.75	5.77
182	1130	A	1	H	1	91.0	0.91	5.96
182	1130	A	1	H	1	107.0	1.07	7.85
182	1130	A	1	H	1	123.0	1.23	5.85
182	1130	A	1	H	1	139.0	1.39	6.65
182	1130	A	1	H	2	11.0	1.61	5.62
182	1130	A	1	H	2	27.0	1.77	5.92
182	1130	A	1	H	2	43.0	1.93	6.50
182	1130	A	1	H	2	59.0	2.09	5.42
182	1130	A	1	H	2	75.0	2.25	6.77
182	1130	A	1	H	2	91.0	2.41	4.96
182	1130	A	1	H	2	107.0	2.57	5.69
182	1130	A	1	H	2	123.0	2.73	5.81
182	1130	A	1	H	3	11.0	3.11	6.27
182	1130	A	1	H	3	27.0	3.27	5.89
182	1130	A	1	H	3	43.0	3.43	7.19
182	1130	A	1	H	3	59.0	3.59	5.85
182	1130	A	1	H	3	75.0	3.75	6.04
182	1130	A	1	H	3	91.0	3.91	3.85
182	1130	A	1	H	3	107.0	4.07	5.39
182	1130	A	1	H	3	123.0	4.23	5.77
182	1130	A	1	H	4	11.0	4.61	5.77
182	1130	A	1	H	4	27.0	4.77	4.50
182	1130	A	1	H	4	43.0	4.93	5.42
182	1130	A	1	H	4	59.0	5.09	5.31
182	1130	A	1	H	4	75.0	5.25	3.54
182	1130	A	1	H	4	91.0	5.41	5.50
182	1130	A	1	H	4	107.0	5.57	5.46
182	1130	A	1	H	4	123.0	5.73	6.35
182	1130	A	1	H	4	139.0	5.89	5.65
182	1130	A	1	H	5	11.0	6.11	9.46
182	1130	A	1	H	5	27.0	6.27	8.27
182	1130	A	1	H	5	43.0	6.43	8.77
182	1130	A	1	H	5	59.0	6.59	6.31
182	1130	A	1	H	5	75.0	6.75	7.23
182	1130	A	1	H	5	91.0	6.91	7.31
182	1130	A	1	H	5	107.0	7.07	8.46
182	1130	A	1	H	5	123.0	7.23	6.50
182	1130	A	1	H	6	11.0	7.61	5.19
182	1130	A	1	H	6	27.0	7.77	6.15
182	1130	A	1	H	6	43.0	7.93	5.39
182	1130	A	1	H	6	59.0	8.09	5.96
182	1130	A	2	H	1	11.0	8.61	6.77
182	1130	A	2	H	1	27.0	8.77	7.50
182	1130	A	2	H	1	43.0	8.93	5.65
182	1130	A	2	H	1	59.0	9.09	7.23
182	1130	A	2	H	1	75.0	9.25	9.08
182	1130	A	2	H	1	91.0	9.41	9.96
182	1130	A	2	H	1	107.0	9.57	7.54
182	1130	A	2	H	1	123.0	9.73	7.08
182	1130	A	2	H	1	139.0	9.89	6.81
182	1130	A	2	H	2	11.0	10.11	6.00
182	1130	A	2	H	2	27.0	10.27	4.39
182	1130	A	2	H	2	43.0	10.43	5.46
182	1130	A	2	H	2	59.0	10.59	4.81
182	1130	A	2	H	2	75.0	10.75	6.08
182	1130	A	2	H	2	91.0	10.91	5.89
182	1130	A	2	H	2	107.0	11.07	6.46
182	1130	A	2	H	2	123.0	11.23	4.15
182	1130	A	2	H	2	139.0	11.39	6.96

Notes: NGR = natural gamma ray. Only a portion of this table appears here. The complete table is available in **ASCII format.**

Table T14. Thermal conductivity measurements, Site 1130.

Leg	Site	Hole	Core	Type	Section	Interval (cm)	Depth (mbsf)	Thermal conductivity (W/[m·K])
182	1130	A	1	H	3	60.0	3.60	0.848
182	1130	A	2	H	3	75.0	12.25	0.906
182	1130	A	4	H	3	75.0	31.25	0.961
182	1130	A	5	H	3	75.0	40.75	0.920
182	1130	A	8	H	2	75.0	67.75	0.954
182	1130	A	6	H	3	75.0	50.25	0.935
182	1130	A	8	H	4	75.0	70.75	0.925
182	1130	A	7	H	3	67.0	59.67	1.002
182	1130	A	8	H	6	75.0	73.75	0.973
182	1130	A	9	H	1	75.0	75.75	0.924
182	1130	A	9	H	3	75.0	78.75	1.094
182	1130	A	12	H	7	15.0	112.65	1.030
182	1130	A	13	H	1	15.0	113.15	1.036
182	1130	A	10	H	3	70.0	88.20	0.933
182	1130	A	10	H	CC	15.0	93.53	0.935
182	1130	A	11	H	3	70.0	97.70	1.080
182	1130	A	11	H	CC	11.0	103.11	1.016
182	1130	A	12	H	3	70.0	107.20	1.007
182	1130	A	13	H	3	70.0	116.70	1.073
182	1130	A	14	H	3	75.0	125.95	1.081
182	1130	A	15	H	3	75.0	135.75	1.050
182	1130	A	16	H	3	75.0	144.23	1.018
182	1130	A	17	H	3	75.0	154.75	1.068
182	1130	A	18	H	3	75.0	164.25	1.069
182	1130	A	19	X	3	75.0	173.75	1.121
182	1130	A	20	X	3	75.0	181.15	0.989
182	1130	A	21	X	3	75.0	190.75	1.035
182	1130	A	22	X	3	75.0	200.35	0.894
182	1130	A	23	X	3	75.0	209.95	1.093
182	1130	A	24	X	3	75.0	219.55	1.150
182	1130	A	25	X	3	75.0	229.15	1.026
182	1130	A	26	X	3	75.0	238.75	1.209
182	1130	A	27	X	3	73.0	248.33	1.328
182	1130	A	28	X	3	75.0	258.05	1.183
182	1130	A	29	X	3	75.0	267.65	1.180
182	1130	A	30	X	3	75.0	277.25	1.121
182	1130	A	31	X	3	60.0	286.70	0.826
182	1130	A	32	X	3	34.0	296.14	1.191
182	1130	A	33	X	3	55.0	305.95	1.070
182	1130	A	34	X	3	75.0	315.75	1.048
182	1130	A	35	X	3	75.0	325.45	1.018
182	1130	B	1	H	3	75.0		0.913
182	1130	B	4	H	3	75.0	26.75	0.877
182	1130	B	5	H	3	75.0	36.25	0.911
182	1130	B	6	H	3	75.0	45.44	0.853
182	1130	B	7	H	3	78.0	55.28	0.932
182	1130	B	8	H	3	78.0	64.78	0.969
182	1130	B	9	H	3	78.0	74.28	0.876
182	1130	B	10	H	3	78.0	83.78	0.975
182	1130	B	11	H	3	75.0	93.25	0.959
182	1130	B	12	H	3	75.0	102.75	0.965
182	1130	B	13	H	3	75.0	112.25	0.927
182	1130	B	14	H	3	75.0	121.75	0.991
182	1130	B	14	H	3	75.0	121.75	0.962
182	1130	B	15	H	3	75.0	131.25	1.119
182	1130	B	16	H	3	75.0	139.66	0.969
182	1130	B	17	H	3	75.0	150.25	0.998
182	1130	B	18	X	3	75.0	159.75	0.997
182	1130	B	19	X	3	75.0	169.35	0.978
182	1130	B	20	X	3	75.0	179.05	1.012
182	1130	B	21	X	3	75.0	188.75	1.037
182	1130	B	22	X	3	75.0	198.45	1.041
182	1130	B	23	X	3	75.0	208.15	1.080

Note: Only a portion of this table appears here. The complete table is available in **ASCII format.**

Table T15. Discrete *P*-wave velocity measurements using PWS1, PWS2, and PWS3, Site 1130.

Leg	Site	Hole	Core	Type	Section	Interval (cm)	Depth (mbsf)	PWS 1, 2, or 3	V_p (km/s)
182	1130	A	1	H	1	124.9	1.25	1	1.5774
182	1130	A	1	H	1	27.1	0.27	2	1.5896
182	1130	A	1	H	1	59.9	0.60	2	1.5852
182	1130	A	1	H	1	93.7	0.94	2	1.5910
182	1130	A	1	H	2	60.2	2.10	1	1.5724
182	1130	A	1	H	2	126.5	2.77	1	1.5919
182	1130	A	1	H	2	24.5	1.75	2	1.5824
182	1130	A	1	H	2	60.2	2.10	2	1.5710
182	1130	A	1	H	2	94.4	2.44	2	1.5809
182	1130	A	1	H	2	125.6	2.76	2	1.5766
182	1130	A	1	H	3	31.6	3.32	1	1.5774
182	1130	A	1	H	3	99.1	3.99	1	1.5984
182	1130	A	1	H	3	31.4	3.31	2	1.5695
182	1130	A	1	H	3	66.5	3.67	2	1.5639
182	1130	A	1	H	3	98.7	3.99	2	1.5496
182	1130	A	1	H	3	124.1	4.24	2	1.5998
182	1130	A	1	H	4	39.7	4.90	2	1.5795
182	1130	A	1	H	4	82.8	5.33	2	1.5781
182	1130	A	1	H	4	99.9	5.50	2	1.5589
182	1130	A	1	H	5	79.4	6.79	2	1.6101
182	1130	A	1	H	5	97.0	6.97	2	1.6191
182	1130	A	1	H	5	128.9	7.29	2	1.6101
182	1130	A	1	H	6	22.4	7.72	2	1.5969
182	1130	A	1	H	6	60.0	8.10	2	1.5910
182	1130	A	2	H	1	55.6	9.06	1	1.6268
182	1130	A	2	H	1	14.6	8.65	2	1.5541
182	1130	A	2	H	1	55.5	9.06	2	1.6171
182	1130	A	2	H	1	125.6	9.76	2	1.6057
182	1130	A	2	H	2	101.2	11.01	1	1.6117
182	1130	A	2	H	2	23.5	10.24	2	1.5466
182	1130	A	2	H	2	67.5	10.68	2	1.5852
182	1130	A	2	H	2	101.0	11.01	2	1.6013
182	1130	A	2	H	2	127.2	11.27	2	1.5766
182	1130	A	2	H	3	57.0	12.07	1	1.6042
182	1130	A	2	H	3	22.1	11.72	2	1.5867
182	1130	A	2	H	3	55.9	12.06	2	1.6087
182	1130	A	2	H	3	97.3	12.47	2	1.6057
182	1130	A	2	H	3	120.2	12.70	2	1.5983
182	1130	A	2	H	4	33.4	13.33	1	1.6130
182	1130	A	2	H	4	33.1	13.33	2	1.6176
182	1130	A	2	H	4	63.3	13.63	2	1.6131
182	1130	A	2	H	4	95.7	13.96	2	1.6146
182	1130	A	2	H	4	125.3	14.25	2	1.6146
182	1130	A	2	H	5	29.6	14.80	1	1.6306
182	1130	A	2	H	5	126.0	15.76	1	1.6159
182	1130	A	2	H	5	29.8	14.80	2	1.6328
182	1130	A	2	H	5	70.6	15.21	2	1.6176
182	1130	A	2	H	5	93.9	15.44	2	1.6252
182	1130	A	2	H	5	124.3	15.74	2	1.6146
182	1130	A	2	H	6	59.1	16.59	1	1.6253
182	1130	A	2	H	6	24.5	16.25	2	1.6042
182	1130	A	2	H	6	59.0	16.59	2	1.6161
182	1130	A	2	H	6	84.5	16.85	2	1.5954
182	1130	A	2	H	7	22.5	17.23	1	1.6245
182	1130	A	2	H	7	22.4	17.22	2	1.6206
182	1130	A	2	H	7	68.9	17.69	2	1.6146
182	1130	A	3	H	1	75.6	18.76	1	1.6245
182	1130	A	3	H	1	75.2	18.75	2	1.6146
182	1130	A	3	H	1	112.9	19.13	2	1.6297
182	1130	A	3	H	2	28.6	19.79	1	1.6299
182	1130	A	3	H	2	100.6	20.51	1	1.6299
182	1130	A	3	H	2	28.3	19.78	2	1.6343
182	1130	A	3	H	2	63.7	20.14	2	1.6027
182	1130	A	3	H	2	72.2	20.22	2	1.6161

Note: Only a portion of this table appears here. The complete table is available in **ASCII format.**

Table T16. Index properties measurements, Site 1130.

Leg	Site	Hole	Core	Type	Section	Top (cm)	Bottom (cm)	Depth (mbsf)	Bulk water content (%)	Dry water content (%)	Bulk density (g/cm^3)	Dry density (g/cm^3)	Grain density (g/cm^3)	Porosity (%)	Void ratio
182	1130	A	1	H	1	89.0	91.0	0.89	41.0	69.4	1.42	0.84	1.95	56.9	1.32
182	1130	A	1	H	2	89.0	91.0	2.39	37.5	59.9	1.46	0.91	1.95	53.3	1.14
182	1130	A	1	H	3	89.0	91.0	3.89	37.7	60.6	1.52	0.95	2.15	55.9	1.27
182	1130	A	1	H	4	89.0	91.0	5.39	34.4	52.4	1.59	1.05	2.25	53.4	1.15
182	1130	A	1	H	5	89.0	91.0	6.89	36.3	57.0	1.48	0.94	1.99	52.6	1.11
182	1130	A	1	H	6	49.0	51.0	7.99	34.9	53.5	1.50	0.98	1.99	51.0	1.04
182	1130	A	2	H	1	89.0	91.0	9.39	37.4	59.7	1.47	0.92	1.98	53.5	1.15
182	1130	A	2	H	2	89.0	91.0	10.89	36.8	58.3	1.51	0.95	2.08	54.2	1.18
182	1130	A	2	H	3	89.0	91.0	12.39	34.5	52.7	1.60	1.05	2.28	54.0	1.17
182	1130	A	2	H	4	89.0	91.0	13.89	36.7	58.1	1.48	0.94	2.00	53.1	1.13
182	1130	A	2	H	5	89.0	91.0	15.39	36.1	56.5	1.54	0.99	2.16	54.3	1.19
182	1130	A	2	H	6	89.0	91.0	16.89	33.7	50.9	1.62	1.07	2.29	53.2	1.14
182	1130	A	3	H	1	89.0	91.0	18.89	34.7	53.2	1.49	0.97	1.97	50.6	1.02
182	1130	A	3	H	2	89.0	91.0	20.39	32.7	48.6	1.55	1.04	2.06	49.3	0.97
182	1130	A	3	H	3	49.0	51.0	21.49	35.0	53.9	1.56	1.02	2.18	53.4	1.15
182	1130	A	4	H	1	79.0	81.0	28.29	31.1	45.1	1.53	1.06	1.97	46.5	0.87
182	1130	A	4	H	2	74.0	76.0	29.74	33.5	50.4	1.52	1.01	2.00	49.7	0.99
182	1130	A	4	H	3	79.0	81.0	31.29	28.5	39.9	1.60	1.14	2.06	44.5	0.80
182	1130	A	4	H	4	74.0	76.0	32.74	29.4	41.6	1.58	1.11	2.03	45.2	0.82
182	1130	A	4	H	5	79.0	81.0	34.29	31.3	45.5	1.57	1.08	2.07	47.9	0.92
182	1130	A	4	H	6	59.0	61.0	35.59	26.6	36.2	1.53	1.13	1.87	39.7	0.66
182	1130	A	4	H	7	49.0	51.0	36.49	27.5	37.9	1.67	1.21	2.20	44.9	0.82
182	1130	A	5	H	2	70.0	72.0	39.20	21.7	27.8	1.65	1.29	1.98	35.0	0.54
182	1130	A	5	H	3	69.0	71.0	40.69	25.4	34.1	1.52	1.13	1.82	37.7	0.61
182	1130	A	5	H	4	69.0	71.0	42.19	20.6	25.9	1.58	1.25	1.83	31.6	0.46
182	1130	A	5	H	5	68.0	70.0	43.68	31.4	45.7	1.47	1.01	1.83	45.0	0.82
182	1130	A	5	H	6	69.0	71.0	45.19	21.1	26.8	1.66	1.31	1.99	34.2	0.52
182	1130	A	5	H	7	69.0	71.0	46.69	23.0	29.9	1.56	1.20	1.86	35.1	0.54
182	1130	A	6	H	1	79.0	81.0	47.29	22.0	28.2	1.61	1.25	1.91	34.5	0.53
182	1130	A	6	H	2	79.0	81.0	48.79	21.9	28.1	1.59	1.24	1.88	34.0	0.52
182	1130	A	6	H	3	79.0	81.0	50.29	22.3	28.7	1.63	1.27	1.96	35.5	0.55
182	1130	A	6	H	4	79.0	81.0	51.79	20.3	25.5	1.68	1.34	2.00	33.2	0.50
182	1130	A	6	H	5	79.0	81.0	53.29	26.3	35.6	1.56	1.15	1.91	39.9	0.66
182	1130	A	6	H	6	79.0	81.0	54.79	23.1	30.0	1.61	1.24	1.94	36.2	0.57
182	1130	A	6	H	7	29.0	31.0	55.79	22.1	28.3	1.66	1.30	2.02	35.8	0.56
182	1130	A	7	H	1	79.0	81.0	56.79	22.0	28.2	1.52	1.18	1.75	32.6	0.48
182	1130	A	7	H	2	79.0	81.0	58.29	19.2	23.8	1.67	1.35	1.97	31.4	0.46
182	1130	A	7	H	3	79.0	81.0	59.79	20.8	26.3	1.69	1.34	2.03	34.2	0.52
182	1130	A	7	H	4	79.0	81.0	61.29	20.8	26.3	1.55	1.23	1.80	31.6	0.46
182	1130	A	7	H	5	79.0	81.0	62.79	24.5	32.5	1.58	1.19	1.92	37.8	0.61
182	1130	A	7	H	6	79.0	81.0	64.29	19.7	24.6	1.65	1.33	1.95	31.8	0.47
182	1130	A	7	H	7	9.0	11.0	65.09	23.6	30.9	1.51	1.15	1.77	34.9	0.54
182	1130	A	8	H	1	79.0	81.0	66.29	21.8	27.8	1.59	1.24	1.88	33.8	0.51
182	1130	A	8	H	2	79.0	81.0	67.79	25.7	34.6	1.60	1.19	2.00	40.3	0.67
182	1130	A	8	H	3	79.0	81.0	69.29	22.4	28.9	1.54	1.20	1.81	33.7	0.51
182	1130	A	8	H	4	79.0	81.0	70.79	22.2	28.5	1.58	1.23	1.87	34.3	0.52
182	1130	A	8	H	5	79.0	81.0	72.29	21.6	27.6	1.68	1.32	2.05	35.5	0.55
182	1130	A	8	H	6	79.0	81.0	73.79	20.5	25.9	1.58	1.26	1.84	31.8	0.47
182	1130	A	9	H	1	79.0	81.0	75.79	28.4	39.6	1.20	0.86	1.29	33.2	0.50
182	1130	A	9	H	2	79.0	81.0	77.29	22.6	29.2	1.62	1.26	1.96	35.8	0.56
182	1130	A	9	H	3	79.0	81.0	78.79	23.3	30.4	1.54	1.18	1.83	35.1	0.54
182	1130	A	9	H	4	79.0	81.0	80.29	19.9	24.9	1.63	1.30	1.91	31.6	0.46
182	1130	A	9	H	5	79.0	81.0	81.79	21.0	26.6	1.66	1.31	1.99	34.1	0.52
182	1130	A	9	H	6	79.0	81.0	83.29	20.4	25.6	1.65	1.31	1.96	32.9	0.49
182	1130	A	10	H	1	72.0	74.0	85.22	21.6	27.6	1.66	1.30	2.00	35.1	0.54
182	1130	A	10	H	2	78.0	80.0	86.78	22.8	29.6	1.63	1.26	1.98	36.3	0.57
182	1130	A	10	H	3	78.0	80.0	88.28	22.6	29.2	1.64	1.27	1.98	36.1	0.56
182	1130	A	10	H	4	78.0	80.0	89.78	21.0	26.6	1.58	1.25	1.84	32.4	0.48
182	1130	A	10	H	5	79.0	81.0	91.29	21.3	27.0	1.67	1.31	2.01	34.7	0.53
182	1130	A	11	H	1	79.0	81.0	94.79	20.3	25.4	1.61	1.28	1.88	31.8	0.47
182	1130	A	11	H	2	79.0	81.0	96.29	26.4	35.9	1.46	1.07	1.72	37.6	0.60
182	1130	A	11	H	3	79.0	81.0	97.79	20.2	25.3	1.66	1.33	1.98	32.8	0.49
182	1130	A	11	H	5	79.0	81.0	100.79	21.1	26.8	1.58	1.25	1.85	32.7	0.49
182	1130	A	11	H	6	79.0	81.0	102.29	22.2	28.5	1.66	1.30	2.02	36.0	0.56
182	1130	A	12	H	1	69.0	71.0	104.19	22.4	28.9	1.65	1.28	2.00	36.1	0.57

Note: Only a portion of this table appears here. The complete table is available in **ASCII format.**

Table T17. Undrained shear strength measurements, Site 1130.

Leg	Site	Hole	Core	Type	Section	Interval (cm)	Depth (mbsf)	Maximum shear strength (kPa)	Peak (kPa)
182	1130	A	1	H	2	133.7	2.84	6.93	8.45
182	1130	A	1	H	3	132.7	4.33	9.63	11.75
182	1130	A	1	H	4	93.6	5.44	3.87	4.72
182	1130	A	1	H	5	118.4	7.18	2.43	2.96
182	1130	A	2	H	1	122.0	9.72	1.08	1.32
182	1130	A	2	H	3	117.6	12.68	4.23	5.16
182	1130	A	2	H	3	131.5	12.81	4.59	5.60
182	1130	A	2	H	4	133.2	14.33	6.84	8.34
182	1130	A	2	H	5	136.2	15.86	5.31	6.48
182	1130	A	2	H	6	72.6	16.73	6.84	8.34
182	1130	A	3	H	1	106.2	19.06	4.86	5.93
182	1130	A	3	H	2	137.5	20.88	4.59	5.60
182	1130	A	4	H	1	139.8	28.90	4.41	5.38
182	1130	A	4	H	2	134.2	30.34	7.92	9.66
182	1130	A	4	H	3	87.9	31.38	6.48	7.90
182	1130	A	4	H	3	126.9	31.77	11.07	13.50
182	1130	A	4	H	4	135.3	33.35	22.59	27.55
182	1130	A	4	H	5	136.3	34.86	18.54	22.61
182	1130	A	5	H	1	133.7	38.34	12.42	15.15
182	1130	A	5	H	2	135.6	39.86	21.06	25.69
182	1130	A	5	H	3	117.7	41.18	10.80	13.17
182	1130	A	5	H	4	135.6	42.86	21.06	25.69
182	1130	A	5	H	5	91.9	43.92	5.67	6.92
182	1130	A	5	H	6	111.6	45.62	7.92	9.66
182	1130	A	5	H	7	56.2	46.56	7.92	9.66
182	1130	A	6	H	1	120.3	47.70	10.26	12.51
182	1130	A	6	H	2	132.7	49.33	2.97	3.62
182	1130	A	6	H	3	109.7	50.60	21.33	26.02
182	1130	A	6	H	4	125.1	52.25	13.05	15.92
182	1130	A	6	H	5	108.1	53.58	16.47	20.09
182	1130	A	6	H	6	114.6	55.15	9.54	11.64
182	1130	A	6	H	7	17.5	55.67	16.02	19.54
182	1130	A	7	H	1	124.9	57.25	9.27	11.31
182	1130	A	7	H	2	125.7	58.76	13.59	16.58
182	1130	A	7	H	3	101.5	60.01	9.72	11.86
182	1130	A	7	H	4	127.1	61.77	20.88	25.47
182	1130	A	7	H	5	120.4	63.20	12.15	14.82
182	1130	A	7	H	6	132.5	64.82	18.63	22.72
182	1130	A	7	H	7	14.9	65.15	9.45	11.53
182	1130	A	8	H	1	130.7	66.81	22.14	27.00
182	1130	A	8	H	2	121.9	68.22	11.61	14.16
182	1130	A	8	H	3	117.7	69.68	16.29	19.87
182	1130	A	8	H	4	110.8	71.11	14.94	18.22
182	1130	A	8	H	5	127.8	72.78	12.06	14.71
182	1130	A	8	H	6	99.7	74.00	22.32	27.22
182	1130	A	9	H	1	117.7	76.18	12.33	15.04
182	1130	A	9	H	2	124.4	77.74	18.99	23.16
182	1130	A	9	H	3	112.6	79.13	21.60	26.34
182	1130	A	9	H	3	126.0	79.26	35.37	43.14
182	1130	A	9	H	5	113.2	82.13	20.61	25.14
182	1130	A	9	H	6	96.0	83.46	14.58	17.78
182	1130	A	10	H	1	111.6	85.62	13.86	16.90
182	1130	A	10	H	2	131.0	87.31	6.30	7.68
182	1130	A	10	H	3	108.8	88.59	7.56	9.22
182	1130	A	10	H	4	131.0	90.31	7.29	8.89
182	1130	A	10	H	5	109.4	91.59	19.35	23.60
182	1130	A	10	H	6	113.6	93.14	17.64	21.51
182	1130	A	11	H	1	116.7	95.17	19.98	24.37
182	1130	A	11	H	2	122.6	96.73	22.23	27.11
182	1130	A	11	H	3	106.3	98.06	14.67	17.89
182	1130	A	11	H	4	131.0	99.81	20.07	24.48
182	1130	A	11	H	5	109.8	101.10	18.54	22.61
182	1130	A	11	H	6	125.7	102.76	15.84	19.32

Note: Only a portion of this table appears here. The complete table is available in **ASCII format.**

Table T18. Summary of tool strings, intervals logged, and logging speeds, Hole 1130C.

Tool string	First pass		Second pass	
	Interval (mbsf)	Speed (m/hr)	Interval (mbsf)	Speed (m/hr)
Triple combo	0-371.5	550	0-322.5	275
FMS/sonic	152.5-368.5	275	0-367.5	275

Note: Triple combo = triple combination logging tool, FMS = Formation MicroScanner.

Table T19. Differences between depths to key horizons and corrected depths.

Seismic horizons	Predicted intersection (mbsf)	Check-shot corrected depth (mbsf)	Difference (m)
Base of Sequence 2	230	238	+8
Top of Sequence 6A	311	326	+15
Top of Sequence 7	343	360	+17

Notes: Predicted intersection depths were derived using high-resolution site-survey seismic data stacking velocities. Corrected depths were based on check-shot data and interval transit-time (ITT) data.